# Control of Fluid Flow and Species Transport within Microchannels of Microfluidic Chips

by

**Zhanjie Shao**

A thesis
presented to the University of Waterloo
in fulfillment of the
thesis requirement for the degree of
Master of Applied Science
in
Mechanical Engineering

Waterloo, Ontario, Canada, 2008

# Authors's Declaration

I hereby declare that I am the sole author of this thesis. This is a true copy of the thesis, including any required final revisions, as accepted by my examiners.

I understand that my thesis copy may be made electronically available to the public.

Zhanjie Shao

# Abstract

Microfluidic chips have drawn great attention and interest due to their broad applications in chemical, biological and biomedical fields. These kinds of miniaturized devices offer many advantages over the traditional analysis instruments, such as reduced cost, shortened time, increased throughput, improved integration/automation/portability, etc. However, the concept of integrating multiple labs on a single chip to perform micro total analysis hasn't been realized yet because of the lack of fundamental knowledge and systematic design of each component, especially for some particular applications. A thorough understanding and grasp of the basic physical phenomenon is the theoretical basis to develop functional devices to utilize them. In this study, we intend to investigate the electrokinetic fluid flow and coherent species transport processes in microchannels, and then try to effectively control them for designing related lab-on-a-chip devices.

Rather than expensive experiments, numerical studies are performed to simulate the different processes involved in various electrokinetic chip applications. In the theoretical models, applied potential field, flow field and species concentration field are considered and corresponding governing equations with initial/boundary conditions are numerically solved by computational fluid dynamics techniques. The flow field is obtained by the developed SIMPLE algorithm and a slip-wall velocity boundary condition is applied in simulating electroosmotic flow. Grid independence tests and convergence studies are performed to ensure economic computation with adequate accuracy and stability. For every application with typical channel layout, parametric studies are performed to investigate different effects through the controlling parameters linked to them.

For surface patterning or microfabrication using laminar flows, various operational parameters are investigated to explore the optimized configurations for multi-stream flow and mass transport control in cross-linked microchannels. Through a series of numerical simulations, it is found that applied potentials, electroosmotic mobilities of solutions and channel dimensions have significant effects on the flow and mass transport after converging in the intersection of channel network. Diffusion coefficient has less

influence than the other parameters due to the presence of high Peclet number for such applications.

For the microwashing with two different electrolyte solutions, a three-dimensional model is numerically solved to reveal the flow structure change. In a straight microchannel with a rectangle cross section, KCl solution and $LaCl_3$ solution are mainly employed for tests. Displacement processes between two solutions in both orders are tested and analyzed. The observed flow structures such as back flow in channel center and distortion of plug-like velocity profile are noticed and discussed. The distortion of the flow field results from the induced pressure gradient, which is due to the non-uniformity of electroosmotic mobilities and electrical conductivities of two replaced solutions. The bigger difference two solutions have in chemical properties, the stronger effects on flow they have. Effect of applied potential field strength is also studied and the approximate linear influences are concluded.

Finally, the unsteady on-chip sample injection and separation processes involved in microchip capillary electrophoresis are studied. Species' electrophoretic migration effect is included and the theoretical model is non-dimensionalized in a unique manner with the key fundamental parameters: the $\mathrm{Re}\,Sc_i$, species' non-dimensional electrophoretic mobility and applied potentials. The species transport characteristics are revealed numerically and well understood for future effective control and innovative chip design. Species front movement during injection and sample plug development in separation are examined with diffusion effect; results include concentration profiles and contour plots over a range of injection and separation time. The influence of $\mathrm{Re}\,Sc_i$ which characterizes the relative role of convection versus diffusion is examined over the commonly encountered range and the diffusion effect is found to have an essentially negligible effect. Through three species, the electrophoretic mobilities difference is demonstrated to be the reason for separation. Real-time monitoring of different species' movements is performed for injection guidance.

# Acknowledgements

I would like to express my overwhelming gratitude to the following people and organizations without whose support the work in this thesis could not be finished.

Firstly, special thanks are presented to my supervisors, Prof. Carolyn Ren and Prof. Gerry Schneider, for all the opportunities and guidance that they have ever given to me. Their encouragement, help and patience throughout my whole graduate studies are highly appreciated forever.

Secondly, I am lucky to pursue my graduate study in the UW microfluidic and bio-chip laboratory. The knowledge and experiences learnt from our research group make me benefit a lot. The valuable advice and discussion from my colleagues, Jay Taylor, Tom Glawdel, Razim Samy, Lin Gui, Shuwen Wang, Zeyad Almutairi and other lab-mates, is an important contribution to the fulfillment of this thesis.

Thirdly, the financial support of a Research Grant of the Natural Sciences and Engineering Research Council (NSERC) of Canada to Prof. Ren and Prof Schneider is gratefully acknowledged.

At last, I will appreciate the sincere support from my wife, daughter and parents. Their invaluable love is always the source for me to go forward.

# Table of Contents

# List of Figures

# List of Tables

# Nomenclature

### Acronyms

| | |
|---|---|
| BCE | Bovine Capillary Endothelial |
| CAE | Capillary Array Electrophoresis |
| CE | Capillary Electrophoresis |
| CFD | Computational Fluid Dynamics |
| DIUF | Distilled Ultra Filtered |
| DNA | Deoxyribo-Nnucleic Acid |
| EDL | Electrical Double Layer |
| EOF | Electroosmotic Flow |
| LIF | Laser-Induced Fluorescence |
| MCE | Microchip Capillary Electrophoresis |
| PCR | Polymerase Chain Reaction |
| PDMS | Polydimethylsiloxane |
| PIV | Particle Image Velocimetry |
| RNA | Ribo-Nucleic Acid |
| SIMPLE | Semi-Implicit Method for Pressure Linked Equations |
| μTAS | Micro-Miniaturized Total Analysis System |

### Mathematical symbols

| | |
|---|---|
| $a$ | Particle radius, $nm$ |
| $c$ | Concentration, $mol/l$ or $M$ |
| $C$ | Non-dimensional concentration |
| $D$ | Diffusion coefficient, $m^2/s$ |
| $D_h$ | Hydraulic diameter, $D_h = 4hw/(h+w)$, $\mu m$ |
| $e$ | Electric charge of an electron, $-1.6\times10^{-19} C$ |
| $E$ | Applied potential field strength, $V/m$ |
| $F$ | Faraday constant, $9.65\times10^4 C/mol$ |
| $F_D$ | Frictional force or drag force, $N$ |

| | |
|---|---|
| $F_e$ | Electrical force, $N$ |
| $h$ | Channel height or depth, $\mu m$ |
| $K_b$ | Boltzmann constant, $1.38\times10^{-23} J/K$ |
| $l$ | Channel length, $mm$ |
| $n$ | Ionic number concentration, $l^{-1}$ |
| $N_a$ | Avogadro number, $6.022\times10^{23} mol^{-1}$ |
| $p$ | Pressure, $Pa$ |
| $P$ | Non-dimensional pressure |
| $P_a$ | Atmospheric pressure, $1.01\times10^{5} Pa$ |
| $Pe$ | Peclet number |
| $Q$ | Amount of net charge, $C$ |
| Re | Reynolds number |
| $Sc$ | Schmidt number |
| $t$ | Time, $s$ |
| $T$ | Temperature, $K$ |
| $v$ | Velocity, $m/s$ |
| $V$ | Non-dimensional velocity |
| $w$ | Channel width, $\mu m$ |
| $x, y, z$ | The x, y, z-coordinate |
| $X, Y, Z$ | Non-dimensional x, y, z-coordinate |

**Greek symbols**

| | |
|---|---|
| $\varepsilon$ | Electrical permittivity of medium, $C/(V\cdot m)$ |
| $\varepsilon_0$ | Vacuum permittivity, $8.854\times10^{-12} C/(V\cdot m)$ |
| $\varepsilon_r$ | Relative permittivity of medium |
| $\zeta$ | Zeta potential, $mV$ |
| $\kappa$ | Debye-Huckle parameter, $\kappa=\sqrt{2n^{\infty}z^2e^2/K_bT\varepsilon_r\varepsilon_0}$ |
| $\lambda$ | Electrical conductivity of solutions, $S/m$ |
| $\mu$ | Viscosity, $N\cdot s/m^2$ |

| | |
|---|---|
| $\mu_{eo}$ | Electroosmotic mobility, $\mu_{eo} = \varepsilon\zeta/\nu$, $m^2/(V \cdot s)$ |
| $\mu_{ep}$ | Electrophoretic mobility, $\mu_{ep} = zFD/RT$, $m^2/(V \cdot s)$ |
| $\nu$ | Kinematic viscosity, $m^2/s$ |
| $\rho$ | Density, $kg/m^3$ |
| $\rho_e$ | Net charge density, $C/m^3$ |
| $\tau$ | Non-dimensional time |
| $\phi$ | Applied electrical potential, $V$ |
| $\Phi$ | Non-dimensional or normalized applied electrical potential |
| $\psi$ | Electrokinetic potential, $mV$ |
| $\Psi$ | Non-dimensional electrokinetic potential, $\Psi = ze\psi/K_bT$ |

**Subscrips**

| | |
|---|---|
| 0 | Original or initial |
| a | Air |
| e | Electrical |
| eo | Eletroosmotic |
| ep | Electrophoretic |
| h | Horizontal |
| i | The i-th species, channel or reservoir number |
| in | Inlet |
| inj | Injection |
| l | The parallel direction to channel wall |
| n | The normal direction to channel wall |
| out | Outlet |
| ref | Reference |
| sep | Separation |
| unif | Uniform |
| v | Vertical |
| x,y,z | Variables in the x,y,z-direction |

# Chapter 1

# Introduction

## 1.1 Background

In the fields of analytical chemistry, biology and biochemistry, there are many analysis processes involved, such as chemical synthesis, cell manipulation and bio-species (protein, DNA, RNA, etc) analysis. For example, DNA amplification is realized by polymerase chain reaction (PCR) and DNA sequencing is performed through electrophoretic separation to decode genetic information stored in genes [1]. To fulfill these kinds of tasks, different experimental measurements and tests have to be performed with the appropriate equipments and devices. Compared to conventional technologies, microfluidic chips or lab-on-a-chip devices provide an excellent platform.

A lab-on-a-chip device or microfluidic chip is a microscale laboratory built on a thin glass or plastic plate with a network of microchannels, electrodes, sensors, power supply system and other integrated functional components. As shown in Figure 1-1, the lab-on-a-chip device generally performs a number of microfluidic functions, such as pumping, mixing, dispensing, thermal cycling and so on. Through external pressure forces or applied electrical forces, the liquid flow and species transport can be controlled in the microchannel networks. Incorporating specific components, different operations and analysis processes can be run on such a small chip.

Lab-on-a-chip devices offer many remarkable advantages over the conventional bench-top analytical instruments [2]. Besides the reduced sample consumption and analysis time, people can benefit a lot from its innovative features, such as easiness for automation, integration and improved portability. Therefore, more and more miniaturized lab-on-a-chip devices and microfluidic chips are being developed in a wide range of various chemical, biological and biomedical applications. However, this area of research is still quite new. Extensive experimental and numerical studies on fundamental

knowledge of microfluidic phenomena and development of new-generation miniaturized devices will continue to be prosperous in the following decades.

The design and construction of microfluidics devices differs from macroscale ones, so it is not generally possible to scale conventional devices down and then expect them to work in microfluidics applications. When the dimensions of a device or system reach a certain small size, the particles of fluid, or particles suspended in the fluid, become comparable in size with the apparatus itself, and the effects dominating fluid motion change. The laws for macroscale flow may not be applicable and system behavior may change dramatically. For example, fluids at micron-scale are primarily dominated by viscous forces and surface tension forces, and there are also other unknown factors involved, the nature of which only further research can reveal.

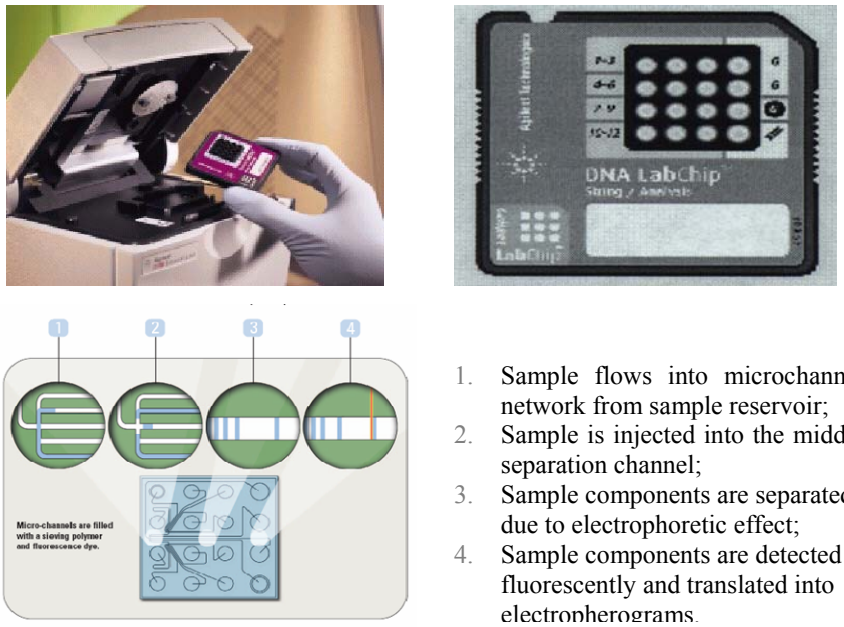


**Figure 1-1** Illustration of a lab-on-a-chip/microfluidic device.

Computational fluid dynamics (CFD) is widely used in prediction and analysis of systems involving fluid flow, heat and mass transfer problems by means of computer based simulations. It is a powerful tool for many industrial and non-industrial

applications. Experimental studies are more expensive, time consuming and sometime operation limited. Many things must be considered like the equipment, facility, materials, human costs, etc. On the contrary, numerical simulations by CFD provide an inexpensive and fast alternative to studying. CFD has the capability to perform parametric studies quickly by altering the values of parameters and it also has the ability to study specific problem where experiments are difficult or impossible to be conducted.

There are many challenges of running CFD simulations. People need to be aware of the underlying physics well with identification and formulation of the problems and then make simplifications and assumptions to reduce the complexity. CFD also has its own limitations and drawbacks. It is limited by available physical models with differential equations. Ideal assumptions and appropriate boundary conditions are important to obtain convergence results. Comparing to analytical solution, some errors in numerical results are unavoidable and a proper numerical algorithm is required to minimize them.

## 1.2 Motivation and objectives

Lab-on-a-chip device or microfluidic chip have been developed as micro-total analysis systems (μTAS) for chemical, biological and biomedical applications in the past decades [3]. There have been many reported quality researches addressing numerous obstacles to be overcome in applying microfluidic devices in natural and life sciences as reviewed by Dittrich [4]. However, the concept of integrating and miniaturizing multiple labs on a single chip to perform micro total analysis has not been realized yet due to the lack of systematic design tools for each component and the ability to control operation. The fundamental knowledge and understanding on microfluidics and microscale transport phenomena, improved theoretical model and effective analysis tool are still required through further studies, especially for some particular applications.

### 1.2.1 Surface pattern and microfabrication

Based on some reported experimental work, laminar flow was utilized to perform surface patterning and microfabricate certain desired structures within microchannels or small

spaces. However, to date, little has been reported regarding the development of analysis tools providing optimized configurations for multi-stream flow control in such miniaturized systems. Electroosmotic flow (EOF) is employed here as the pumping method to facilitate the liquid flow in a cross-linked microchannel network.

A numerical model is developed to study the applied potential field, flow field and concentration field in such geometries. Effects of various controlling parameters, such as applied potentials, channel geometries and buffer solution properties, will be investigated based on the simultaneous solution to this model. Using this analysis tool, the goal of this project is to provide an optimized configuration of operational parameters to realize on-chip microfabrication through precise control of laminar flow and mass transport, which allow two or three streams of solutions pumped into a main channel.

### 1.2.2 Microwashing for sample preparation

Multiple washing procedures are usually required in most sample preparation processes, in which one solution is designed to replace another one in microchannels or capillaries. It is very important to fully understand this displacement transport processes prior to effective controls of them. To potentially exploit this replacement phenomenon, the details of complex three-dimensional EOF structure during this process will have to be grasped. The objective of present study is to investigate the solution displacement process in rectangular microchannel using a special three-dimensional numerical model. Electroosmotic flow is employed as a pumping method and the induced pressure gradient due to the balance of discontinuity of velocity at the interface of two solutions will be included as well. The time evolution of the interface between different solutions, pressure field within microchannel, EOF velocity profile and the concentration distribution of two solutions will be revealed and discussed for improved understanding and control.

### 1.2.3 Injection and separation for capillary electrophoresis

A classical on-chip capillary electrophoresis (CE), which normally consists of a two-step task of injection and separation, has been widely utilized for chemical and biological

separation analysis. Although relevant experimental work has been published by chemistry people with real bio-samples, theoretical studies on fluid flow control and mass transport involved in this on-chip analysis process are critical important to provide prediction and guidance.

In this study, the focus is on the development of a theoretical model and subsequent numerical investigation of species injection and separation processes based on a cross-linked microchannel network. A two-dimensional numerical model will be developed and completely non-dimensionalized to identify the key controlling parameters which affect the injection sample plug and sample separation resolution. Parametric studies will be performed to investigate the effects of species' properties on the whole transport process. This fundamental study will be helpful to acquire a thorough understanding of fluid flow and species transport in microchannels, which will provide guidance to chip design and practical operation/control in on-chip capillary electrophoresis applications.

## 1.3 Overview

With different research concerns, three projects for various particular applications are included through a series of numerical studies. The developed theoretical models are presented in details and numerically solved with our own codes. Under the specific control schemes, some fluid flow problems and mass transport phenomenon within microchannel network are revealed and discussed. Fundamental knowledge and improved understanding are achieved through these parametric studies. Different effects with corresponding controlling parameters are investigated, which will contribute to future chip design and practical control.

For the introduction chapter of this thesis, the background knowledge is firstly given, which includes the necessity and application scope of lab-on-a-chip device, brand new microfluidics research and the methodology of CFD adopted in our study. Next, the motivation and objectives of every individual project are expressed respectively. A brief overview of the whole thesis is presented chapter by chapter and a summary of every chapter is made with emphasis at the last section.

A comprehensive literature review on related topics of our studies is presented in Chapter 2. At first, the basic knowledge encountered in microfluidics studies is reviewed. The growing chip technology and the long-term goal of micro total analysis system are simply introduced by pointing out its remarkable advantages, broad applications and potential lack. The fundamental microfluidic concepts are then explained, which include the electrical double layer, zeta potential and the governing Poisson-Boltzmann equation. Secondly, some basic aspects of microflow and microscale mass transport are discussed. The usual electrokinetic flow and pressure driven flow are compared and so are their different control mechanisms. Thermal effect due to the Joule heating is found to have important influences on electrokinetic flows and mass transfer involved in them. Some effective methods to remove the negative effects from hydrostatic pressure and meniscus Laplace pressure are expressed. Electrophoresis which accounts for electrophoretic separation is discussed in details by the derivation of charged particle's electrophoretic mobility. Diffusion related effects are talked about finally, and the Taylor dispersion and Brownian motion can be neglected in the scale of our applications. Thirdly, according to the three particular applications, related literature reviews are presented to show the technical problems and research developments for each of them. In the last section of research methods, comparison of experimental studies and numerical studies are made to highlight the focus of our studies.

In chapter 3, the project of surface patterning and microfabrication by controlling laminar flows is summarized. In this numerical study, the mathematical model is developed to describe the applied potential field, flow field and concentration field. Through investigating the different controlling parameters, a three-steam flow and two-stream flow is generated to fulfill the desired surface patterning and fabrication in microchannels.

In a straight microchannel, the displacement process for two different solutions is disclosed in Chapter 4. The characteristics of EOF with replaced solutions are described by the simulated three-dimensional flow structure. Some specific phenomenon during this process, such as the back flow and circulation, are found and explained. The uniform applied electrical field is destroyed by the presence of two solutions with different electrical conductivities in the same microchannel.

In Chapter 5, a complete model is developed to simulate the on-chip species injection and separation process, which is same to the procedure of microchip capillary electrophoresis (MCE). Using the simple cross injector and common pinched injection mode, the unsteady species transport characteristics are revealed in details. Effects of species' diffusion coefficients are investigated through the developed parameter of $\mathrm{Re}\,Sc_i$. And the species' electrophoretic mobilities are also studied, which helps us construct the intuitive understanding of on-chip capillary electrophoretic separation.

In last Chapter, a summary is given with the emphasized effects we studied in every project. Regarding the numerical investigation of three different applications, corresponding contributions and recommendations are outlined; and the extended future work is also pointed out in the end. The findings of this research will provide useful reference for relevant experiments and further numerical studies as expected.

# Chapter 2

# Literature Review

## 2.1 Fundamentals

### 2.1.1 μTAS and chip technology

Biochips or lab-on-a-chip devices have drawn a great deal of attention over the last decade due to their great potential in chemical and biomedical diagnostics and treatments [5-7]. Major advantages of such miniaturized devices versus their traditional macro-scale counterparts include reduced sample consumption, shortened processing time, and increased portability, integration and automation[8, 9]. Despite of the great potential of lab-on-a-chip to various applications, few practical devices exist due to the difficulties in the integration, automation and systematic design of each component. Microfluidic chip is one of the major components and has been applied to improve various chemical and biomedical processes, such as cell sorting [10], DNA sequencing [11-13], protein analysis [14], PCR amplification [15] and electrophoresis applications [16, 17]. Rapid development of microfluidic chip technology has allowed many chemical and biomedical analyses to be performed on a palm-size plastic or glass chip [18-22] with significantly improved resolution and efficiency [11, 23].

Integrating and optimizing different small analysis units into one single micro total analysis system is the long-term goal. These built-in labs on a chip can duplicate the specialized functions as performed by their room-size counterparts. Such portable devices would be convenient for home and bedside use, thereby eliminating the time consuming laboratory analysis procedures. The progress of lab-on-a-chip has been accelerated by the novel soft lithography technique [24]. Compared to the conventional photolithography, it provides an easy, fast, safe and inexpensive method to manufacture prototype chips. The chip fabrication can be achieved in-house with low cost and high speed. Moreover, mass production can be easily realized by replication with one mold or master in soft lithography. However, the concept of integrating and miniaturizing multiple labs on a

single chip to perform micro total analysis has not been realized yet due to the lack of systematic design tools for each component and the ability to control various operations. Fundamental studies are still required to grasp the basic mechanisms and influencing effects on flow and transport inside microchannel network. And then, novel design and improved control can be developed for μTAS with high performance.

### 2.1.2 Microfluidics

The rapid growth of microfluidics is driven by new technological applications in chemical, biological and biomedical areas. Microfluidics is defined as the science of designing, manufacturing and formulating devices and processes that deal with volumes of fluid on the order of nanoliters or even picoliters. Microfluidic devices and their components have dimensions ranging from millimetres down to microns. Due to the small dimensions of microchannels and small quantities of fluids and samples within them, the Reynolds number of microflow is usually quite small (in the order of 1 and less). The flow is completely laminar and no turbulence occurs, which provides a means by which samples can be transported in a relatively predictable manner inside microchannels. In addition to pressure driven flow, electrokinetic phenomenon has often been employed to run different chip-based analysis processes. Understanding of this microfluidic phenomenon is necessary in order to utilize the microflow properly.

According to the interfacial electrokinetics and colloid science, an electrical double layer (EDL) shown in Fig 2-1 will appear at the two-phase interface when an aqueous solution is contacting a microchannel wall. The formation of this surface charge layer is complicated and is caused by a variety of mechanisms [25]. One important mechanism is due to the ionization of surface groups. A wall with acid groups will give rise to a negatively charged surface due to the $H^+$ dissociation. Conversely, a basic surface takes on a positive charge by releasing $OH^-$. The charged wall surface will attract the counter-ions in the solution and form a thin layer of non-uniform charged ions.

Because of the net charge layer, there is an elecktrokinetic potential distribution in the direction normal to the microchannel wall. According to the theory of electrostatics, it can be described by Poisson equation.

$$\varepsilon_r \varepsilon_0 \nabla^2 \psi = -\rho_e \qquad [2\text{-}1]$$

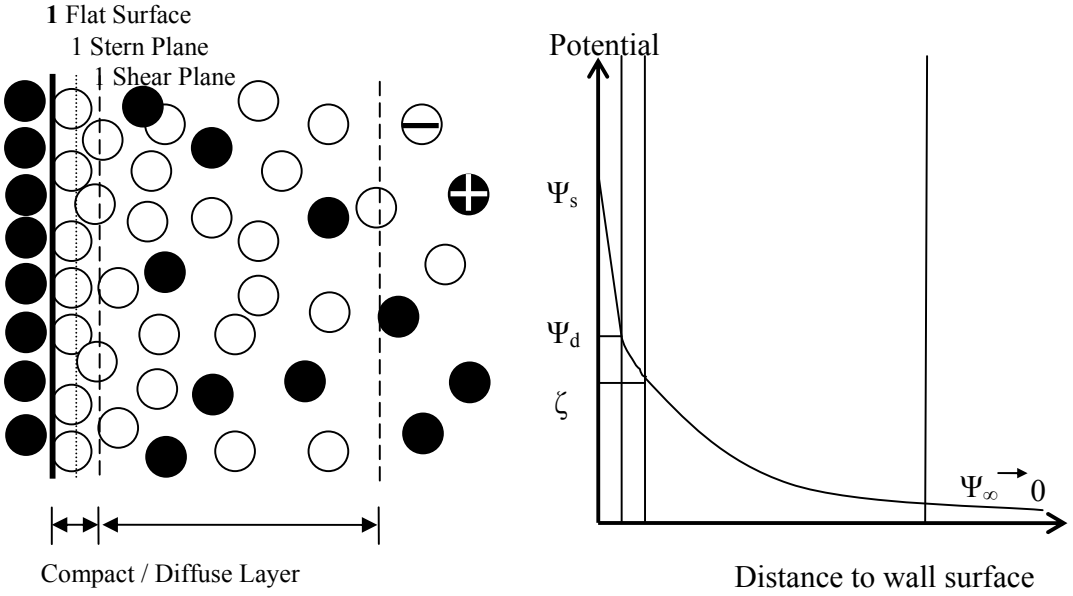


**Figure 2-1** Schematic diagram of ion distribution in the EDL (left) and electrokinetic potential distribution on the interface of channel wall and aqueous solution (right).

In EDL, equilibrium is established for electrical force and diffusive force on the ions. Boltzmann equation is then formulated to reveal the ion concentration distribution and then the net charge density. For a symmetric electrolyte solution (valance $|z_+| = |z_-| = z$),

$$\rho_e = -2n^\infty ze Sinh(\frac{ze\psi}{K_b T}) \qquad [2\text{-}2]$$

where $n^\infty$ is the bulk ionic concentration. Incorporating equation [2-1] and [2-2], the complete Poisson-Boltzmann equation is obtained for the electrokinetic potential [26].

$$\nabla^2 \psi = \frac{2n^\infty ze}{\varepsilon_r \varepsilon_0} Sinh(\frac{ze\psi}{K_b T}) \qquad [2\text{-}3]$$

Normally, the surface potential is as small as the order of mili-volts and the term satisfies $ze\psi / K_b T << 1$. Therefore, a Debye-Huckle linear approximation can be applied to simplify the Poisson-Boltzmann equation [2-3] as follows.

$$\nabla^2\psi = \frac{2n^{\infty}z^2e^2}{\varepsilon_r\varepsilon_0 K_b T}\psi = \kappa^2\psi \qquad [2\text{-}4]$$

where, $\kappa$ is known as Debye-Huckle parameter with $\kappa = \sqrt{2n^{\infty}z^2e^2/K_bT\varepsilon_r\varepsilon_0}$ . The thickness of EDL can be estimated by the inverse Debye-Huckle parameter $\kappa^{-1}$, which is typically on the order of second nano-meters. Actually without any assumption and simplification, it is difficult and expensive to solve the Poisson-Boltzmann equation directly, especially for non-symmetric electrolyte solutions. As shown in Figure 2-1, the electrokinetic potential $\psi$ will drop to zero quickly within the thin EDL. An important parameter is the zeta potential, $\zeta$ , which is denoted as the electrokinetic potential at the interface of compact layer and diffuse layer.

Zeta potential is influenced by the environmental pH value, ionic strength of electrolyte solution, temperature and the concentration of some additives. Measurement of zeta potential has been realized by one of the three electrokinetic effects which are electroosmosis, electrophoresis and streaming potential. A fine particle's mobility is firstly determined experimentally in electrophoresis method and then zeta potential can be obtained by the Smoluchowski equation ( $\mu_{ep} = \varepsilon_0\varepsilon_r\zeta/\mu$ ). The streaming potential technique [27] utilizing pressure driven flow is good for flat channel surfaces, but is difficult to achieve accurate measurements. Electroosmotic flow is also found to be suitable to measure zeta potential and the only thing we need to determine is the electroosmotic velocity, which can be measured by some developed techniques, such as slope method by current-time monitoring [28], micro-particle image velocimetry (μPIV), advanced electroacoustic technique and so on. Once the electroosmotic velocity is known, the electroosmotic mobility can be determined and zeta potential can be calculated accordingly by the equation of $\mu_{eo} = -\varepsilon_0\varepsilon_r\zeta/\mu$ . The basic knowledge on electrokinetic phenomena has been well documented in classical reference books by Hunter [25], Masliyah [29] or Tabeling [30]. Electroosmotic flow and electrophoresis phenomena involved in electrokinetic microfluidics will be reviewed in the following sections.

## 2.2 Fluid flow and mass transfer in microscale

### 2.2.1 Microflow and its control

The flow in microchannels can be facilitated by several different ways, namely, applied electrical potential, external pressure difference, surface tension, gravity, etc. Driven by electrical forces and pressure difference respectively, electrokinetic flow and pressure driven flow are commonly used as pumping methods in lab-on-a-chip devices [31-35], however, electroosmotic flow, where an applied electrical field induces flow motion, is preferred over pressure driven flow because of the degree of flow-rate control it allows, and the characteristic plug-like velocity profile it produces [36].

For the EOF in microchannels, once an applied electrical field is employed through the microchannel, net charges in the EDL will move forward due to the electrical force exerted on them, which will then create motion of the fluid near the wall and transfer via viscous forces into convective motion of bulk fluid. Since the driving force is uniformly distributed along the thin EDL adjacent to microchannel wall, there is no pressure drop and flow is nearly uniform throughout, which will produce a plug-like or flat electroosmotic velocity profile as shown in Figure 2-2.

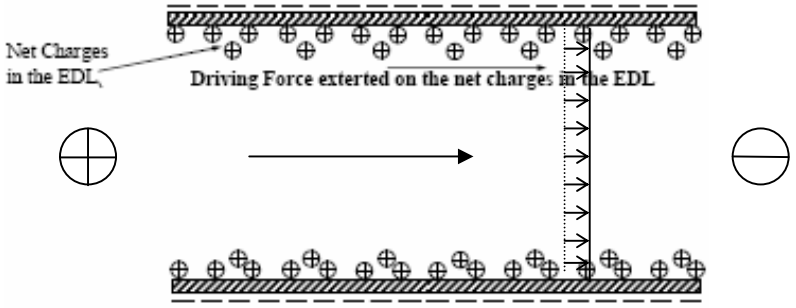


**Figure 2-2** Electroosmotic flow with plug-like velocity profile in microchannel.

There is almost no velocity gradient in the cross-section direction except for the thin EDL, which will make the Taylor dispersion effect [37] very small and the slip-wall velocity boundary assumption reasonable. The electroosmotic velocity can be simulated by the electroosmotic mobility and local applied electrical field strength,

$v_{eo} = \mu_{eo} E = (-\varepsilon_0 \varepsilon_r \zeta / \mu) E$ , which can be derived by the momentum equation and Poisson equation [25]. This feature will also avoid the irregular sample plugs produced by pressure driven flow, which has the so-called no-slip velocity boundary condition at wall and exhibits a parabolic velocity profile under the influence of pressure and viscous force. In addition, electrokinetic flow is easy to control by adjusting applied voltages on embedded electrodes and also convenient to be coupled with other on-chip electronic applications. As a result, electroosmotic flow is often employed as sample introduction method in many chemical and biomedical applications.

Control of electrokinetic flow is critically important to run successful sample handling in microfluidic chip. There are many effects to influence the EOF in microchannels. The applied electrical field is the primary way to control electrokinetic flow, but it is limited by Joule heating because most fluid properties (like viscosity, permittivity, conductivity, etc) are sensitive to environmental temperature. Another important role is from zeta potential, which is influenced by a group of factors including pH values, ionic strength concentration of buffer solution, temperature, wall properties, surfactant additive and so on. Instability of external pressure field like hydraulic pressure and Laplace pressure by surface tension will also cause dramatic changes to electrokinetic flows.

### 2.2.2 Thermal and pressure effect

**Joule heating**

Thermal effect results from the inevitable volumetric Joule heating when the conducting electrolyte is driven under an applied electrical field. The power generation may exceed heat dissipation that is restrained by the wall and both ends of microchannel. Consequently, elevated temperature with local gradient occurs in the buffer solution and surrounding material, which is not anticipated in most microfluidic chip applications. The Joule heating effect in electrokinetic flow has been reviewed by Xuan [38] in terms of material properties, influences on flow and entire microfluidic chip, and applications utilizing Joule heating. The magnitude of Joule heating is determined by many different effects, such as the applied potential field strength, buffer solution properties, chip

materials, etc. Tang et al [39] investigated the influences from the concentration of buffer solution and chip material. Under the applied potential field strength of 60kV/m, the temperature of a dilute $NaHCO_3$ (0.1mM) solution based on PDMS/glass chip almost didn't change (room temperature, 25$^o$C). However, the corresponding temperature for the same solution with a higher concentration of 50mM went to 45$^o$C, and another increment of 20$^o$C applied for PDMS/PDMS chip. The thermal conductivity of PDMS is only one-tenth of that for glass.

Some properties of buffer solution, such as permittivity, viscosity, electrical conductivity and pH value, are dependent on temperature, which will in turn influence the electrokinetic flow. For example, the non-uniform applied potential field strength within microchannel will appear due to discontinuous electrolyte's electric conductivity which is temperature relevant. The desired plug-like velocity profile is replaced by a velocity field of concave shape near the channel ends and convex shape in the middle channel [40]. Temperature deviation will also affect species transport processes because their diffusion coefficients are influenced by temperature according to Einstein's relation. Tang et al [39] found that Joule heating effect would not only speed up the transport of samples, but also increase the dispersion. Velocity distortion might cause the sample plug distortion in electrophoretic separations. In addition, the analytes or bio-samples themselves are also sensitive to temperature. More importantly, too much heat will increase the temperature and generate bubbles in the microchannel, which will produce two-phase flow and even terminate the electric current.

Naturally, the high surface to volume ratio of microchannel produces stronger heat dissipation capability than conventional macrochannel. However, effective controls should also been taken to avoid the negative consequences associated with Joule heating. Actively, different cooling systems can be employed to assist heat dissipation, such as mechanical fan with forced air convection or liquid coolant cycling to minimize heat accumulation. Passively, one appropriate buffer solution and chip material with high thermal conductivity should be adopted. Low applied potential field strength and short running time is also helpful to minimize the Joule heating. In our simulation, the average applied potential field strength is only about $12.5kV/m$ and the maximum injection time

is less than 30 seconds. Therefore, the assumption of constant room temperature (25°C) with negligible Joule heating is reasonable.

**Hydrostatic and Laplace pressure**

In electrokinetic flow, some unpredictable pressure effects may cause the flow field deviation and influence subsequent species transport process [41]. The pressure effects in microfluidic applications mainly come from three aspects, hydrostatic pressure, induced pressure and meniscus Laplace pressure.

Hydrostatic pressure is generated by the height difference of buffer level through the continuous fluid flow from injection reservoir to waste reservoir, but its magnitude is found to be very small compared to Laplace pressure [42]. Moreover, the effect of hydrostatic pressure can be minimized by utilizing large reservoirs and periodical buffer supply to the injection reservoir. In one of our applications, the electroosmotic velocity is about 0.56mm/s under the applied electrical field strength of 12.5kV/m in the horizontal straight channel (l/w/d : 8mm/50$\mu$m/20$\mu$m). A pressure difference of 134Pa is required to produce the same velocity and corresponding buffer height difference will have to be 13.7mm, which is remarkable during experiments. As for the induced pressure near the cross-channel corners, it has been identified negligible (in the order of $10^{-2}$Pa).

Surface tension happens in the interface of buffer solution and air in reservoirs and the surface curvature is changing dynamically during the whole operation. Although a same reservoir will be applied in all channel ends, the surface tension forces will be different except for the initial stage. To balance those forces, Laplace pressure is generated at the curvature interface of buffer and air. The magnitude of Laplace pressure for a spherical meniscus can be estimated by

$$\Delta P = \frac{2\gamma}{r} = \frac{2\gamma \cdot \cos\theta}{R} \qquad [2\text{-}5]$$

where, $\gamma$ is the surface tension value (water-air at 25°C: $71.97\times10^{-3}\,N/m$). The radius of the curvature $r$ can be estimated by reservoir radius $R\,(10^{-3}\,m)$ and contact angle of liquid-solid $\theta$ (water-glass: $0^o$). Based on the typical values chosen above, the

corresponding Laplace pressure is found to be 144Pa. It means that this meniscus Laplace pressure will produce an electroosmotic velocity of 0.60mm/s in the same horizontal microchannel. In practice, we will try to minimize the surface tension forces and the noticeable Laplace pressure by employing large reservoirs and reasonable electrodes alignments. A shallow microchannel design will also help to minimize the flow deviation caused by pressure effects, either Laplace pressure or hydrostatic pressure.

### 2.2.3 Species transport process

Microfluidic chips have been developed as total analysis systems for chemical, biological and biomedical applications. For those various on-chip applications, some species transport processes have to be studied, such as sample mixing [43-45], focusing [46], switching [47], loading [48], dispensing [49], etc. Among them, capillary elecrophoretic separation has been extensively studied and applied in practical separation analysis, especially after it was introduced to be run in microfluidic chips in early 1990s. DNA sequencing is one of the most popular applications of capillary electrophoresis [11]. The labeled DNA fragments with buffer solution will be pumped into a separation channel and they will move at different actual velocities due to various electrophorrtic mobilities. Detector mounted in the separation channel end will record and recognize the nucleotides (A, T, C or G). The basic separation mechanism and those influencing effects should be well understood and investigated for advanced design and control.

**Electrophoretic migration**

Motion of charged particles induced by the applied potential field is called electrophoresis. Based on the colloid and interface science, small chemical particles and biological species are usually charged when immersed into an aqueous solution. The EDL and zeta potential will also appear in the interface of solid and electrolyte solutions. Under the external applied electric field, those charged particles or species will have an effect of electrophoretic migration. Their mobility and velocity difference will cause the separation process of mixed particles or species. The individual migration rate of a

certain particle or species results from its own electrophoretic mobility and the applied electric field strength.

$$v_{epi} = \mu_{epi} E \qquad [2\text{-}6]$$

The magnitude of species's electrophoretic mobility is normally denoted as the charge over mass ratio and it can be approximated by Nernst-Einstein relation, $\mu_{epi} = z_i F D_i / RT$ [29]. In microfluidics, the flow is usually laminar with pretty low Reynolds number and the assumption of Stokes flow can be applied. The electrical forces exerted on the charged particles will be balanced by the Stokes frictional force. For an ideal spherical particle with a radius of $a$, this relationship will be expressed by,

$$ElectricalDrivingForce = StokesFricationalForce$$

$$Q_i E = 6\pi a_i \mu v_{epi} \qquad [2\text{-}7]$$

As a result, the electrophoretic velocity and electrophoretic mobility will be,

$$v_{epi} = \mu_{epi} E = \frac{Q_i}{6\pi a_i \mu} E \qquad [2\text{-}8]$$

If the density of species was constant, the mass of particle can be replaced by its size. The above electrophoretic mobility is consistent with its physical meaning of charge over mass ratio. The species' diffusion coefficient is determined by the Einstein-Stokes equation, $D_i = K_b T / 6\pi a_i \mu$ . Using this relationship as a bridge, the expression of electrophoretic mobility in equation [2-8] is same to the approximation by Nernst-Einstein relation.

Although we have had a spherical assumption with radius ($a_i$), there is still a problem to determine the net charges ($Q_i$) in order to obtain the analytical electrophoretic mobility. In two limit conditions, the electrophoretic mobility can be achieved theoretically. As shown in Figure 2-3, one is the small particle with big Debye-Huckel length ($\kappa a << 1$) and another one is the big particle with small Debye-Hunkel length ($\kappa a >> 1$). For the case of $\kappa a << 1$, the net charges can be solved using the Poisson-Boltzmann equation.

$$Q_i = 4\pi\varepsilon_0 \varepsilon_r a_i \zeta \qquad [2\text{-}9]$$

And corresponding electrophoretic mobility is,

$$\mu_{epi} = \frac{2\varepsilon_0 \varepsilon_r \zeta}{3\mu} \qquad [2\text{-}10]$$

For a big $\kappa a >> 1$, the EDL is extremely thin compared to the particle size. Thus, we can neglect the curvature effect and consider the relative movement of ions with respect to a planar surface. i.e., the electrophoretic motion can be reverted to the EOF in a long straight microchannel. The magnitude of electrophoretic mobility will be same to the electoosmotic mobility determined by Helmholtz–Smoluchowski equation. However, the sign will be different because of the reverse direction they move.

$$\mu_{epi} = \frac{\varepsilon_0 \varepsilon_r \zeta}{\mu} \qquad [2\text{-}11]$$

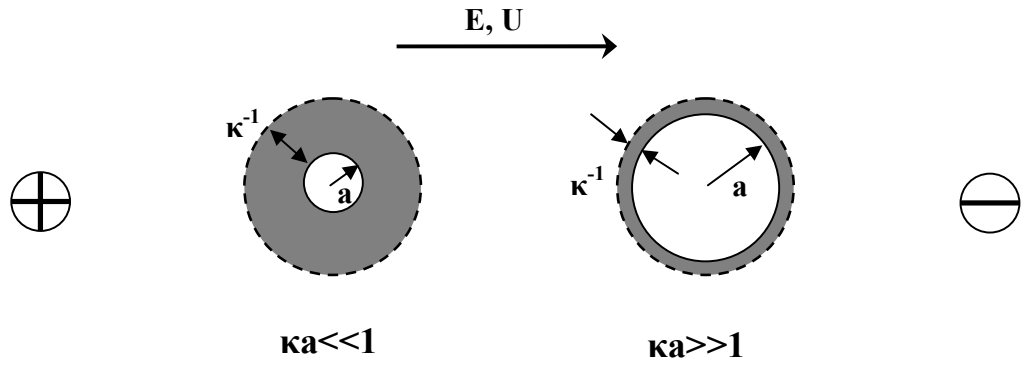


**Figure 2-3** A schematic diagram of electrophoresis of a spherical particle in two limits: $\kappa^{-1}a<<1$ and $\kappa^{-1}a>>1$.

Actually, particles are not like the two limit cases discussed above. Henry [50] presented a correlation to simulate the electrophoretic mobility, where a correction function of the parameter $\kappa a$ is added. Certain assumptions were made in his derivation. For example, it is applicable for low surface potentials and the relaxation effect of particle was ignored.

$$\mu_{epi} = \frac{2\varepsilon_0 \varepsilon_r \zeta}{3\mu} f(\kappa a_i) \qquad [2\text{-}12]$$

where $f(\kappa a_i) = 1.5 - \frac{1}{2[1 + 0.072(\kappa a_i)^{1.13}]}$ and the $\kappa a_i$ is in the whole range ($0 \sim \infty$).

**Diffusion related effects**

The diffusion effect usually becomes non-negligible for small chemical or biological fragments. As a spontaneous and thermodynamically favourable process, species' diffusion effect due to the concentration difference has to be considered in microscale transport phenomena. Based on Fick's law, the diffusing flux is a product of species' diffusion coefficient and concentration gradient. The diffusion coefficient is approximated by Einstein–Smoluchowski relation and later by Einstein-Stokes relation for particles in low Reynolds number flow. Its magnitude is found to be proportional to absolute temperature and has an inverse relation of medium viscosity and particle size. The diffusion coefficient of common biological species like DNA fragments and proteins is estimated to be in the range of $10^{-9} \sim 10^{-11} m^2 / s$. In our on-chip species injection and separation processes, the diffusion-dispersion effect will be obvious at the interfaces of sample plug and pure buffer solution due to the local high concentration gradient. Therefore, diffusion effect will account for the band broadening problem during the sepration process.

In the EOF with plug-like velocity profile, the diffusive forces will cause the sample plug broadening only in the flow direction. Once a velocity gradient occurs in the cross-stream direction like the parabolic velocity profile in pressure driven flow, the Taylor dispersion [51] will happen with increased diffusion especially at high Peclet number flow. The shear flow is found to increase the effective diffusivity of species and enhance the spread rate dramatically, which is not anticipated in our electrophoretic separation. Besides the easiness and convenience for control, lowering or even avoiding the Taylor dispersion is another advantage of employing electrokinetic flow other than pressure driven flow.

According to the particle theory, Brownian motion is the random movement of particles suspended in a liquid. Due to the instantaneous imbalance in the collision forces exerted by the small liquid molecules on the particle, Brownian motion is a temperature-dependant stochastic process and is very difficult to control. However, the Brownian displacements are proved to be very small compared to electrophoretic motion by Oddy [52]. Through investigating the effects on micro-PIV measurement, Santiago [53] found

that Brownian motion of small seed-particle (sub-micron) in low speed flow (less than $10\,\mu m/s$) would introduce considerable error into velocity measurements. In our application, the combined movement of a large number of species is different to the seed-particle in micro-PIV measurement and the flow speed is super high as $0.56mm/s$. As a result, Brownian motion effect is considered as negligible, especially for the environment with a constant room temperature.

## 2.3 Specific on-chip applications of electrokinetic flow

### 2.3.1 Microfabrication and microchannel surface patterns

The flow in microfluidic devices is laminar characterized by a low Reynolds number, which allows multiple streams flowing next to each other without turbulent mixing. Chemical reactions in such flow regimes only occur either between the adjacent streams and the interior surface of microchannel, or at the interface between the streams. Such a laminar flow feature opens up the ways for surface patterning [54] and microfabrication of the desired structures inside capillaries or enclosed spaces [55-57].

For example, by pumping different patterning components into a microchannel, the cells on channel surface can be selectively patterned by different medium. Kane et al. [54] has successfully used laminar flow patterning technique to pattern bovine capillary endothelial (BCE) cells in a network of capillaries. In their experiments, different solutions were pumped into three channels which converged into a main channel. BCE cells were pre-deposited on the bottom surface of capillary network, and only the cells on which the solution with a fluorescent dye was allowed to flow were stained. In this application, fluid flows must be well controlled in order to selectively pattern the cells.

Kenis et al. [55] applied multi-stream laminar flow to fabricate a three-electrode system inside a microchannel with a width of 200 microns. Firstly, a two-electrode system (working and counter electrodes) was generated by flowing three streams of different solutions (one gold etchant with two flanking streams of water) from three inlets of microchannels converging into the main channel, where gold strip was deposited. Secondly, the reference silver electrode was fabricated at the interface of a two-stream

laminar flow containing components of electroless silver plating solution. Microfabrication inside the capillaries using multi-stream laminar flow avoids the use of multiple photolithography processes and allows a wider range of chemistries in patterning. During these kinds of fabrications, control of flow streams is the key since it will determine the spatial resolution and precision of fabricated electrodes which have great influences on electrochemical reactions [58] involved heavily in lab-on-a-chip applications.

Zhao et al. [57] presented a method to fabricate pressure-sensitive switches inside microchannels through patterning their surface free energies to achieve liquid flow directed by surface tension. In their study, multi-stream laminar flow and self-assembled monolayer chemistry are combined to pattern surface free energies inside a microchannel network and the control of flow streams is very important for the resolution of hydrophilic pathways which are the channels allowing liquid to flow after patterning.

It can be seen that, multi-stream laminar flow is a promising method for in situ fabrication, surface patterning and on-chip cell culturing. The success of this method lies in the effective control of multiple flow streams. The above experimental studies focus on the exploration of different applications of multi-stream laminar flow in microfluidics. So far, little has been reported regarding the development of analysis tools providing optimized configurations for multi-stream flow control in such miniaturized systems.

### 2.3.2 Microwashing with replaced solutions for sample preparation

To date, most studies on microfluidic chips have focused on the analysis of simple and pre-purified biological samples, such as Oligonucleotides [59], DNA [60, 61], RNA [62, 63] and single cell analysis [10, 64]. The major challenge to achieve the concept of lab-on-a-chip lies on the integration of sample preparation processes starting from real-world samples (like blood drops) obtained in clinical labs. Preparation of biomedical samples for DNA, RNA or protein analysis tends to be complex. Generally speaking, three major steps must be followed [65]: cell separation through fluorescence- [66] or magnetic- [67] activated cell sorting; cell lysis using chemical [68, 69], thermal [70], electrical [71] and

recently mechanical methods [72]; and molecular extraction and purification by gel electrophoresis [73, 74] or capillary electrophoresis [14, 75, 76].

Most of these sample preparation processes involve multiple washing procedures where one solution is designed to displace another different solution in a controlled manner [7, 77, 78]. For example, the sample preparation for DNA analysis reported by Taylor *et al* [79] involves the following procedures: the white blood cells extracted from a sample of whole blood through a filter, were first washed with an aqueous buffer solution using an optimized washing scheme; then 200 μl elution buffer was used to displace the wash buffer, and following ultrasonic cell lysis, additional buffer solution was used to wash the white blood cells' lysate in order to finally obtain the pure DNA samples. The automatic and precise control of washing procedures which involve one solution displacing another solution becomes extremely important for integration of sample preparation processes with the total analysis system. Therefore, it is crucial to gain a better understanding of the fundamental transport phenomena of on-chip solution displacement processes.

Electrokinetic flow is normally preferred than pressure driven flow due to its remarkable features. Most studies of EOF so far have focused on the flow of a uniform solution [80-87]. However in many practical applications, electroosmotic flow with displacement between different solutions is often encountered as mentioned above. In such a displacement process, if the two solutions are very different in terms of ionic type, valence and concentration, the zeta potential, which depends on the pair of solid-liquid interface and the electrical potential field in EDL, will vary along the channel length. The driving forces exerted on the net charges in EDL by the externally applied electrical field will be different at different locations, which will bring non-uniformity into the flow field and will induce pressure driven flows as well.

Deviations of plug-like electroosmotic flow due to the presence of surface heterogeneity have been studied extensively both theoretically [88-91] and experimentally [92-94]. Whereas, the non-uniform flow field induced by solution displacement in microchannels, where non-uniform surface potential will vary with time, has received little attention. Solution displacement between two similar solutions with the

same chemical composites and a slight concentration difference has been used to measure electroosmotic velocity in microchannels [95, 96] and nanochannels [97]. Ren *et al* [95] also reported a 1-D numerical model and their experimental results agree with the numerical model reasonable well. However, displacement process between two different solutions will be much more complicated than that between two similar solutions and therefore related studies on electrokinetic flow with various replaced solutions were chosen to be performed.

### 2.3.3 On-chip injection and separation analysis

Electrophoretic separation for DNA and/or protein samples is one of the key processes in achieving micro total analysis. Gel electrophoresis has been commonly used for such applications, however, this method is time consuming due to manually loading gels and also has a few other disadvantages like excessive Joule heat generation. Since Harrison et al. [20] introduced the concept of on-chip electrophoresis separation, many have followed including both experimental and numerical studies, such as different chip designs, various sample injection schemes, multi-channel microchip development for high throughput and efficiency analysis, etc. Normally, microchip capillary electrophoresis includes two steps which are the loading and dispensing process conducted on a perpendicularly cross-linked microchannel. By altering applied source fields in the reservoirs (pressure or electrical), the buffer solution and samples can be manipulated into different flow directions, which serves to perform on-chip sample handling tasks successfully. Due to its remarkable features like the easy controllable flow-rate and characteristic plug-like velocity profile, electroosmotic flow is often employed to pump buffer solutions and drive samples in most microfluidic applications.

There have been a number of studies on chip-based electrokinetic sample loading and dispensing which examine different concerns. For example, extensive experimental studies were performed to develop microfluidic devices with advanced injection schemes and high efficiency separation in Ramsey's group [45, 46, 98]. Different design features were realized and tested with chemical and biological samples. In addition, the same group has also investigated microchip electrophoretic separation under reduced gravity

and hypergravity conditions which would be experienced in space-based platforms [99]. Sinton et al. [100] proposed a dynamic loading method to control the loaded sample size and inject a wide and highly-concentrated sample plug. There are some other experimental studies [17, 101, 102] focusing on the integration of multi-channel microfluidic chips for DNA sequencing separation where a cross-linked microchannel was used as a basic injection and separation component.

A couple of numerical studies have also been performed to investigate the species transport process for on-chip analysis. Patankar and Hu [103] reported a three-dimensional model studying the flow field in a cross-linked microchannel. In this study, they thoroughly discussed the effects of different parameters on the flow pattern in the intersection based on a non-dimensionalized numerical model and found that the sample plug can be affected by applied potentials and pressure gradients. Ermakov et al. [104] investigated sample focusing and mixing based on various channel geometries and good agreement between numerical and experimental results were achieved. The same group [105] also proposed and numerically studied two different injection methods, pinched and gated injection methods.

Based on the Guoy-Chapman approximation, Bianchi [106] numerically studied the influences of various parameters, such as the zeta potential distribution, Reynolds number and relative channel widths, on the flow distribution. Mohammadi [107] presented a numerical model combining state control and shape optimization techniques, which was proposed for a microfluidic device, aimed at extracting a small amount of sample with minimal band dispersion and with separate species present in the band. Ren et al. [49, 108] studied the loading and dispensing processes on a conventional cross channel by investigating the effects of applied potential, electroosmotic mobility, solution conductivity, diffusion coefficient and channel geometry, on the loaded and dispensed samples. Artificial boundaries were employed to truncate the physical domain into a small computational domain containing the intersection where 2-D phenomena exist. This method concentrates computation power on the small domain aiming to improve numerical simulation accuracy while considering a practical injection and separation microfluidic chip with a long separation channel.

Lee et al. [109] reported a method to improve electrokinetic separation performance through controlling surface wall properties by embedding electrodes close to the channel walls. Turn-induced dispersions can be controlled by altering the zeta potentials of a U-shape separation channel, which can correct the band tilting phenomena and reduce the race-track effect. Yang et al. [47] developed an effective model for flow control analysis, and their numerical results agreed well with their experimental findings. Fu et al. [110] developed a multi-T-form injection system which can successfully guide multiple samples to desired outlet ports. The multi-T injection scheme was also employed by Tsai et al. [111] to minimize the sample leakage effect and enhance separation and detection performance.

Most studies focused on the control of fluid flow and the injected sample plug in the channel intersection. The species transport characteristics and effects of sample proprieties on injection/separation processes have been seldom covered and revealed numerically and experimentally. A thorough understanding of them will definitely offer help to effective controls and innovative designs. Also, less attention has been paid to the effects of the controlling parameters on the separation resolution through non-dimensional parametric studies which can be used to develop an optimized design for certain separation resolution in terms of the channel dimensions, buffer solutions, and applied potentials.

## 2.4 Research methods

Electrokinetic flow and microscale transport phenomena for on-chip chemical, biological and biomedical analysis have been studied numerically and experimentally. Many experimental studies have been reported with different research concerns, such as design of integrated multi-channel chip [112], advanced microfluidic devices [14] and detection techniques development [51], various on-chip analyses with chemical and biological samples [17], etc. Most of them rely on experienced design or expensive trial and error experiments.

Just for the multi-channel DNA sequencing chip, many designs have been proposed and studied experimentally with real DNA fragments as reviewed by Gao in 2001 [113].

After that, designs with more integrated channels in one chip were proposed to achieve high efficiency and high throughput separation. Recently, another two capillary array electrophoresis (CAE) microchips with 384 and 768 channels were introduced by Tian *et al* [102] and Aborn *et al* [114] respectively. With the development of fabrication technology, the analysis capability of one single microfluidic chip becomes extremely strong. In general, most of them have a similar radial channel layout. Although some proposed new design features like different injectors and folded separation channel, the bottleneck is the lack of thorough understanding of fluid flow and mass transport phenomena in microchannel networks. The complete analysis model and effective design tool will be pretty useful and necessary prior to the expensive experimental work.

Related theoretical studies should be performed to provide valuable ideas and guidelines. Numerical simulations allow parametric studies in an easier and cost-effective manner, which can shorten the time period for developing a new chip and provide insight into the physics behind the phenomena. By offering useful prediction and direction, numerical studies have been shown to be an excellent alternative to experimental studies in microfluidics [115]. Some different models have been developed for various applications (focusing, mixing, cell sorting, loading, etc) with a couple of controllable parameters (applied potential, channel geometry, pressure effects, zeta potential, etc). Different numerical schemes of finite difference, finite element and finite control volume method have been adopted. Although some effects have been investigated more or less in some specific applications, fundamental studies are still required to be performed for comprehensive understandings.

Rather than the expensive and time-consuming experiments, numerical studies are the focus of current study. The reported work mentioned above will definitely offer valuable advice and help. Comparison with previous studies will lead to a deeper understanding and better control. For example, the experimental work provides us an intuitive insight to the application of our theoretical study. The basic knowledge and related results achieved from the published numerical work will offer help to construct the complete model and determine the parameters and their range to be studied.

# Chapter 3

# Control of Laminar Flow and Mass Transport for Microfabrication

Tremendous interests have been drawn into developing micro technologies towards the integration and automation of biochips or lab-on-a-chip devices due to their wide applications in environmental, chemical and biomedical engineering fields. The laminar flow nature in microfluidic devices offers opportunities to fabricate the desired structures and pattern culturing medium inside microchannels. However, no analysis tools are available to provide optimized configurations to control the flows for those applications. Therefore the motivation of this study is to develop a numerical model to study the transport phenomena in a cross-linked microchannels aiming to explore an optimized configuration for the microfabrication of specific desired features inside microchannel networks. Electroosmotic flow with induced pressure field is employed and the model consists of a set of equations describing the applied potential field, flow field and concentration field. Effects of various operational parameters on multi-stream flow are investigated based on the simultaneous solution to theoretical model.

## 3.1 On-chip cross-linked microchannel network

Here, we consider the cross-linked microchannels as shown in Figure 3-1. The microchannel depth and width are assumed to be 20 μm and 100 μm, respectively. Channel 1, 2 and 3 are chosen as same as 4 mm and channel 4 is 8 mm. There are four reservoirs connected to the four ends of microchannels. Electrodes are inserted into these reservoirs to set up the applied electrical field across the whole channel network. When the chosen electrical potentials are applied to four reservoirs, solutions in reservoir 1, 2 and 3 will be driven to flow passing the intersection and converging into the channel downstream towards reservoir 4. For the following on-chip injection and sepration

studies, where species dissolved in buffer solution are firstly loaded into the intersection and then dispensed into the perpendicular channel for further separation analysis, sample transport during those two different processes is the focus. However in this study, control of the width of flow streams and the width of their interfaces is the goal, which will be achieved through varying the controlling parameters. Therefore, without losing generality, an electroosmotic mobility for fluid in microchannels is assumed to be $4.5\times10^{-8}\ m^2/(V\cdot s)$ which is close to commonly used buffer solutions and chemical etchants [116], and the diffusion coefficient of solution is assumed to be $1.0\times10^{-10}\ m^2/s$, except stated otherwise.

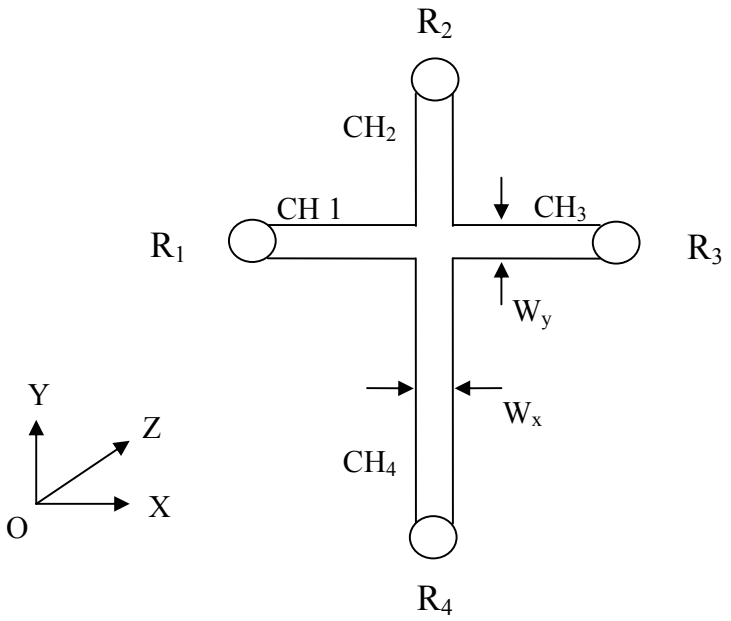


**Figure 3-1** Illustration of the chip configuration and coordinates employed.

## 3.2 Theoretical model and simulation

**Electrical field**

A thin electrical double layer and no net charge density are considered in the bulk liquid. According to the theory of electrostatics, the applied electrical potential, $\phi$, can be described by

$$\vec{\nabla} \cdot \left( \lambda \vec{\nabla} \phi \right) = 0 \qquad [3\text{-}1]$$

where, $\lambda$ is electrical conductivity of solution. If different buffer solutions are applied in the microchannels, the applied potential field will exhibit a non-uniform distribution. The effect of solution electrical conductivity will be investigated in the following project of replaced solutions. Here, a same buffer solution is utilized and we can neglect the solution electrical conductivity difference, which is true for many practical applications. This choice simplifies equation [3-1] to Laplace's equation.

$$\nabla^2 \phi = 0 \qquad [3\text{-}2]$$

The numerical model presented in this work takes the assumption of two-dimensionality (in the plane of the chip) commonly employed in modeling similar processes [49, 104, 105]. It is assumed that the dependent variables do not exhibit significant gradients in the third, thickness dimension. Through comparing two- and three-dimensional models, Patankar et al. [103] showed this assumption to be reasonable for EOFs in similar cross microchannels, in which variables in the x- and y- dimension are more important. Therefore, equation [3-2] can be rewritten as,

$$\frac{\partial^2 \phi}{\partial x^2} + \frac{\partial^2 \phi}{\partial y^2} = 0 \qquad [3\text{-}3]$$

Introducing non-dimensional parameters,

$$\Phi = \frac{\phi}{\phi_{ref}}, \qquad X = \frac{x}{w}, \qquad Y = \frac{y}{w}$$

where $\phi_{ref}$ is a reference electrical potential and $w$ is the microchannel width. Equation [3-3] can be non-dimensionalized as,

$$\frac{\partial^2 \Phi}{\partial X^2} + \frac{\partial^2 \Phi}{\partial Y^2} = 0 \qquad [3\text{-}4]$$

The associated wall boundary conditions are:

$$\frac{\partial \Phi}{\partial n} = 0 \qquad [3\text{-}4a]$$

where $n$ represents the direction normal to the channel wall. Specific potential values are applied to all reservoirs,

$$\Phi\big|_{(R=1-4)} = \Phi_{applied}\big|_{(R=1-4)} \qquad [3\text{-}4b]$$

Once the applied electrical potential distribution is numerically solved in the whole channel network, the local electric field strength can be calculated by

$$\vec{E} = -\vec{\nabla}\phi \qquad [3\text{-}5]$$

**Flow field**

For incompressible liquid buffer solutions, the basic equations describing the flow field are the continuity equation,

$$\vec{\nabla} \cdot \vec{v} = 0 \qquad [3\text{-}6a]$$

and the momentum equation,

$$\rho\left[\frac{\partial \vec{v}}{\partial t} + \left(\vec{v} \cdot \vec{\nabla}\right)\vec{v}\right] = -\vec{\nabla}p + \mu\nabla^2\vec{v} + \rho_e\vec{E} \qquad [3\text{-}6b]$$

where $\vec{v}$ is the mass average velocity vector. In the electroosmotic flows, Reynolds number, $\mathrm{Re} = vw/\nu$, which gives the ratio between the inertial forces and the viscous forces, is very small (e.g. $\mathrm{Re} \le 0.1$). Hence, the left hand side of momentum equation [3-6b] can be neglected.

The driving force in electrokinetic flow is electrical force, $\rho_e\vec{E}$, which appears as the third term of the right hand side of momentum equation. It exists and is balanced by viscous forces only in the thin EDL. Coupled with the definition of EDL and induced zeta potential distribution, the velocity field is found to develop from zero on the wall to a maximum electroosmotic velocity at the interface of the EDL and bulk fluid flow. In the neutral bulk fluid zone of EOF, the electrical force is zero, as is the viscous force, and then the resulting flow field is uniform at the electroosmotic velocity.

As a result, the velocity is constant everywhere except in the region very close to the wall (i.e. within the EDL). However, it has been demonstrated that the thickness of EDL is negligible compared to the dimensions of microchannel cross-section. Rather than applying the electrical force directly in momentum equation, a slip wall velocity boundary condition is employed to reflect that. This assumption and arrangement has been identified reasonable and employed by other researchers. The slip wall velocity boundary is simulated by $\vec{V}_{wall} = \mu_{eo}\vec{E}$ and the electroosmotic mobility is assumed to be same through all the tests except indicated otherwise. Taking into account of the above considerations, equation [3-6] can be rewritten as,

$$\frac{\partial v_x}{\partial x} + \frac{\partial v_y}{\partial y} = 0 \qquad [3\text{-}7a]$$

$$-\frac{1}{\rho}\frac{\partial p}{\partial x} + \nu\left(\frac{\partial^2 v_x}{\partial x^2} + \frac{\partial^2 v_x}{\partial y^2}\right) = 0 \qquad [3\text{-}7b]$$

$$-\frac{1}{\rho}\frac{\partial p}{\partial y} + \nu\left(\frac{\partial^2 v_y}{\partial x^2} + \frac{\partial^2 v_y}{\partial y^2}\right) = 0 \qquad [3\text{-}7c]$$

Introducing the following non-dimensional parameters,

$$P = \frac{p - p_a}{\rho(\nu/w)^2}, \quad V_x = \frac{v_x \cdot w}{\nu}, \quad V_y = \frac{v_y \cdot w}{\nu}$$

Accordingly, equation [3-7] can be non-dimensionalized as,

$$\frac{\partial V_x}{\partial X} + \frac{\partial V_y}{\partial Y} = 0 \qquad [3\text{-}8a]$$

$$-\frac{\partial P}{\partial X} + \frac{\partial^2 V_x}{\partial X^2} + \frac{\partial^2 V_x}{\partial Y^2} = 0 \qquad [3\text{-}8b]$$

$$-\frac{\partial P}{\partial Y} + \frac{\partial^2 V_y}{\partial X^2} + \frac{\partial^2 V_y}{\partial Y^2} = 0 \qquad [3\text{-}8c]$$

Corresponding non-dimensional boundary conditions at reservoirs are

$$\left.\frac{\partial V_x}{\partial X}\right|_R = 0, V_y\big|_R = 0 \text{ for reservoirs 1, and 3} \qquad [3\text{-}9a]$$

$$\left.\frac{\partial V_y}{\partial Y}\right|_R = 0, V_x\big|_R = 0 \text{ for reservoirs 2 and 4} \qquad [3\text{-}9b]$$

$$P\big|_{(R=1-4)} = 0 \qquad [3\text{-}9c]$$

The slip velocity boundary conditions at the walls of microchannels are

$$V_x\big|_{wall} = \mu_{eo} E_x w/\nu \qquad [3\text{-}9d]$$

$$V_y\big|_{wall} = \mu_{eo} E_y w/\nu \qquad [3\text{-}9e]$$

**Concentration field**

In order to obtain the information about the widths of multiple streams and the widths of their interfaces, the solution concentration in each stream has to be found. The distribution of solution concentration can be described by the conservation law of mass, which takes the form of

$$\frac{\partial c_i}{\partial t} + v_x \cdot \frac{\partial c_i}{\partial x} + v_y \cdot \frac{\partial c_i}{\partial y} = D_i\left(\frac{\partial^2 c_i}{\partial x^2} + \frac{\partial^2 c_i}{\partial y^2}\right) \qquad [3\text{-}10]$$

where $c_i$ is the concentration of the $i-th$ stream and $D_i$ is the diffusion coefficient of the $i-th$ solution. In this work, we are interested in how to control the volume of each flow stream, which depends on the solution's electroosmotic mobility, diffusion coefficient, the applied electrical potential and the dimensions of microchannels. Introducing the non-dimensional parameters,

$$C_i = \frac{c_i}{c_{i\_0}}, \qquad \tau = \frac{t}{w^2/\nu}$$

where $c_{i\_0}$ is the original concentration for the $i-th$ solution, equation [3-10] can then be non-dimensionalized as,

$$\frac{\partial C_i}{\partial \tau} + V_x \frac{\partial C_i}{\partial X} + V_y \frac{\partial C_i}{\partial Y} = \frac{D_i}{\nu}\left( \frac{\partial^2 C_i}{\partial X^2} + \frac{\partial^2 C_i}{\partial Y^2} \right) \qquad [3\text{-}11]$$

Wall boundary conditions are,

$$\frac{\partial C_i}{\partial n} = 0 \qquad [3\text{-}12a]$$

For a three-stream flow scenario, there are three concentration fields to be calculated totally. For the solution flowing into the channel network from the $i-th$ reservoir, the boundary conditions in the reservoirs are specified as,

$$C\big|_{i\_Ri} = C_{i\_original} \qquad [3\text{-}12b]$$

$$C\big|_{i\_Rj(j\neq i, j\neq 4)} = 0 \qquad [3\text{-}12c]$$

For a two-stream flow scenario, two different solutions will be pumped into the intersection from reservoir 1 and 3 by applying potentials to these two reservoirs and leaving reservoir 2 floating and reservoir 4 grounded. The channel 2 will be filled with water. Therefore, there are two concentration fields to be calculated. For the solution flowing into the channel network from the $i-th$ reservoir, boundary conditions in the reservoirs are specified as,

$$C\big|_{i\_Ri\,(i=1\,or\,3)} = C_{i\_original} \qquad [3\text{-}13a]$$

$$C\big|_{i\_Rj(j\neq i, j\neq 4)} = 0 \qquad [3\text{-}13b]$$

The same outflow boundary condition is applied to the reservoir 4 for both three-steam and two-stream flows,

$$\left.\frac{\partial C_i}{\partial Y}\right|_{R4} = 0 \qquad [3\text{-}14]$$

The complete set of non-dimensional equations of [3-4], [3-8] and [3-11], were solved using the semi-implicit method for pressure linked equations (SIMPLE) algorithm developed by Patankar [86], which is based on a finite control volume discretization of the governing equations. In order to capture all the features near the four corners of

microchannel network, a non-uniform staggered grid system is employed. The control volume size next to the channel wall is the minimum. The size of successive control volumes away from the channel wall is increased by a factor of 1.1. In this implementation, the solution to this set of discretized equations is obtained by a line-by-line iterative procedure. This numerical scheme has been verified previously [51] by comparing with experimental studies.

### 3.3 Applied potential field and flow field with induced pressure field

Under the influence of applied electrical potentials in four reservoirs, an electrical field is set up across the microchannel network to pump the liquid flow. Therefore, the applied potentials play a key role in controlling the flows within the microchannels. Figure 3-2 shows the applied potential field over the entire chip and near the intersection for a typical case, where the non-dimensional applied electrical potentials at $R_1$, $R_2$ and $R_3$ are 1.0 and reservoir 4 is grounded. One can see that the applied potentials change linearly along the microchannel except near the intersection and the direction of potential drop indicates the direction of fluid flow in each channel. Because four reservoirs are open to atmosphere, no pressure differences are applied across the channels. However, cross-stream velocity gradients may arise due to the momentum interactions of the perpendicular EOFs and the pressure gradient is induced near the intersection to satisfy the continuity as shown in Figure 3-3(left). As implied by the applied potential field in Figure 3-2, three flow streams are expected to be pumped into the intersection and merge downstream towards reservoir 4. Figure 3-3(right) shows the flow field, and one can see that indeed under the applied potentials, three different streams from $R_1$, $R_2$, and $R_3$ converge into the channel 4.

### 3.4 Different influencing effects on three stream flow

There are numerous combinations of applied potentials that can generate different multi-stream flow patterns in the microchannel network, which in turn affect the resolution and precision of fabrication inside the channels. Figure 3-4(left) shows the concentration field

of the stream flowing from reservoir 2 to 4 in a three-stream flow system, where applied potentials for four reservoirs are 1.0, 1.4, 1.0, and 0 for $\Phi_1$~$\Phi_4$ respectively, (where $\Phi$ indicates normalized applied voltage and the subscripts correspond to reservoir number). The concentration decreases from white to black region (same for future description).

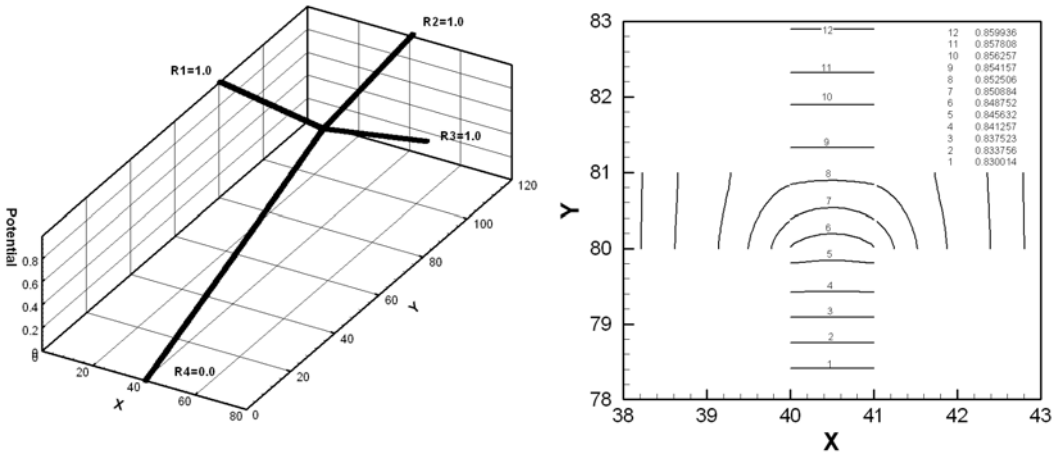


**Figure 3-2** Model predicted potential field for the entire chip (left) and the region near the intersection (right).

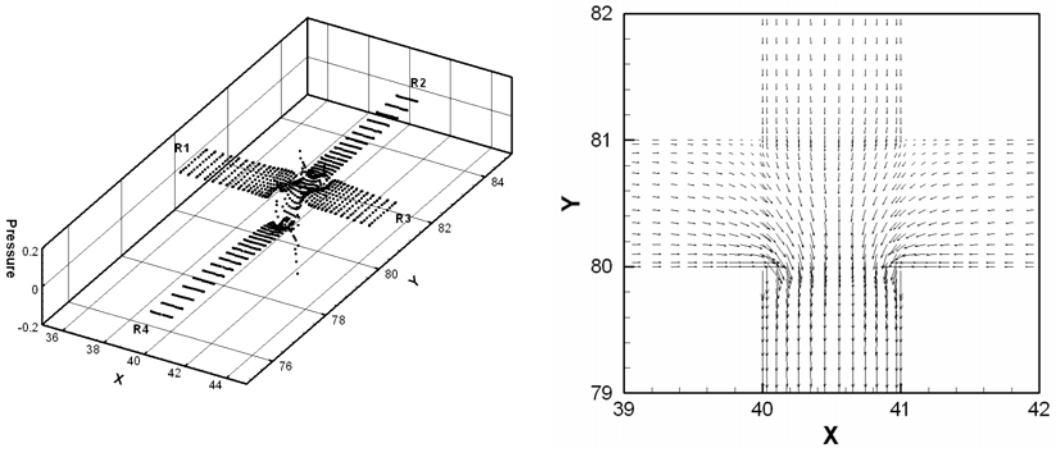


**Figure 3-3** Model predicted induced pressure field for the entire chip (left) and flow field near the intersection (right).

It can be seen that, the channel 4 is nearly completely filled with the solution from reservoir 2 and almost no flow coming into this stream from reservoir 1 and 3. This is

also seen from Figure 3-4(right), which shows the concentration profile cross the width of channel 4 at the location of two channel widths down from the intersection (Y=78). It indicates that the concentrations of solutions from reservoir 1 and 3 quickly drop to zero from the wall to the center of channel 4. If this set of potentials was applied to three-stream flows to fabricate a three-electrode system, no working and counter electrodes can be fabricated since the etchant from reservoir 2 completely will remove the deposited gold substrate in channel 4. Therefore, the optimized configuration for particular applications must be explored through extensive numerical simulations using the developed model in order to provide guidance for expensive trial-and-error experiments.

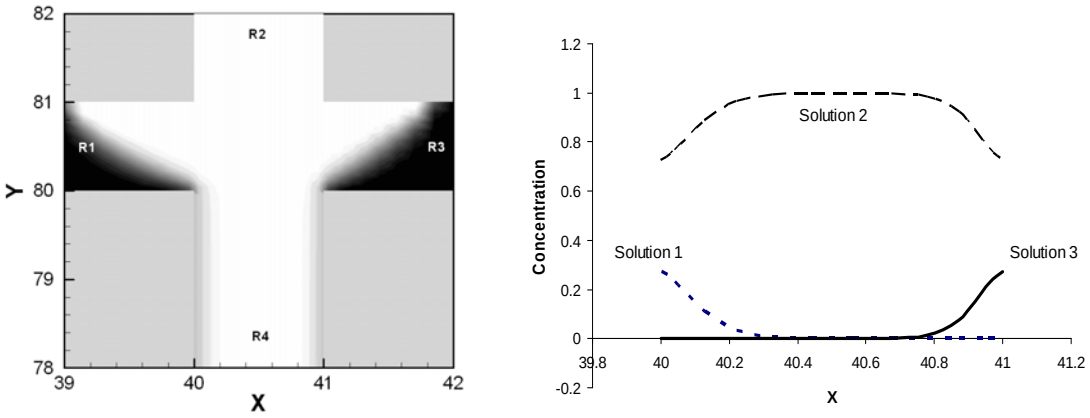


**Figure 3-4** Iso-concentration contour (left) and concentration profile (right) of three solutions at the location of Y=78, of a typical case with the less-focused main stream.

Figure 3-5(top) displays a controlled three-stream flow where the applied potentials for $\Phi_1$~$\Phi_4$ are 1.0, 1.0, 1.0, 0. One can see that three laminar flows move smoothly side by side in channel 4 and the concentration decreases from white to dark for each solution. Figure 3-5(bottom) shows the concentration profiles for each solution in a specific location downstream the channel 4 (Y = 78), which more clearly indicates the interfaces between three streams. Depending on the specific application, an optimized combination of applied potentials can be explored to achieve the desired three-stream laminar flows. In addition, from the middle stream's concentration for three different grid systems, the scheme of 12 control volumes is found the best and then applied in all simulations.

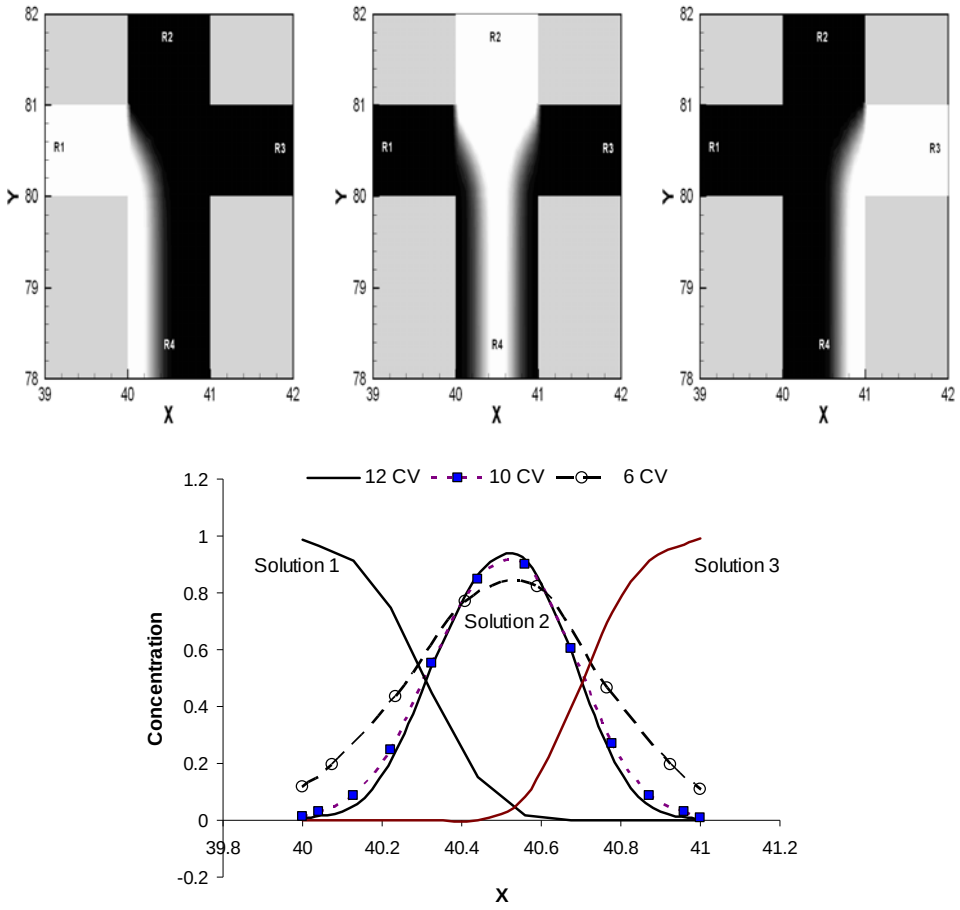


**Figure 3-5** Iso-concentration contour (top) for three solutions flowing from reservoir 1, 2 and 3; concentration profile (bottom) for three solutions at the location of Y=78.

As reported by Ren and Li [49], the ratio of channel widths has significant effects on EOF in cross-linked microchannels, which may provide more controls to multi-stream laminar flows. If we define $w_x$ as the width of vertical channel and $w_y$ as the width of horizontal channel as illustrated in Figure 3-1, under the same applied potentials of 1.0, 1.0, 1.0 and 0 for $\Phi_1$~$\Phi_4$, the shape of middle stream flow is different between the case of $w_x/w_y = 1$ and the case of $w_x/w_y = 1/2.3$ as shown in the left two figures of Figure 3-6. The ratio of $1/2.3$ is chosen for convenience of grid generation. With a wider channel size in horizontal channels, the side-wing flows from reservoir 1 and 3 are stronger than that with uniform channel size, which focuses the middle-stream flow near the

intersection and downstream channel 4. However, the width of middle-stream flow can also be controlled by altering the applied potentials in reservoir 1 and 3. As validated in the right two figures of Figure 3-6 with the same channel dimension of $w_x/w_y = 1/2.3$, when the applied potential is changed from 1.0/1.0/1.0/0.0 to 0.8/1.0/0.8/0 for $\Phi_1$~$\Phi_4$, the middle-stream is less focused.

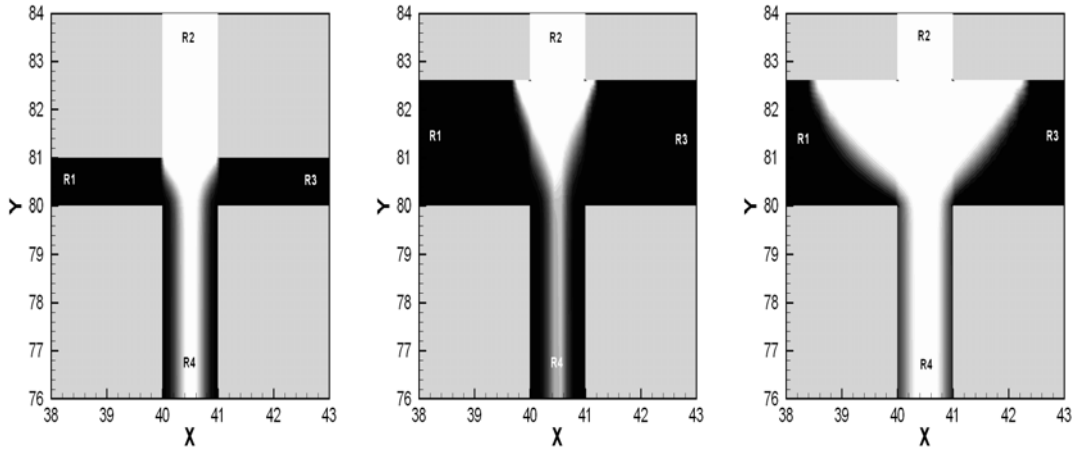


| | | |
|---|---|---|
| $w_x / w_y = 1.0:1.0$ | $1.0:2.3$ | $1.0:2.3$ |
| $\Phi_1/\Phi_2/\Phi_3/\Phi_4 = 1.0/1.0/1.0/0.0$ | $1.0/1.0/1.0/0.0$ | $0.8/1.0/0.8/0.0$ |

**Figure 3-6** Effects of channel dimensions (left two figures) and applied potentials (right two figures), on iso-concentration contour for the main stream flow from reservoir 2 to 4.

Interactions between different streams depends both convection and diffusion, which can be evaluated by the Peclet number ($Pe = vw/D$) reflecting the ratio of convection and diffusion effects. Normally, the magnitude of $v$ is in mm/s, $w$ is the microchannel width chosen as 100 μm, and $D$ is the typical diffusion coefficient of $1.0\times10^{-10} m^2/s$. The corresponding Peclet number is very big (on the order of $10^3$), which implies that the convection effects dominate the concentration distribution of multi-stream laminar flow. This agrees with the results from Pantankar and Hu [103]. Actually, when the diffusion coefficient is increased from $1.0\times10^{-10} m^2/s$ to $4.3\times10^{-10} m^2/s$ in Figure 3-7 where the applied potentials are 1.0, 1.0, 1.0, 0 for $\Phi_1$~$\Phi_4$, no significant difference in concentration

field is observed due to the dominating convection effects for this application. Therefore, control of multi-stream flow transport is most likely relying on the control of velocity through either applied potentials or electroosmotic mobility of solutions.

With the applied electrical field of 1.0, 1.0, 1.0, 0 for $\Phi_1$~$\Phi_4$, effects of different electroosmotic mobilities are investigated. In a three-stream flow system, two flanking streams have the same electroosmotic mobility of $2.0\times10^{-8}\ m^2/(V\cdot s)$ and the middle-stream has an electroosmotic mobility of $4.5\times10^{-8}\ m^2/(V\cdot s)$. It is found that, flows from reservoir 1 and 3 with larger electroosmotic mobility in Figure 3-8(a) enter the channel 4 more than the lower one as shown in Figure 3-8(b), giving rise to a focused middle-stream flow in channel 4.

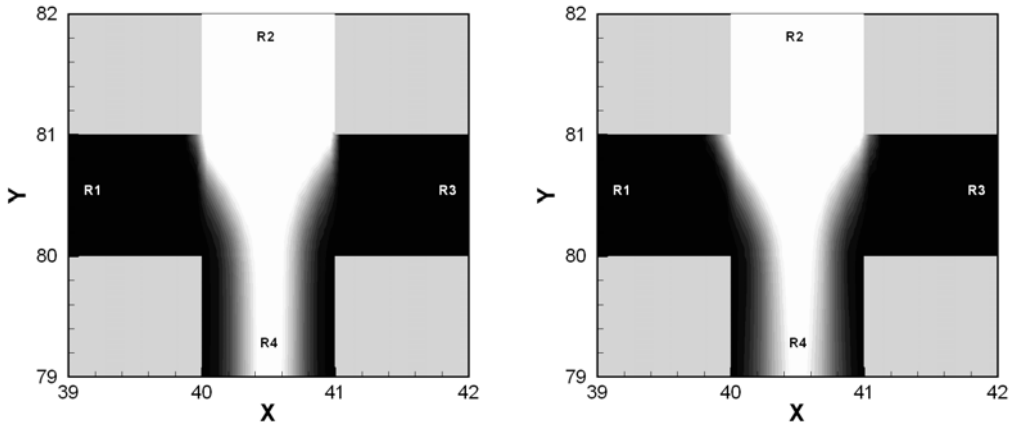


(a) $D=1.0\times10^{-10}\ m^2/s$ (b) $D=4.3\times10^{-10}\ m^2/s$

**Figure 3-7** Effects of diffusion coefficients on the iso-concentration contour of the flow stream from reservoir 2 to 4.

### 3.5 "T"- channel: two stream flow control

In above sections, we studied the effects of different parameters on the control of three-stream flows in cross-linked microchannels. In many other applications [55], however, two-stream flows are required in such geometry, where two different solutions are pumped into the intersection by applying electrical potentials at $R_1$ and $R_3$ and floating potential in reservoir 2. This arrangement results in no noticeable flow from reservoir 2

towards the intersection. Through controlling the parameters discussed above, the width of the interface between two solutions can be controlled. Figure 3-9 shows a width of the interface of 20 μm, where the normalized applied potential at $R_1$ and $R_3$ are both 1.6 and the floating potential is set on reservoir 2.

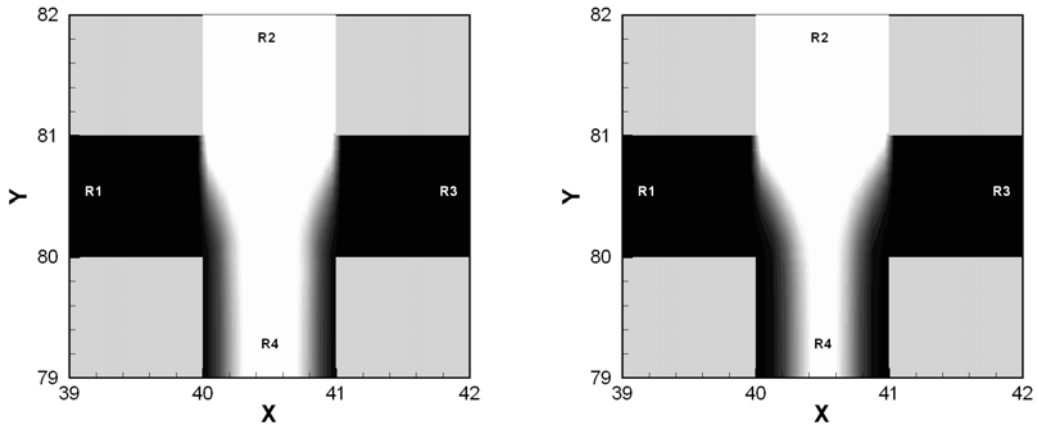


(a) $\mu_{eo_{1,3}} = 2.0\times10^{-8}, \mu_{eo_2} = 4.5\times10^{-8}\ m^2/(V\cdot s)$; (b) $\mu_{eo_{1,2,3}} = 4.5\times10^{-8}\ m^2/(V\cdot s)$

**Figure 3-8** Effects of electroosmotic mobility on the concentration field of the flow stream from reservoir 2 to 4.

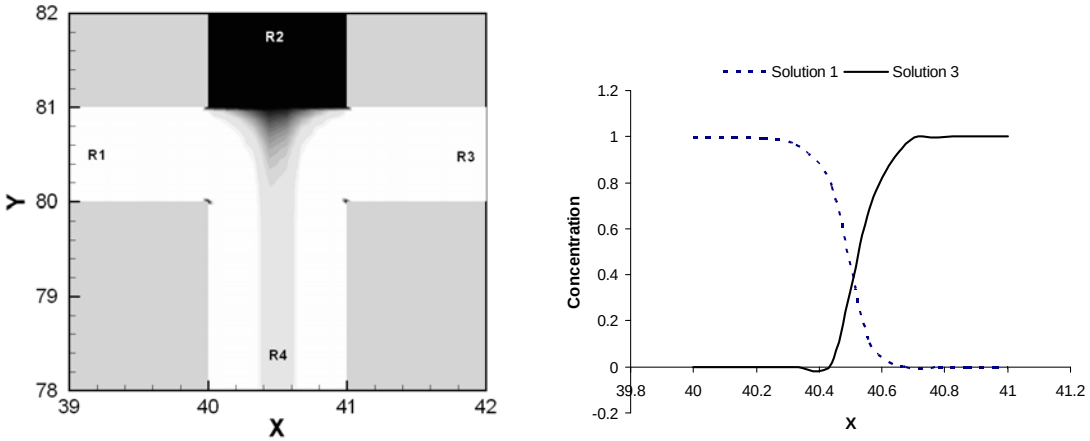


**Figure 3-9** Iso-concentration contour (left) for two stream flows and concentration profile (right) for two solutions flowing from reservoir 1 and 3 converging into the channel 4 at the location of Y=78.

## 3.6 Conclusions

Based on a simple cross-linked microchannel network, the fluid flow and mass transport processes are attempted to be controlled for applications of patterning or fabricating some featured structures within microchannel wall surfaces. In current theoretical studies, the mathematical model with a whole set of governing equations was developed in details and a series of numerical simulations were then performed to investigate the effects of different controlling parameters on multi-stream flows in cross-linked microchannels. The applied potential field, flow field and concentration field were solved in sequence for various scenarios and grid independence test was also implemented during the numerical simulations of some typical cases.

The width of middle stream and the interface width of adjacent flow streams in the downward microchannel (CH4) were found to be controllable through adjusting the developed controlling parameters, no matter which flow scheme (three-stream or two-stream) was utilized. According to our numerical results, the applied potentials, the electroosmotic mobilities of solutions in different streams, and the channel dimensions (like the ratio of horizontal channel width to vertical channel width) have significant effects on the multi-stream flow and mass transport after converging in the intersection of cross-linked microchannels. However, diffusion coefficients of different solutions have less influence than the other parameters because of the presence of high Peclet number for such kinds of applications.

Generally, through the simulations using the model developed in current study, the optimized configurations in terms of these controlling parameters for some particular applications can be numerically explored and then used as guidance for further expensive experiments and corresponding devices designs.

# Chapter 4

# Three-Dimensional Electoosmotic Flow of Replaced Solutions in Straight Microchannel

Electroosmotic flow with solution displacement in microchannels is often encountered in many lab-on-a-chip devices where washing procedures are designed. In order to investigate the detailed flow structures for a displacement process between two different electrolyte solutions, a three-dimensional numerical model is developed. KCl solution and $LaCl_3$ solution are mainly used as sample solutions. A 2 mm long straight microchannl with a rectangle cross sectional area (height of 100μm and width of 200 μm) is employed for study. The governing equations of applied electrical field, flow field and concentration field are numerically solved based on a finite control volume scheme. The fluid flow coupled equations are solved using the developed SIMPLE algorithm. The observed flow structures, such as back flow in the channel center and distortion of plug-like electroosmotic velocity profile, are discussed in details. It is found that the distortion of flow field is due to the induced pressure gradient, which is a result of the non-uniformity of electroosmotic mobilities and electrical conductivities of two solutions. Finally, the displacement between a pair of different solutions, distilled ultra filtered (DIUF) water and $LaCl_3$ solution, is briefly studied for further verification.

## 4.1 Physical model and theoretical basis

In this study, a straight microchannel with a dimension of 2 mm ($l$) x 100 μm ($2h$) x 200 μm ($2w$) is considered and the solutions will flow along the Z-direction. Due to the symmetric conditions, one quarter of the whole channel is chosen as computational domain (ABCD & A'B'C'D') as highlighted in Figure 4-1(a). During a displacement process, an electrical field is applied to the solutions in the microchannel through two electrodes inserted into two reservoirs connected at the two ends of the microchannel.

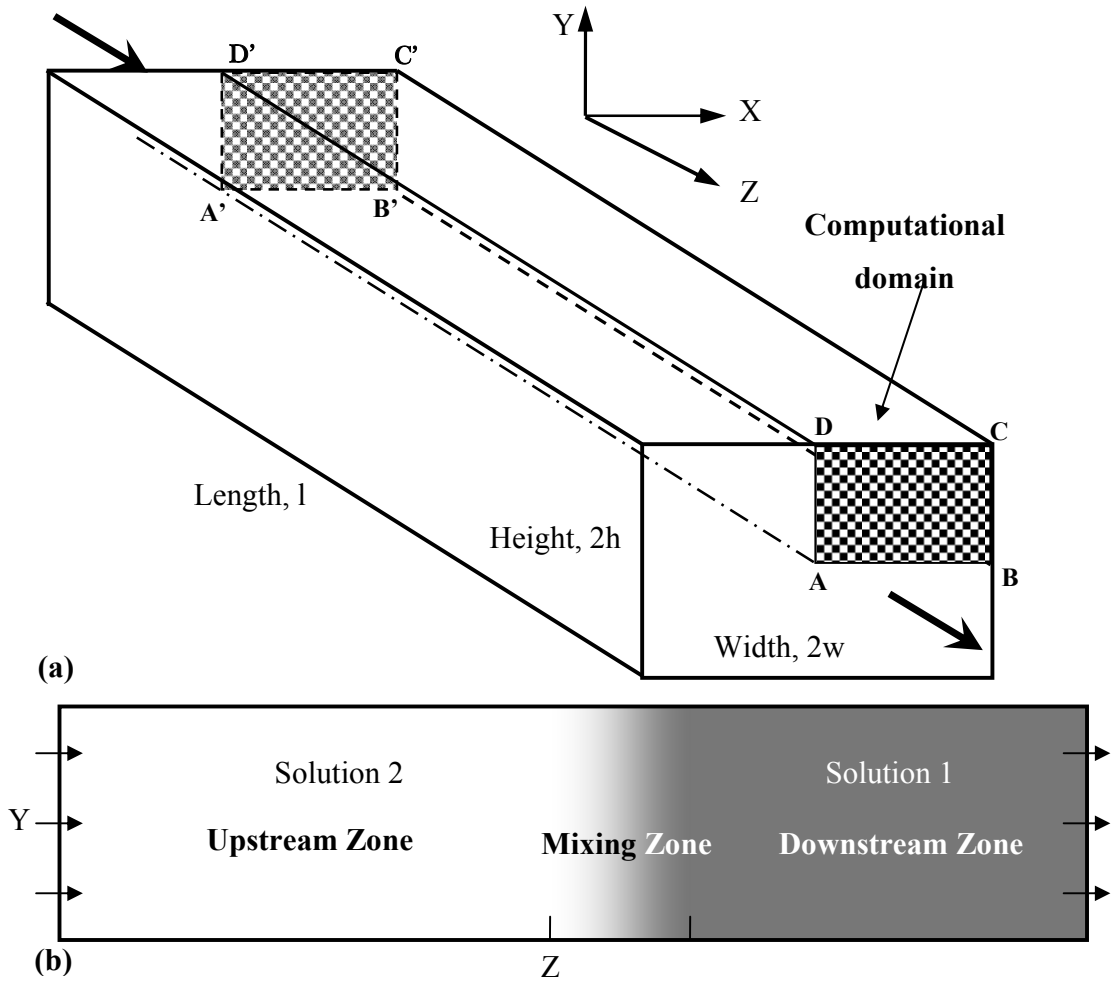


**Figure 4-1** (a) Illustration of the rectangular microchannel and computational domain; (b) Schematic diagram of the process of one solution displacing another one at a Y-Z Plane.

Initially, the whole channel is filled with one uniform solution, referred to as solution 1. Once the exerted electrical field is applied, the electrical force drives another solution (solution 2) into the microchnnel from the left inlet. At the same time, solution 1 will flow out of the channel. Due to the presence of non-uniform flow fields for different solutions, pressure gradients will be induced, which are not present for uniform solution. As shown in Figure 4-1(b), during a displacement process, the microchannel can be divided into three zones according to the concentration distribution. The upstream zone is filled with uniform solution 2 with a concentration of $C_{0\_2}$, the downstream zone is filled

with uniform solution 1 with a concentration of $C_{0\_1}$, and the mixing zone is filled with a mixture of both solution 1 and solution 2. No chemical reaction between two solutions is considered because most washing buffer solutions are designed to not react with reagents. The mixing zone length is defined as follows: The position where $C = 99.99\%C_{0\_2}$ will be the left boundary of the mixing zone. The position where $C = 99.99\%C_{0\_1}$ will be the right boundary of the mixing zone. It is obvious that the length of the mixing zone and the lengths of the other two sections all change with time. In the simulation, the properties of the electrolyte solution in the mixing zone are obtained using linear interpolation of two solutions.

**Flow field**

The applied electrical field results in electroosmotic flow in the microchannel and the basic equations describing flow field are the continuity equation,

$$\vec{\nabla} \cdot \vec{V} = 0 \qquad [4\text{-}1a]$$

and the Navier-Stokes momentum equation for incompressible liquid,

$$\mathrm{Re}\left[\frac{\partial \vec{V}}{\partial \tau} + \left(\vec{V} \cdot \vec{\nabla}\right)\vec{V}\right] = -\vec{\nabla}P + \nabla^2 \vec{V} + \vec{F}_e \qquad [4\text{-}1b]$$

In general, the Reynolds number for microchannel flow is very small: the velocity is on the order of mm/s, the channel dimension is on the order of μm, the viscosity is on the order of $1.0\times10^{-3}\ N\cdot s/m^2$ and the density is about $1.0\times10^{3}\ kg/m^3$. To simplify equation [4-1b], we ignore transient and convective terms and consider laminar cases where $\mathrm{Re} < 0.1$. $F_e$ stands for the non-dimensional electroosmotic body force [29] described by

$$F_e = \frac{\phi_{\max}\varepsilon_0\varepsilon_r K_b T\rho}{ze\mu^2}\vec{\nabla}\Phi\nabla^2\Psi \qquad [4\text{-}1c]$$

In order to fully capture the complete solution, the electrokinetic potential distribution in the EDL, $\Psi$, has to be solved. However, the presence of large variations of length scales,

which include the mixing length (mm), the channel cross-sectional dimensions (μm) and the double layer thickness (nm), will make the three-dimensional numerical simulation of such displacement processes very complicated and expensive. The electroosmotic velocity variation only occurs within the EDL region and exhibits plug-like velocity profile in the rest of the channel cross-sectional plane. It is true that a velocity variation in the transverse direction exists in the mixing region, however, it is mostly caused by induced pressure driven flow rather than by EOF. Therefore, the EDL can be treated as an ultra thin film with net charges for the entire channel. The electrical driving force only exists in this thin film, which allows the further simplification of equation [4-1b] by dropping the electrical force term and applying a slip velocity boundary condition, $\vec{V}_{wall} = \mu_{eo}\vec{E}$, where $\mu_{eo}$ is the electroosmotic mobility for each solution. This approach has been applied successfully in many numerical studies [94, 104] and validated by experimental results. For detailed justification of applying this approach to non-uniform EOF, readers are also referred to the publication of [89]. It is considered that the both channel ends are open to air. Thus, the corresponding inlet (reservoir 2) and outlet (reservoir 1) boundary conditions are

$$P = 0,\ V_x = 0,\ V_y = 0,\ \frac{\partial V_z}{\partial Z} = 0 \quad \text{on the ABCD and A'B'C'D' planes} \quad [4\text{-}2a]$$

The boundary conditions at the CC'D'D plane (the upper wall of microchannel) are

$$\frac{\partial P}{\partial Y} = 0,\ V_x = \mu_{eo}E_x(D_h\rho/\mu),\ V_y = 0,\ V_z = \mu_{eo}E_z(D_h\rho/\mu) \quad [4\text{-}2b]$$

and at the CC'B'B plane (the side-wall of microchannel) are

$$\frac{\partial P}{\partial X} = 0,\ V_x = 0,\ V_y = \mu_{eo}E_y(D_h\rho/\mu),\ V_z = \mu_{eo}E_z(D_h\rho/\mu) \quad [4\text{-}2c]$$

For the other two planes (BB'A'A and DD'A'A planes), the symmetric boundary conditions are applied

$$\frac{\partial P}{\partial Y} = 0,\ \frac{\partial V_x}{\partial Y} = 0,\ V_y = 0,\ \frac{\partial V_z}{\partial Y} = 0 \quad \text{on the DD'A'A plane} \quad [4\text{-}2d]$$

$$\frac{\partial P}{\partial X} = 0,\ V_x = 0,\ \frac{\partial V_y}{\partial X} = 0,\ \frac{\partial V_z}{\partial X} = 0 \quad \text{on the BB'A'A plane} \quad [4\text{-}2e]$$

**Electrical field**

The distribution of applied potential field will be influenced by the solution displacement. Since the two solutions have different electrical conductivities, the electrical resistance, the electrical current and the applied electrical field gradient will all change with time. At a given time, the electrical field will vary along the channel length due to the instantaneous electrical current and different electrical resistance from location to location. According to the theory of electrostatics, the applied electrical potential, $\Phi$, can be described by,

$$\vec{\nabla} \cdot (\lambda \vec{\nabla} \Phi) = 0 \qquad [4\text{-}3]$$

which varies from the traditional Laplace equation in that a non-uniform electrical conductivity along the channel has been included. The insulation boundary conditions ($\partial\Phi/\partial n = 0$) are applied to the channel walls and symmetric boundary conditions are applied to symmetric axes ($\partial\Phi/\partial X = 0$ at $Y = 0$ and $\partial\Phi/\partial X = 0$ at $X = 0$). The specific potential values are applied to the inlet of the channel ($\Phi_{in} = 1$) and the outlet of the channel is grounded ($\Phi_{out} = 0$).

**Concentration field**

During the displacement process, diffusion will happen near the interface of two solutions. At the same time, the bulk solution is pumped by applied potential field, which will influence the concentration as well. The concentration distribution of the $i-th$ solution can be described by the conservation of mass law,

$$\frac{\partial C_i}{\partial \tau} + \left(\vec{V} \cdot \vec{\nabla}\right) C_i = \frac{D_i \rho}{\mu} \nabla^2 C_i \qquad [4\text{-}4]$$

The zero flux boundary conditions are applied to the channel walls ($\partial C_i/\partial n = 0$) and symmetric boundary conditions are applied to the symmetric plane ($\partial C_i/\partial X = 0 \text{ at } Y = 0$ and $\partial C_i/\partial Y = 0 \text{ at } X = 0$). For the inlet and outlet, the boundary conditions for the $i-th$ solution are specified as $C_i = 1$ at $Z = 0$ and $\partial C_i/\partial Z = 0$ at $Z = l/D_h$.

**Numerical Scheme**

One thing that should be noted here is, a series of scaling parameters in equation [4-5] are applied in the course of non-dimensionalization, where $D_h$ is the hydraulic diameter of $4hw/(h+w)$.

$$\begin{cases} V = v/(\mu/D_h\rho);\ P = (p - p_a)/(\mu^2/\rho D_h^2) \\ \Phi = \phi/\phi_{ref} \\ C = c/c_0;\ \tau = t/(D_h^2\rho/\mu) \end{cases} \quad [4\text{-}5]$$

The fluid flow set of non-dimensional equation [4-1] and [4-2], was solved using the SIMPLE algorithm, which is based on a finite control volume discretization of the governing equations on a staggered grid. At a given time-step, the concentration distribution for both solutions is known from the previous time-step. With this concentration profile, the electrical conductivity, the electrical resistance and the local electrical field can be determined. Considering the changing electroosmotic mobility of the liquid near the mixing zone, the boundary conditions for flow field are updated. A converged flow field is achieved. Then, the equation of concentration can be solved to obtain the concentration distribution for the current time-step and the unsteady term in the concentration equation is solved with an alternative-direction implicit method in the numerical simulation. The above procedure is repeated for next time-step until the accomplishment of whole displacement.

The accuracy of the numerical solution has been validated by evaluating grid independence. In the real simulation, the grid Peclet number plays an important role in evaluating this effect. The balance between accuracy and reasonable calculation time leads to a selection of the grid Peclet number of 67.5 in the current simulations.

## 4.2 Characteristics of EOF with replaced solutions

The objective of this study is to investigate the three-dimensional flow structures during a displacement process between two different solutions using the specially developed three-dimensional numerical model. To this end, two aqueous electrolyte solutions with different ionic valence ratio (z:z) are employed in tests and their running conditions are

listed in Table 4-1. Some other physical properties listed in Table 4-2 are assumed for the selected solutions. It should be noted that for all the concentration plots unless indicated otherwise, the concentration of $LaCl_3$ solution decreases from black to white, whereas the reverse trend for the other solutions. The default applied electrical field strength is 15 kV/m for all the tests unless indicated otherwise.

**Table 4-1** The comparative physical parameters of the selected electrolyte solutions.

| **Solution** | **Conductivity $\lambda$ (S/m)** | **Zeta potential $\zeta$ (mV)** | **Electroosmotic mobility $\mu_{eo}$ ($m^2$/V·s)** |
|---|---|---|---|
| **KCl $10^{-4}$M** | $15.14\times10^{-4}$ | - 107 | $7.58\times10^{-8}$ |
| **$LaCl_3$ $10^{-4}$M** | $40.20\times10^{-4}$ | - 39.2 | $2.78\times10^{-8}$ |
| **DIUF water** | $0.7269\times10^{-4}$ | - 240 | $1.7\times10^{-7}$ |

**Table 4-2** The approximate physical parameters of general aqueous electrolyte solutions.

| **Density $\rho$ ($kg/m^3$)** | **Viscosity $\mu$ (N·s/$m^2$)** | **Relative permittivity $\varepsilon_r$** | **Permittivity Vacuum $\varepsilon_0$ (C/V·m)** | **Diffusion coefficient D ($m^2$/s)** |
|---|---|---|---|---|
| $1\times10^3$ | $1\times10^{-3}$ | 80 | $8.854\times10^{-12}$ | $2\times10^{-9}$ |

In a displacement process between two different solutions, the presence of different electroosmotic mobilities and electrical conductivities for two solutions, and thus the non-uniform applied electrical field, will result in non-uniform electroosmotic flow field and induced pressure gradient along the channel, which is not present for uniform solution applications. Figure 4-2 shows the concentration field of $LaCl_3$ solution, the flow field and the pressure field for the process where $10^{-4}$M $LaCl_3$ solution displaces $10^{-4}$M KCl solution at 0.09s. In order to clearly show the detailed flow structure, different sections of the total channel length are plotted in Figure 4-2(a) ( $Z = 1 \sim 4$ ), Figure 4-2(b) ( $Z = 5 \sim 9$ ) and Figure 4-2(c) ( $Z = 10 \sim 14$ ).

For each plot, the velocity profile and corresponding iso-pressure contours are plotted in the upper area, and the concentration field is presented in the lower half area. As

shown in this figure, when $LaCl_3$ solution gradually displaces KCl solution, plug-like electroosmotic velocity profiles are distorted by the induced pressure gradients, which have a non-dimensional peak value of -115 in the mixing zone. $LaCl_3$ solution has small electroosmotic mobility (as listed in Table 4-1) and this region has lower electrical field strength due to its high electrical conductivity, which gives rise to a lower electroosmotic velocity and the KCl solution region has a higher velocity.

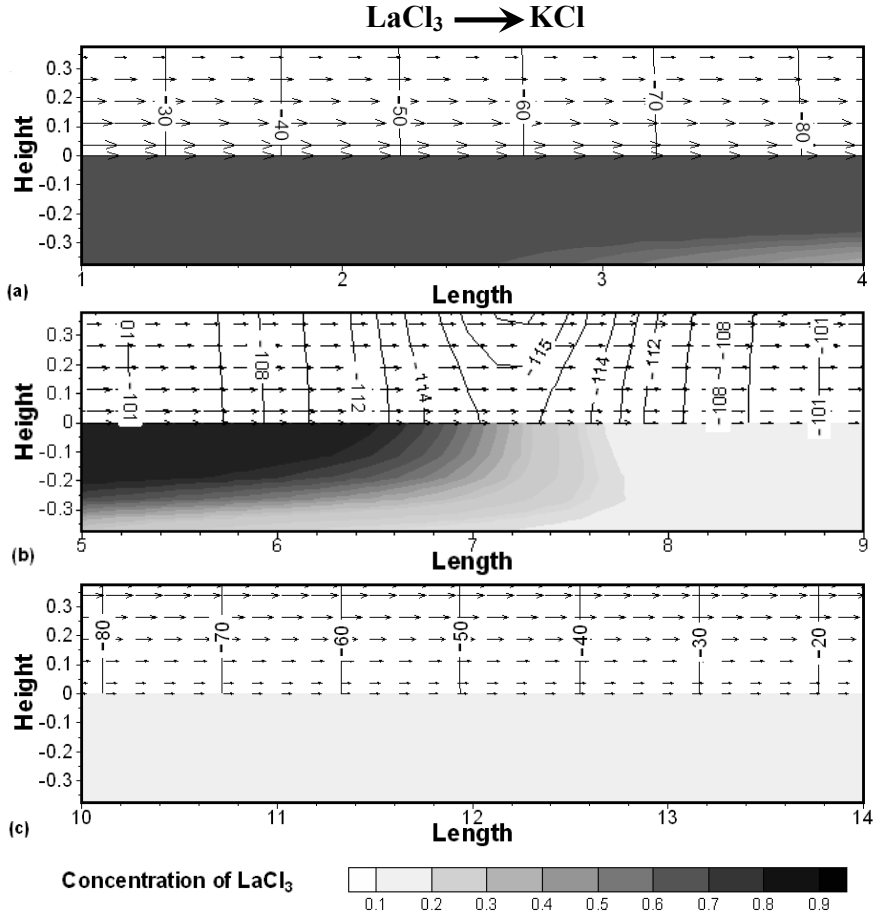


**Figure 4-2** The flow field, pressure field and concentration field in the Y-Z plane (X=0.3375) for the process of $LaCl_3$ solution displacing KCl solution at t = 0.09s at (a) $1 \le Z \le 4$; (b) $5 \le Z \le 9$; and (c) $10 \le Z \le 14$.

In order to satisfy the continuity condition, pressure gradients are induced to balance the non-uniformity in the flow field. As shown in Figure 4-2(a), a negative pressure gradient exists in the region with $LaCl_3$ solution to speed up the liquid in this region and

generate a parabolic-like velocity profile and a positive pressure gradient is induced in the region with KCl solution to slow down the liquid in this region and generate a concave velocity profile.

Figure 4-3(top) shows the concentration field of KCl solution in the entire microchannel at the plane of $X = 0.3375$ for the case of $10^{-4}$ M KCl solution displacing $10^{-4}$ M $LaCl_3$ (0.18s after the displacing). The concentration decreases from white to dark. It can be seen that KCl solution gradually displaces $LaCl_3$ solution from the left inlet to the outlet as expected, however, it should be noted that there exists a region in the upstream zone (the region of high concentration of KCl solution) with a much lower concentration in the center of the channel than near the wall, which can also be observed by comparing the iso-concentration contours at the planes of $Z = 0.525$, $Z = 3.975$ and $Z = 7.425$ as shown in Figure 4-3(bottom). The presence of lower concentration region near the center of the microchannel is mainly due to the presence of the induced pressure driven backflow (flow in the opposite direction to the main flow) in this region.

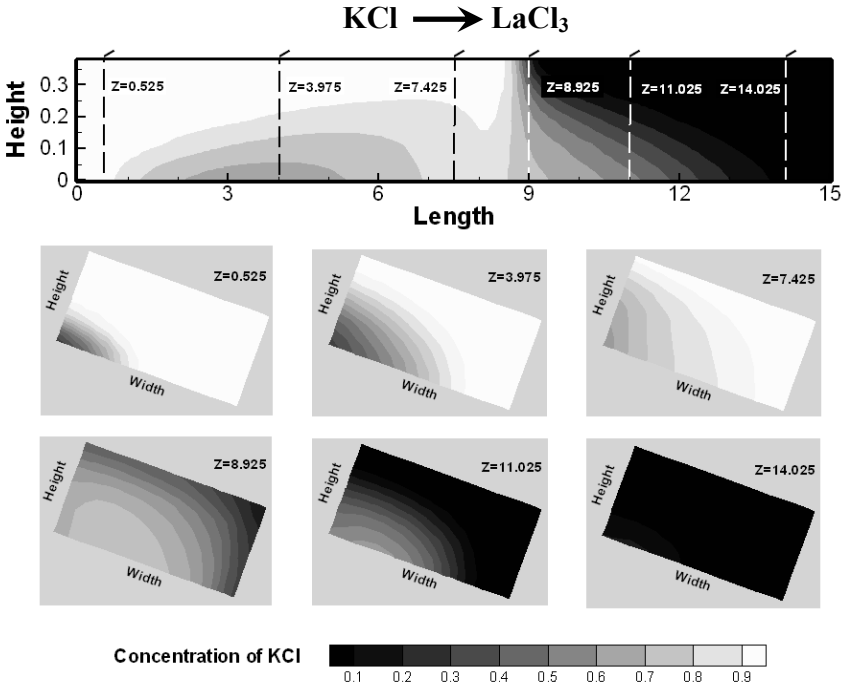


**Figure 4-3** Concentration field in the Y-Z plane (X=0.3375) (top) and X-Y Planes (bottom) along the whole microchannel for the process of KCl solution displacing $LaCl_3$ solution at t = 0.18s.

As discussed above, a positive pressure gradient exists in the KCl solution region (also shown in Figure 4-4(a)), which will cause a flow in the opposite direction to the main flow and the maximum velocity of the back flow exists in the center of the channel. This back flow will significantly slow down the forward movement of KCl solution in the center of the channel generating this region with lower concentration than that near the wall. However, after one solution completely displaces another solution, the microchannel is filled with a uniform solution, where a plug-like electroosmotic velocity profile is expected as shown in Figure 4-4(c) and no pressure gradient exists in the entire channel as indicated by the iso-pressure contour in this figure.

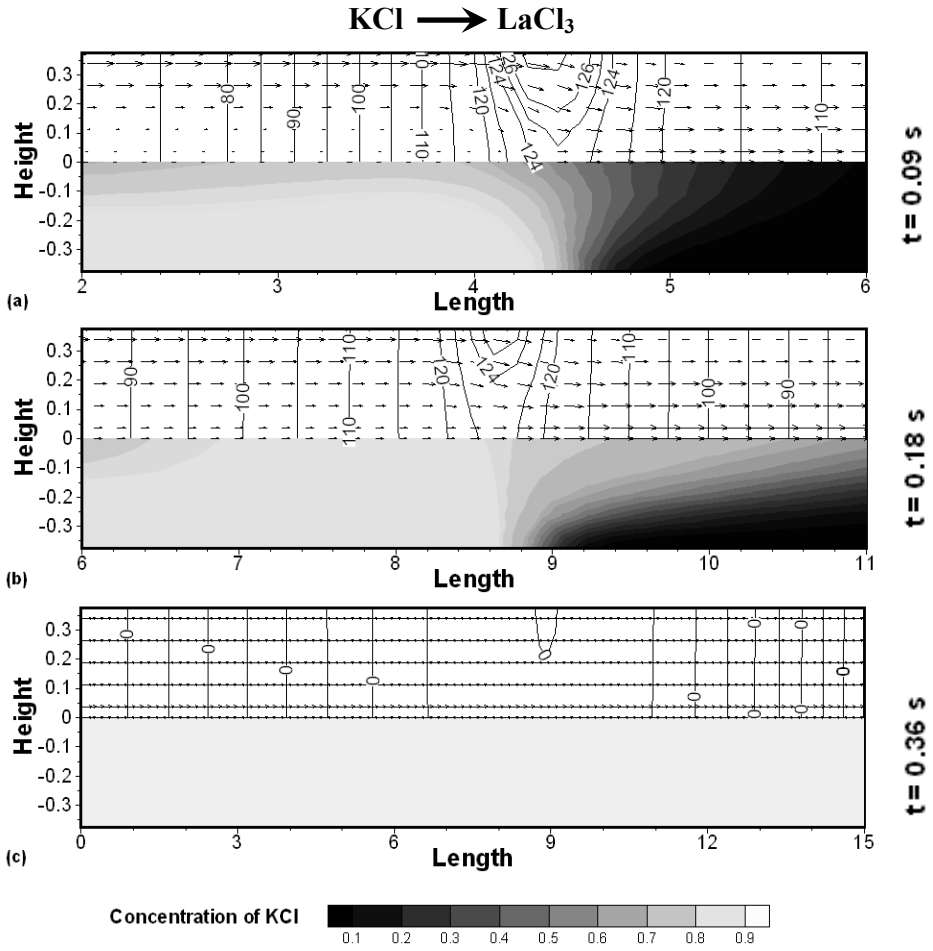


**Figure 4-4** Flow field, pressure field and concentration field in the Y-Z plane (X=0.3375) for KCl solution displacing $LaCl_3$ at different time steps, (a) t = 0.09s and near the mixing zone, (b) t = 0.18s and near the mixing zone, and (c) t = 0.36s for the entire channel.

### 4.3 Specific phenomena: back flow and circulation

The flow structure (the presence of back flow near the center of the microchannel) during the displacement process can be clearly seen from Figure 4-5, where liquid flows from the bottom (the inlet) to the top (the outlet). Figure 4-5(a), (b) and (c) shows the flow field for $10^{-4}$M KCl solution displacing $10^{-4}$M $LaCl_3$ solution at $t = 0.09\,s$, $t = 0.18\,s$, and $t = 0.36\,s$, respectively, and Figure 4-5(d) shows the flow structure for $10^{-4}$M $LaCl_3$ solution displacing $10^{-4}$M KCl solution at $t = 0.09\,s$.

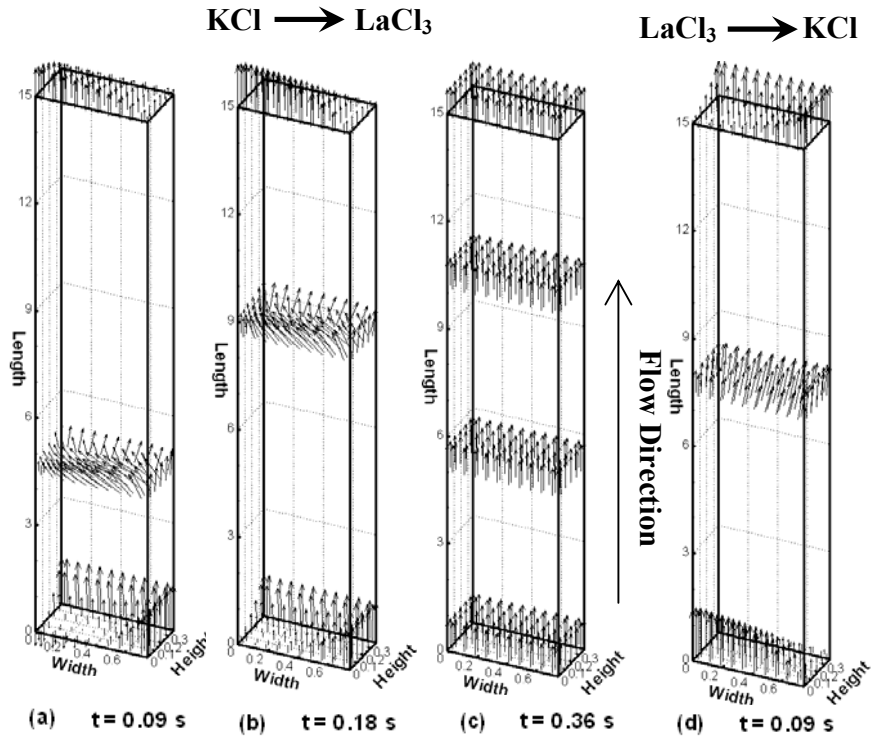


**Figure 4-5** Typical 3-D flow fields along the whole channel for the process of KCl solution displacing $LaCl_3$ solution at (a) t = 0.09s, (b) t = 0.18s, (c) t = 0.36s, and (d) for the process of $LaCl_3$ displacing KCl at t = 0.09s.

As discussed above, when the KCl solution displaces the $LaCl_3$ solution, there exists a back flow in the upstream zone (where the electroosmotic velocity is higher than that of the downstream zone) at the early stage of the displacement process due to the induced pressure gradient, which can be clearly seen from Figure 4-5(a) at the inlet region. The strong deviation of the electroosmotic plug-like velocity profile near the mixing zone is also observed in Figure 5(a) and (b) where the displacement is running. However, a

perfect plug-like velocity profile emerges after one solution completely displaces another solution as expected and shown in Figure 4-5(c). For the reverse displacing process where $10^{-4}$M $LaCl_3$ solution displaces $10^{-4}$M KCl solution, one would expect the plug-like velocity profile to be distorted in the opposite direction to that shown in Figure 4-5(a). Indeed, Figure 4-5(d) clearly indicates that the velocity near the mixing zone deviates in the opposite direction to that shown in Figure 4-5(a).

It is very interesting to note that a similar flow structure should be expected at the beginning of the process of KCl solution displacing $LaCl_3$ solution and the ending stage of the process of $LaCl_3$ solution displaces KCl solution because for these two scenarios, the portion of the channel filled with a certain solution (either KCl or $LaCl_3$ solution) is about the same. This understanding has been tested and the flow structures for both cases are plotted in Figure 4-6, where the upper half shows the ending stage of the process where $LaCl_3$ solution almost completely displaces KCl solution, whereas the lower half shows the beginning stage of the process where the reverse displacement takes place. For both cases, the majority of the channel is filled with $LaCl_3$ solution. As seen in this figure, two flow structures are very similar, which validates the previous discussion.

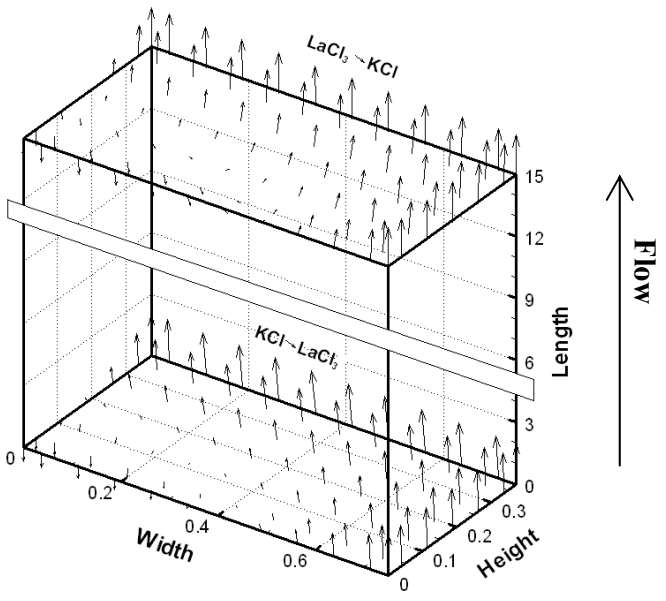


**Figure 4-6** Comparison of the flow field between the early stage of the process of KCl solution displacing $LaCl_3$ solution and the ending stage of the process of $LaCl_3$ solution displacing KCl solution.

From all the test cases of displacement process between different solutions, circulation is found in the mixing zone, which is caused by the induced pressure driven flow as discussed above. The circulation patterns for the plane at $Z = 8.625$ for KCl solution displacing $LaCl_3$ solution and for the plane at $Z = 7.425$ for KCl solution displacing $LaCl_3$ solution are shown in Figure 4-7(a) and (b), respectively. The iso-pressure contour values indicate the flow direction, which is also shown by the velocity vectors (arrows). The circulation pattern occurs in the transverse direction, which can not be predicted by the previous developed one-dimensional model [95].

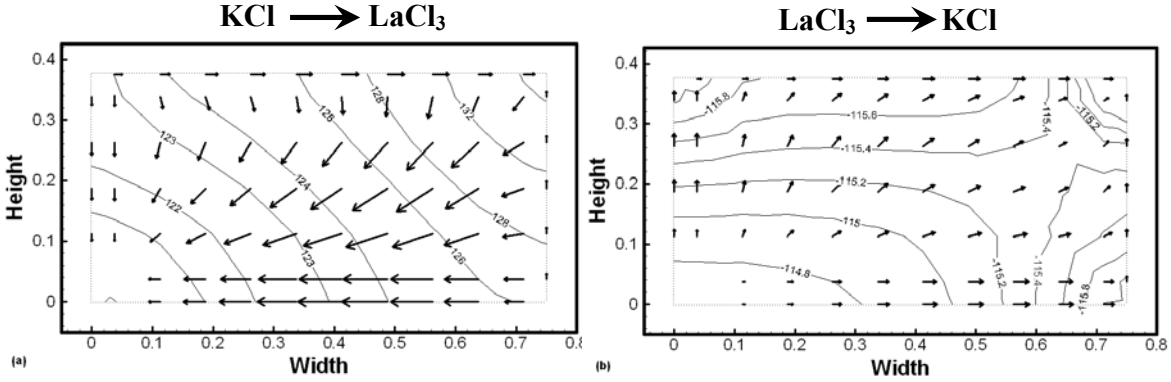


**Figure 4-7** Flow field and pressure field at (a) the X-Y plane (Z=8.625) for the process of KCl displacing $LaCl_3$ at t = 0.18s, (b) the X-Y plane (Z=7.425) for the process of $LaCl_3$ displacing KCl at t = 0.09s.

## 4.4 Comparison of solution displacement

Figure 4-8(a) shows the time sequence of the interface between two solutions (the contour line has a half original concentration value of the solution 2, the displacing one) during the displacement processes. The solid lines represent the interface when KCl solution displaces $LaCl_3$ solution (i.e. the iso-concentration line has $0.5C_{0\_KCl}$) and the dashed lines are for the displacement in the reverse order (i.e. the iso-concentration line has $0.5C_{0\_LaCl_3}$). As shown in the figure, at a given time, the interface is very different for the two cases. The dashed lines shows the effects of parabolic-like velocity on the concentration field (due to induced pressure driven flow) and the solid lines shows the effects of concave velocity on the concentration field. This is because at a given time the

velocity field is different due to different applied electrical field strength (see Figure 4-9(a) and (b) for comparison of the electrical field strength for these two cases) and the non-uniform electroosmotic mobility through the channel.

This phenomenon is also observed for the displacement between DIUF water and $LaCl_3$ solution as shown in Figure 4-8(b). Normally for the EOF of DIUF water in a microchannel, the full Poisson-Boltzmann equation is required to obtain the detailed electrical potential distribution in the EDL region because of its big double layer thickness (i.e. about 300 nm) as compared with the channel size. However, the purpose here is to illustrate that a similar phenomenon can be also observed for the displacement between other pairs of solutions; therefore, the developed model is used here.

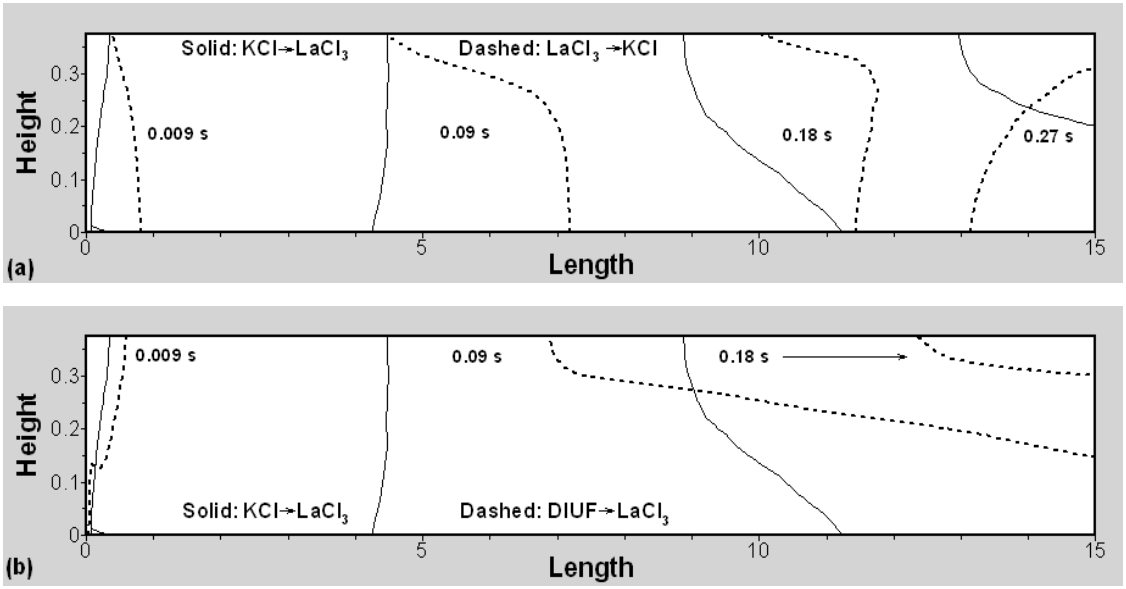


**Figure 4-8** Comparison of the sequence of the iso-concentration line, $c = 0.5c_0$ of solution 2 (i.e. displacing solution) for different displacing processes.

In addition, the difference in the solution interface profile is exaggerated for the displacement between DIUF water and $LaCl_3$ solution. This is because a bigger difference in electroosmotic mobility and electrical field strength (see Figure 4-9(c)) exists for this pair of DIUF water and $LaCl_3$ solution than the pair of KCl and $LaCl_3$ solution, which results in stronger distortion in the flow field and thus the concentration

profile of the interface. The comparison of the pressure, flow and concentration fields between the displacement processes for the pair of DIUF water and $LaCl_3$ solution and the pair of KCl and $LaCl_3$ solution is shown in Figure 4-10(a) and (b).

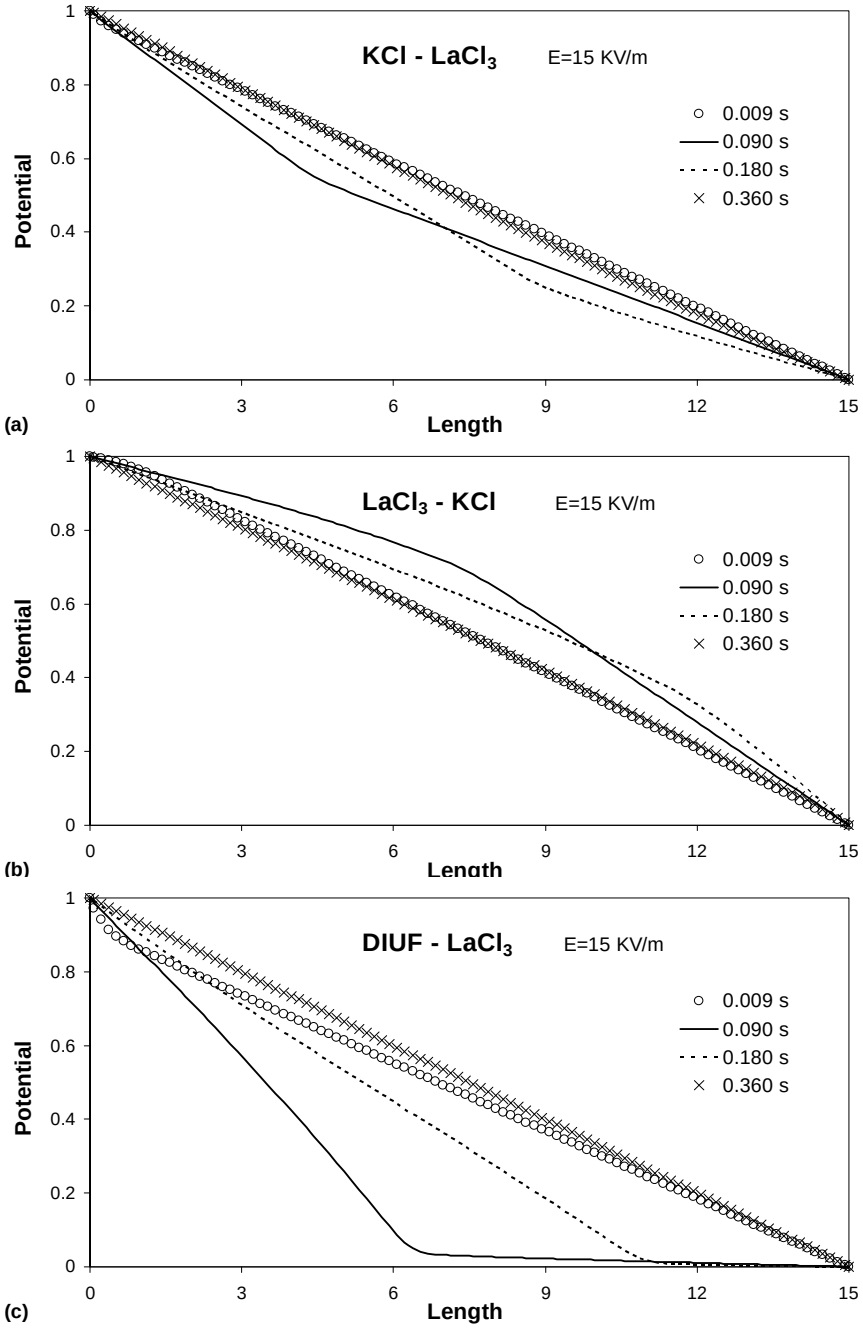


**Figure 4-9** Potential field along the centerline of the computational domain at different time steps for (a) KCl displacing $LaCl_3$, (b) $LaCl_3$ displacing KCl, and (c) DIUF water displacing $LaCl_3$.

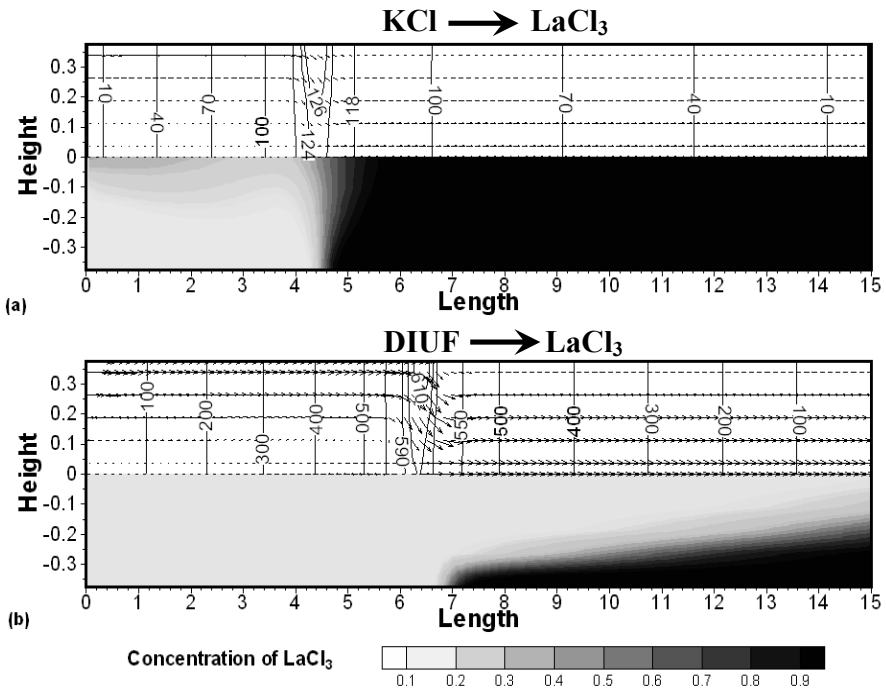


**Figure 4-10** Comparison of the flow field, pressure field and concentration field in the Y-Z plane (X=0.3375) at t = 0.09s for (a) KCl solution displacing $LaCl_3$ solution, and (b) DIUF water displacing $LaCl_3$ solution.

## 4.5 Influence of applied electrical field

The time required to complete the whole displacement process depends on the applied electrical field and the solution involved. For a given condition, if the applied electrical field is higher, the average velocity is higher and less time is required to complete the whole displacement. For EOF in a microchannel with uniform solution, the applied electrical field strength has a linear effect on the velocity, which can be understood from the formula, $u_{eo} = \mu_{eo}\vec{E}$ . Figure 4-11 shows the sequence of the iso-concentration contour for KCl solution at $C = 0.5C_0$ at 0.09s intervals under different applied electrical fields. The approximate linear effect of the applied electrical fields on displacement process is shown in this figure by comparing the iso-concentration contours at $t = 0.09s$ for all the four plots. It can be seen that when the applied electrical field strength is doubled (from $\vec{E} = 7.5kV/m$ in Figure 4-11(a) to $\vec{E} = 15kV/m$ in Figure 4-11(b)), the time required for the interface to reach the same place is reduced by about half. For

example, $t = 0.18s$ is required for a smaller electrical field ( $\vec{E} = 7.5kV/m$ ) to reach about the same location (i.e. Figure 4-11(a)), where $t = 0.09s$ for the interface to reach under a doubled electrical field ( $\vec{E} = 15kV/m$ ) as shown in Figure 4-11(b).

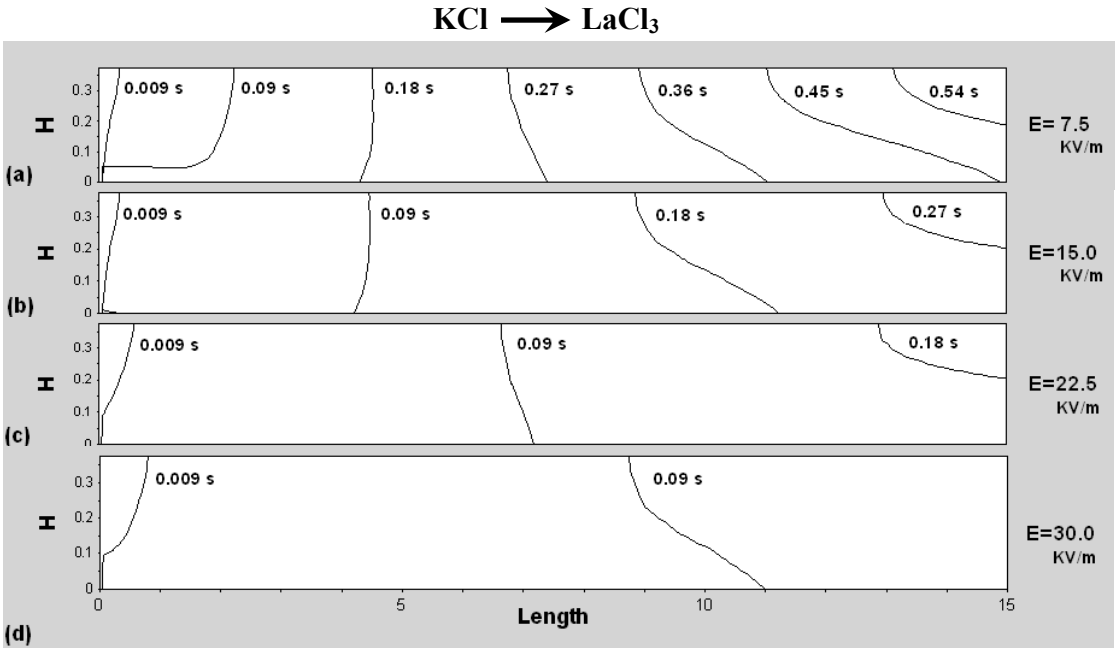


**Figure 4-11** Effects of the applied electrical field strength on the iso-concentration contour at $C = 0.5C_{o\_KCl}$ for KCl displacing $LaCl_3$ at 0.09s intervals.

## 4.6 Summary

It's important to fully understand the solution displacement phenomenon in microchannels, which is often applied for washing purposes in many sample preparation applications. Because of the characteristic velocity profile and easiness control, electrokinetic flow is normally employed rather than pressure-driven flow. Electroosmotic flow during this kind of displacement process between two different solutions depends on the chemical properties of them.

A three-dimensional numerical model to study the displacement process between two various electrolyte solutions is developed across a straight rectangular microchannel. Numerical schemes based on a finite control volume method are established and numerical simulations are consequently performed to investigate the change of

electroosmotic flow structure, pressure distribution and concentration field for a certain solution displacement process.

In current study, the displacement processes between two solutions in both orders (solution 1 displaces solution 2 and vise versa) have been tested and analyzed. The effects of the induced pressure driven flow on the flow field and concentration field are discussed in detail. It can be concluded that, the non-uniformity in chemical properties of the two solutions, especially their electrical conductivities and electroosmotic mobilities differences, has significant effects on the flow field and thus induces pressure driven flows and concentration fields. The bigger difference the two solutions have in their chemical properties, the stronger effects they have on the flow field. The effects of the applied electrical field strength on the displacement process are studied and approximate linear effects are observed.

# Chapter 5

# On-chip Multi-species Transport for Separation Applications

Microchip capillary electrophoresis has been widely employed in chemical and biological applications for separation analysis. Basically, a task of injection/separation (or loading/dispensing) is conducted in this chip-based analyzing technique. Fundamental studies are required to fulfill the complete understanding of fluid flow and species transport in microchannels and effective control through various controlling parameters. Using a developed numerical model, studies are performed of the loading and dispensing processes in on-chip cross-linked microchannels. The model is non-dimensionalized in a unique manner to reveal effects of some key fundamental parameters. The influence of $\mathrm{Re}\,Sc_i$ is examined over the commonly encountered range and the effect of electrophoretic mobilities on separation is investigated for three different types of samples. Species movement and sample plug development with diffusion are examined and related results include concentration profiles and concentration contour plots over a range of injection and separation times. Real-time monitoring of different species movements is performed for injection guidance. Due to electrophoresis effect, migration influence of every species is considered in the model and then solved for separation analysis. Through parametric studies, the electrokinetic transport characteristics are revealed and well understood for future effective control and innovative chip design.

## 5.1 Physical consideration

### 5.1.1 Problem statement

As reviewed earlier, there are different designs like Tee-, cross, double-Tee and multi-Tee injectors; and various operation modes such as pinched, gated and double-L injection, to run the on-chip capillary electrophoresis analysis. In this study, the pinched injection is

employed as default based on a simple cross injector. As illustrated in Figure 5-1, microchip capillary electrophoresis is operated through two processes of injection/separation in a cross-linked microchannel network. Species are loaded with sample carrying buffer solution from the left sample reservoir 1 to the right waste reservoir 3 along the horizontal microchannel. After it reaches a certain state, the separation process will be initiated in the perpendicular direction by switching the applied potential field instantly. The sample driving buffer solution is pumped downward under the influence of potential difference across the top buffer reservoir 2 and bottom waste reservoir 4. At the channel cross, a sample plug is truncated and pushed into the down wing channel. Due to their electrophoretic mobility differences, various species within the sample plug will move at different speeds and become separated. Detectors can be mounted at different locations in the down wing channel to indentify the species and record separation results.

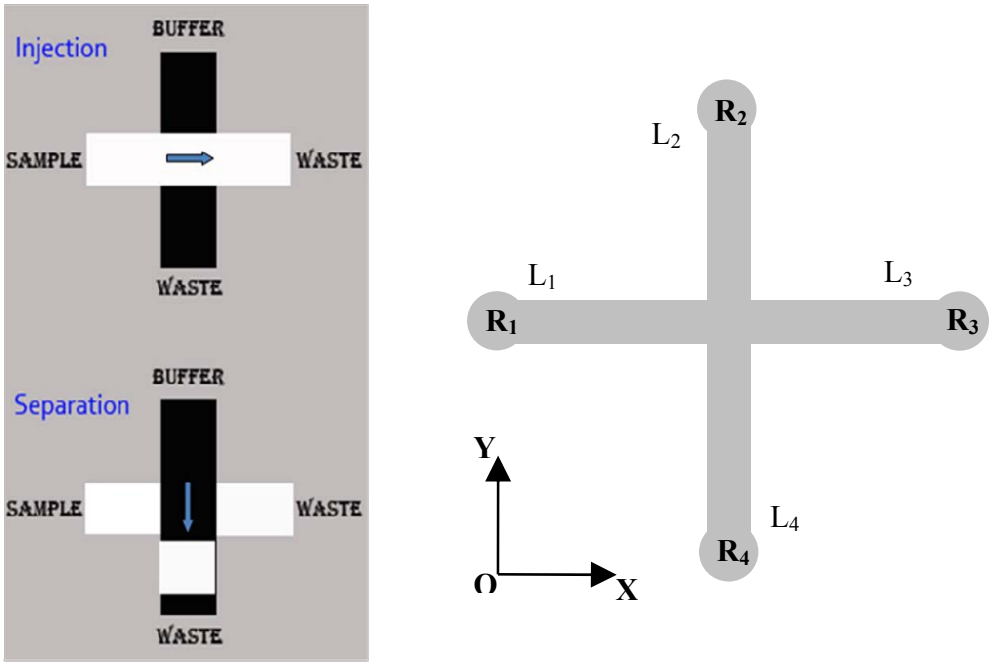


**Figure 5-1** Illustration of on-chip pinched injection and separation process on cross-linked microchannel (left); and layout of reservoirs and microchannel network (right).

### 5.1.2 Physical model

A typical injection-separation unit with a simple cross-linked channel and four reservoirs is shown in Figure 5-1. Within a double-layer microfluidic chip, two microchannels are fabricated perpendicularly sharing with the same intersection. The horizontal channel connecting $R_1$ and $R_3$ is used for injection, while another one is denoted as separation channel. The channel length ($L_i$) is defined as the distance between the intersecting wall and the i-th reservoir ($R_i$), and the channel widths of horizontal and vertical channel are same. Typical channel length, width and depth are 4mm, 50μm and 20μm, which are the values considered here. It is noted that the non-dimensional model reported herein has the flexibility to alter the channel length easily. In the injection mode, the sample solution (i.e. sample species dissolved in the buffer solution) will be pumped from $R_1$ to $R_3$ and the sample plug is controlled by applied potentials. By switching off the applied electrical fields, the loaded sample plug in the intersection can be dispensed into the channel 4 and separation occurs as the sample plug is transported downstream through differences in the electrophoretic mobilities.

### 5.1.3 Running parameters

The magnitude of applied potential field strength for the default injection scheme is $12.5kV/m$ and the corresponding electroosmotic velocity under this uniform potential field is used to non-dimensionalize the velocity field. The same buffer solution is utilized for both sample carrying in the horizontal injection and sample driving in the vertical separation. Therefore we can neglect the influence of liquid electrical conductivity which will lead to a non-uniform applied potential field distribution. The employed buffer solution corresponds to one with an electroosmotic mobility of about $4.5\times10^{-8}\ m^2/(V\cdot s)$ and kinematic viscosity of $1.0\times10^{-6}\ m^2/s$. Other physical properties of this buffer are assumed to be those of water. A negatively charged species, rhodamine dye 110, with an approximate electrophoretic mobility of $-2.0\times10^{-8}\ m^2/(V\cdot s)$ and diffusion coefficient of $4.37\times10^{-10}\ m^2/s$ is typified by the values. One neutral species and another positively charged sample with the electrophoretic mobility of $1.5\times10^{-8}\ m^2/(V\cdot s)$ are also typified

by the values chosen for the study. In the range of $10^{-9} \sim 10^{-10}\ m^2/s$ for most biological fragments, four different diffusion coefficients of samples are investigated in current study. All these values are determined from reported studies and experimental findings. It is considered as a constant room temperature of 20°C with negligible Joule heating. Generally, the default value of physical property of buffer solution or samples will be kept the same except when stated otherwise.

## 5.2 Mathematical model development

### 5.2.1 General fields and governing equations

There are two potential fields established in electroosmotic flows. One is the applied potential along the microchannel and another is the electrokinetic EDL potential in the cross-stream direction. The commonly used buffer solutions for microfluidic applications are on the order of mM, which give rise to a very thin EDL (i.e. <10nm). A brief example is presented here to show this feature of electroosmotic flow.

The electrokinetic EDL potential distribution is described by the Poisson-Boltzmann equation, where a symmetric ($|z_+| = |z_-| = z$) electrolyte solution is used for demonstration.

$$\varepsilon_r \varepsilon_0 \nabla^2 \psi = -\rho_e = 2n^\infty ze Sinh(\frac{ze\psi}{K_b T}) \qquad [5\text{-}1]$$

For the simplified case of an EOF through a slit microchannel with a height of 2H, the above Poisson-Boltzmann equation becomes

$$\frac{d^2\psi}{dy^2} = \frac{2zen^\infty}{\varepsilon_r \varepsilon_0} \sinh(\frac{ze\psi}{K_b T}) \qquad [5\text{-}2]$$

With B.C. (1) $y = 0$, $d\psi/dy = 0$

(2) $y = H$, $\psi = \xi$

Applying Debye-Huckle linearization, the approximate solution is found to be,

$$\psi = \frac{\zeta}{\sinh(\kappa H)} \sinh(\kappa y) \qquad [5\text{-}3]$$

and therefore the net charge density will be

$$\rho_e = -\frac{2z^2e^2n^\infty\psi}{K_bT} = -\frac{2z^2e^2n^\infty\zeta}{K_bT}\frac{\sinh(ky)}{\sinh(kH)} \qquad [5\text{-}4]$$

which has the similar distribution to the induced electrokinetic EDL potential field.

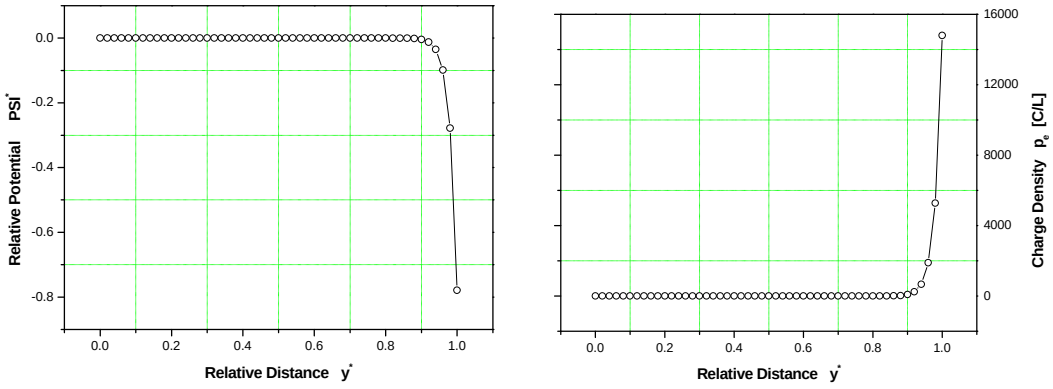


**Figure 5-2** A typical simulation result of simplified Poisson-Boltzmann equation.

From the simulation result shown in Figure 5-2, it is easy to find a very thin EDL whose thickness is negligible as compared to the magnitude of channel width. Thus, there is a very flat plug-like velocity profile in this electroosmotic flow and it is reasonable to decouple the applied electrical potential and the electrokinetic EDL potential. At the same time, the electrokinetic EDL potential is governed by the complicated Poisson-Boltzmann equation which is expensive to solve and need not be. As employed before and will be proved next, a slip-wall velocity boundary condition is usually applied to the flow equations rather than obtaining electrical force $\rho_e\vec{E}$ by solving the Poisson-Boltzmann equation.

This study focuses on the introduction of a complete non-dimensional model of the processes and on the impact of using the non-dimensional model to perform parametric studies. Therefore, a uniform buffer solution is employed and corresponding applied potential field will be governed by

$$\nabla^2 \phi = 0 \qquad [5\text{-}5]$$

Once the applied potential field inside the microchannels is determined numerically, the local electrical field strength can be calculated as the gradient of the local potential.

As known, the flow field in the microchannel is governed by the continuity equation and the momentum equation,

$$\vec{\nabla} \cdot \vec{v} = 0 \qquad [5\text{-}6]$$

$$\rho\left[\frac{\partial \vec{v}}{\partial t} + \left(\vec{v} \cdot \vec{\nabla}\right)\vec{v}\right] = -\vec{\nabla} p + \mu \nabla^2 \vec{v} + \rho_e \vec{E} \qquad [5\text{-}7]$$

The Schmidt number, which represents the ratio between two characteristic time scales of mass diffusion and momentum diffusion, is found to be in the order of $10^4$ ( $Sc = \nu / D$ ). Mass transfer occurs much more slowly than momentum transfer, and therefore the fluid flow can be assumed to be steady state. Like most microchannel flows, the fluid flow considered in this project is laminar with a Reynolds number of 0.028 in this work. The Reynolds number represents the ratio between inertial forces and viscous forces and therefore the convection terms in momentum equation can also be neglected.

The electroosmotic flow has a flat velocity profile except for the pretty thin EDL region, in which velocity will quickly drop to zero at the wall. Therefore, we will consider the electrical driving force term in momentum equation with a replacement slip wall velocity boundary condition. Next, attempts are tried to derive the electroosmotic velocity from driving forces theoretically. For a simple one-dimensional EOF, the momentum equation can be simplified by neglecting inertial and pressure term.

$$\mu \frac{d^2 v_x}{dy^2} + \rho_e E = 0 \qquad [5\text{-}8]$$

Since the net charge density will be zero in the region beyond EDL, bulk flow velocity will have to be constant according to above differential equation. However, in the thin EDL, the net charge density is not zero and corresponding flow velocity will increase

from zero(wall) to a certain value(interface of EDL and bulk fluid) quickly. Incorporating with the Possion equation, equation [5-8] will become,

$$\mu \frac{d^2 v_x}{dy^2} - \varepsilon_0 \varepsilon_r \frac{d^2 \psi}{dy^2} E = 0 \qquad [5\text{-}9]$$

Integrate this differential equation twice over EDL with following boundary conditions,

$$\begin{cases} Wall : v_x = 0, \psi = \zeta \\ Interface : v_x = v_{eo}, \psi = 0 \end{cases} \qquad [5\text{-}10]$$

Then, we'll get the Helmholtz-Smoluchowski velocity,

$$v_{eo} = -\frac{\varepsilon_0 \varepsilon_r \zeta}{\mu} E = \mu_{eo} E \qquad [5\text{-}11]$$

Here the electroosmotic mobility is defined as $\mu_{eo} = -\varepsilon_0 \varepsilon_r \zeta / \mu$, which is a function of zeta potential, fluid viscosity and permittivity. It is far easier to achieve the electroosmotic mobility than to solve the complicated Poisson-Boltzmann equation directly.

For unsteady species transport in microchannels, the distribution of sample concentration field is governed by conservation of mass, which takes the form of

$$\frac{\partial c_i}{\partial t} + \left(\vec{v} \cdot \vec{\nabla}\right) c_i = D_i \nabla^2 c_i + \frac{z_i F D_i}{RT} \vec{\nabla} \phi \cdot \vec{\nabla} c_i \qquad [5\text{-}12]$$

where $z_i$ is the valence of ionic species. The above equation includes an additional migration term, which is a result of electrophoretic forces [29]. Under the applied electrical field, charged samples will experience a velocity difference from the buffer solution, due to these forces, and this will then influence the concentration distribution. The resulting velocity is the electrophoretic velocity and can be modeled using the electrophoretic mobility and local electrical field strength, $\vec{v}_{epi} = \mu_{epi} \vec{E}$ , where $\mu_{epi} = z_i F D_i / RT$ known as Nernst-Einstein relation. Using this model, the above convection-diffusion-migration transport equation can be re-arranged to

$$\frac{\partial c_i}{\partial t} + \left((\vec{v} + \vec{v}_{epi}) \cdot \vec{\nabla}\right) c_i = D_i \nabla^2 c_i \qquad [5\text{-}13]$$

Regarding the electrophoretic mobility of charged particles, it is normally defined as the charge/mass ratio. Our very low Reynolds flow can be considered as Stokes flow and therefore a force balance between electrical force and frictional force is established on the charged samples (spherical shape assumption),

$$F_e = QE = 6\pi a \mu v_{epi} = F_D \qquad [5\text{-}14]$$

Actually, equation [5-8] can also be considered as a balance analysis of viscous force and electrical force. Thus, we will have,

$$\frac{v_{epi}}{E} = \frac{Q}{6\pi a \mu} = \mu_{epi} \qquad [5\text{-}15]$$

This formula satisfies the above physical meaning of charge/mass ratio. Although we may not determine the net charge and radius of a certain particle, the electrophoretic velocity (difference with bulk flow speed) under applied electrical field is measurable. Using Einstein-Stokes relation $D_i = K_b T / 6\pi a \mu$ , the calculation of electrophoretic mobility of charged spherical particle in equation [5-15] is identified essentially same to the term defined by Nernst-Einstein relation in equation [5-12].

### 5.2.2 Initial/boundary conditions

For the applied electrical field, some specific potential values are directly applied to the reservoirs and there are zero potential gradients normal to the wall boundaries. As noted above, there is no initial condition needed for steady state flow. The slip velocity boundary conditions ($v_{eo,l} = \mu_{eo} E_l$) are employed at the walls. In the direction normal to wall, the corresponding velocity component is zero. At the inlet/outlet or reservoirs, zero normal velocity gradients are applied. The normal velocity at the microchannel walls is zero. The microchannel is enclosed except for connecting the reservoir, which is open to air at atmospheric pressure.

Both injection and separation are unsteady transport processes. At the initial state of injection, concentration will be zero in the entire microchannel except for the sample reservoir, where it will be the original concentration for each species. At the point where the applied potential is switched from injection to separation, the concentration field of this final state injection is used as the initial condition for the separation process. There are zero gradients of concentration at the walls and all reservoirs except for the sample reservoir in injection mode.

### 5.2.3 Non-dimensionalization

The microchannel width is used as the length scale for non-dimensionalization. The reference potential from reservoir 2 to reservoir 4 (during separation) is used to non-dimensionalize the applied potentials. The electroosmotic velocity corresponding to the average separation potential is chosen as the velocity scale parameter. By doing so, the magnitude of the non-dimensional buffer velocity is close to 1. Since all the reservoirs are open to air, the reference pressure is chosen to be atmosphere pressure and then pressure is non-dimensionalized with $P = w(p - p_a)/(\mu \cdot \mu_{eo} E_{unif})$. In order to reduce the sensitivity and dependence of the results on parameters, a unique time scale parameter of $w/(\mu_{eo} E_{unif})$ is chosen for the unsteady species transport problem. This renders the advance of the concentration front independent of the value of $\mathrm{Re}\, Sc_i$ and it provides great intuitive interpretation of both the injection and separation phenomena. For every sample, we choose its own original value as the concentration scaling parameter, so the non-dimensional concentration will all vary between 0 and 1. As listed in Table 5-1, the individual electrophoretic mobility of every species is non-dimensionalized by the electroosmotic mobility of buffer solution. A series of $\mathrm{Re}\, Sc_i$ related to different sample diffusion coefficients in the range of $10^{-9} \sim 10^{-10}\ m^2/s$ are investigated.

In view of the geometric structure of this cross-linked microchannel, the flow will only come with the x- and y- direction. It is assumed that the dependent variables do not exhibit significant gradients in the third dimension (z- for depth). With above

assumptions, the whole set of differential equations can be simplified and discretized in the form of two-dimensional expansion.

$$\frac{\partial^2 \Phi}{\partial X^2} + \frac{\partial^2 \Phi}{\partial Y^2} = 0 \qquad [5\text{-}16]$$

$$\frac{\partial V_x}{\partial X} + \frac{\partial V_y}{\partial Y} = 0;\ \frac{\partial^2 V_x}{\partial X^2} + \frac{\partial^2 V_x}{\partial Y^2} = \frac{\partial P}{\partial X};\ \frac{\partial^2 V_y}{\partial X^2} + \frac{\partial^2 V_y}{\partial Y^2} = \frac{\partial P}{\partial Y} \qquad [5\text{-}17]$$

$$\frac{\partial C_i}{\partial \tau} + (V_x + V_{x-epi})\frac{\partial C_i}{\partial X} + (V_y + V_{y-epi})\frac{\partial C_i}{\partial Y} = \frac{1}{\mathrm{Re}\, Sc_i}\left(\frac{\partial^2 C_i}{\partial X^2} + \frac{\partial^2 C_i}{\partial Y^2}\right) \qquad [5\text{-}18]$$

**Table 5-1** Species properties and corresponding test parameters.

| Species Property | Dimensional | Non-Dimensional |
|---|---|---|
| **Electrophoretic Mobility** | $\mu_{epi}$ $[m^2/(V\cdot s)]$ | $\mu_{epi}^*$ |
| | $-2.0\times10^{-8}$ | $-0.44$ |
| | 0 | 0 |
| | $1.5\times10^{-8}$ | 0.33 |
| **Diffusion Coefficient with** $\mathrm{Re}\, Sc_i$ | $D_i$ $[m^2/s]$ | $\mathrm{Re}\, Sc_i$ |
| | $1.13\times10^{-9}$ | 25 |
| | $5.63\times10^{-10}$ | 50 |
| | $4.37\times10^{-10}$ | 64 |
| | $3.75\times10^{-10}$ | 75 |
| | $2.81\times10^{-10}$ | 100 |

## 5.3 Numerical studies

### 5.3.1 Numerical scheme

As shown in Figure 5-3(a), a set of non-uniform staggered grids is used for simulations. In order to capture the detailed features near the walls and intersection area, the size of control volumes is increased by a factor of 1.1 from walls to channel center. For the control volume size in another direction, it is also increased by the same factor for the first couples of control volumes from the exact channel square down to the reservoirs. After those non-uniform ones, the size will be kept constant to the end of channel. By this setting, a scheme of tight grids near the intersection will be formulated, where there are

multi-dimensional effects occurring. A finite control volume method and a line-by-line Gauss-Seidel iterative procedure is implemented in the numerical simulations. The SIMPLE algorithm is employed to solve the fluid flow and pressure fields. For the unsteady species transport process, a fully-implicit method in time method is utilized.

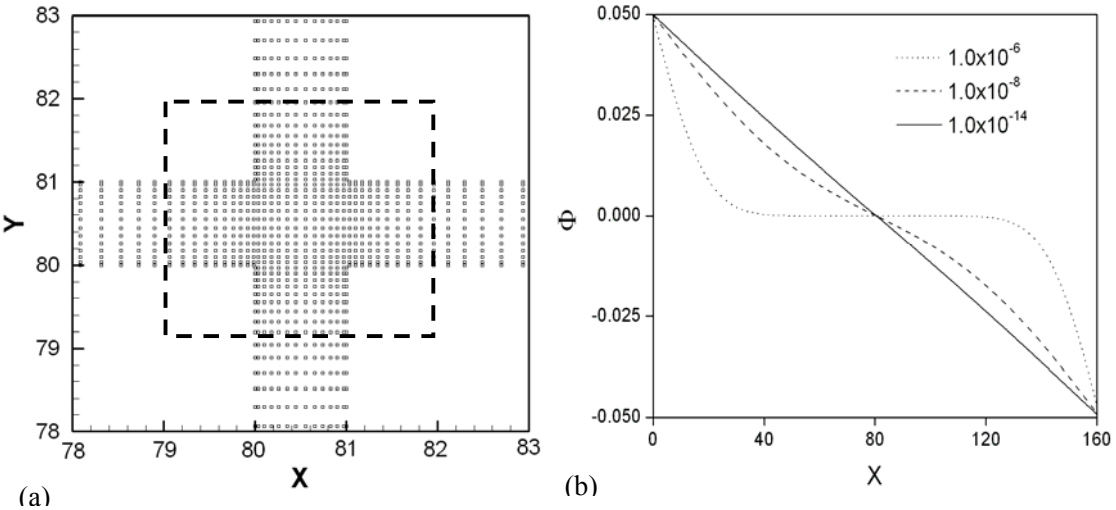


**Figure 5-3** Numerical scheme: (a) non-uniform staggered grid system; (b) convergence study of applied potential field.

### 5.3.2 Tests for reliable and accurate simulations

Grid independence tests and iteration convergence studies have been performed to ensure stable and accurate computations. Convergence studies have been performed in solving the velocity field, pressure field and concentration field. The current grid scheme (10 non-uniform control volumes across the width and 211 control volumes in each channel from the intersection to the reservoir) provided grid-independent results. For iterative procedures in numerical simulations, a fully convergence result is essential and necessary. The precise applied potential field will obviously have an important influence, because it will determine the flow field through the slip wall velocity boundary conditions and also dominate the electrophoretic flows of different species at various locations. An example of the applied electric field convergence is used to illustrate the dramatic importance of convergence studies. In Figure 5-3(b), the potential along the center of the horizontal microchannel is presented for three different convergence criteria. In this injection mode

with power supply of 0.05/0.0/-0.05/0.0 (reservoirs $R_1/R_2/R_3/R_4$), the theoretical result of potential distribution should be a straight line. It is apparent that a high convergence criteria like $1.0\times10^{-6}$ or $1.0\times10^{-8}$ will produce an inaccurate potential field. Using a much lower value of $1.0\times10^{-14}$, that used for this study, provides a fully convergent solution. Finally, a convergence study was also performed for the non-dimensional time step. It was found that the results for a non-dimensional time step of 0.01 were indistinguishable from those for 0.001 but significantly improved from those for 0.1. The results presented herein are all for the 0.01 case.

## 5.4 Results

### 5.4.1 Applied potential field and flow field

Fluid flow and mass transport in microchannel networks can be controlled by applying different potential fields to produce electrokinetic flows. In our specific application, it is operated in two different modes by switching the applied voltages on the four reservoirs within this cross-linked separation unit. Based on this symmetric microchannel network, the multi-species sample can be loaded from the sample reservoir $R_1$ to waste reservoir $R_3$ along the horizontal channel. This loading process is known as injection. After it reaches a certain state, e.g. arrival at the intersection or fully developed in the whole horizontal channel, the separation process can be initiated by switching off the voltages of the four reservoirs instantly. By applying a potential difference across reservoirs 2 and 4, the driving buffer solution will be pumped out of $R_2$ and flow downward to another waste reservoir $R_4$. At the crossing section, the sample plug from the horizontal flow will be truncated and pushed into the separation channel of $L_4$. Under the influence of the applied electrical field, the individual diffusion coefficient, and electrophoretic mobility differences, the different species in this sample plug separate as they flow through channel $L_4$.

According to two-step injection and separation processes, two typical power supply schemes are presented for injection and separation respectively in Figure 5-4. The pinched injection method is adopted here due to easy operation and symmetric sample plug. As seen from the left figure, the non-dimensional corresponding potential of $\Phi_1$~$\Phi_4$

is 0.05/F/-0.05/F and the linear drop of potential field from $R_1$ to $R_3$ is clearly predicted by numerical results. Because of the uniform buffer solution and almost uniform applied potential field, the bulk fluid velocity is going to be almost same everywhere except for the crossing section area. There is some fluid and species flowing into the vertical channel and back to horizontal channel. Two factors account for this phenomena. One is the local potential distribution which governs the bulk fluid flow. There will be zero potential at the exact centerline of vertical channel, but the potential gradient on both sides is not zero, especially near the intersection. The other factor is species diffusion, which is dependent on time. Both factors will draw some sample concentration into vertical channel and make the non-dimensional species concentration in $L_3$ less than 1.

The separation phase with non-dimensional potential of F/0.05/F/-0.05 is shown in the right figure with analogous potential and velocity fields. An induced non-uniform pressure field appears near the intersection due to the special channel structure as has been presented in our previous study. The relative pressure between peak values at the channel corners and atmosphere pressure is found to be essentially negligible. Similarly, different configurations of applied voltages in all reservoirs will produce various potential fields and then cause corresponding electrokinetic flows and species transport inside the channel network. Prior to study how species spread, the applied potential field and subsequent flow field should be solved in advance.

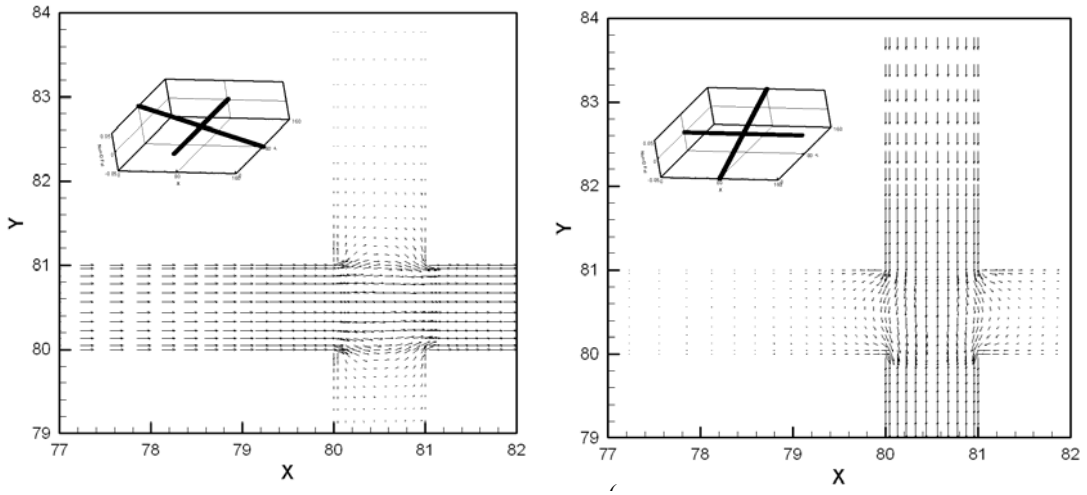


**Figure 5-4** Typical potential and velocity field for injection (left) and separation (right) process.

### 5.4.2 Single species transport process

In order to understand the species movement intuitively, the negatively charged species which has the lowest speed is utilized as default for the investigation. Under the above injection potential setup, species are gradually pumped into the microchannel from sample reservoir $R_1$. In Figure 5-5, three typical stages during the whole injection process are presented by its concentration field in two-dimensional format. They are pre-cross, on-cross and post cross, and corresponding injection time are 8.9s, 17.8s and 36.7s respectively. It should be noted that species concentration decreases from white to black in the figures. If not specially stated, the white region inside the microchannel refers to pure species, while the black area means pure buffer solution. In a mixed zone, the degree of grey is proportional to the ratio of buffer/species amount.

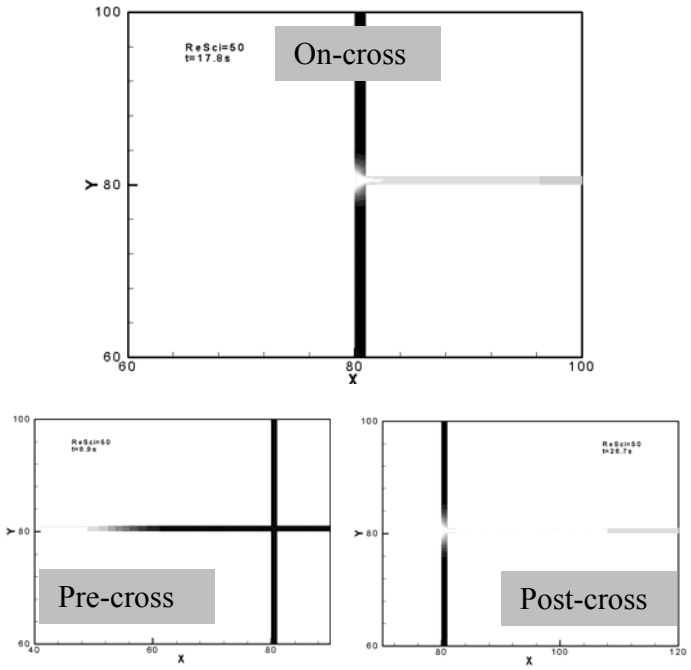


**Figure 5-5** Three typical stages during injection process expressed by concentration contour: pre-, on- and post-cross.

By an alternative way, the centerline concentration is utilized to reveal the transient loading process in Figure 5-6. In the left figure, the concentration profile along the horizontal channel is displayed at a constant time interval of 4.5s. A series of sample

fronts clearly indicate the species transport with time development. It will take 13.5s for the sample front to arrive at the intersection. After the species front passes the intersection, the magnitude of the maximum concentration is found to be smaller than 1, which is caused by buffer leakage from the vertical channel to the right wing. The slope change of the sample front profile vividly shows the diffusion development which occurs at the interface between the species and pure buffer.

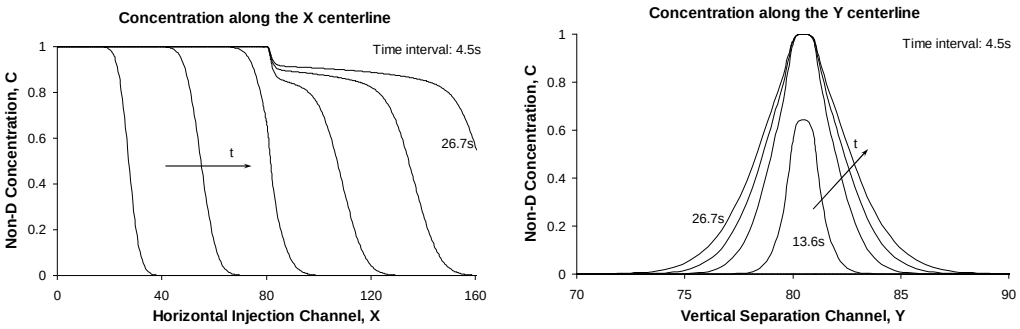


**Figure 5-6** Description of single species injection by concentration profile along the microchannel centerlines: species front movement in the horizontal channel (left) and sample plug growth in the vertical channel (right).

Concentration development along the vertical channel centerline is recorded in the right figure. There are two contours at the early injection stage where the sample front hasn't yet reached the cross and this region is still occupied by pure buffer. The sample dispersion into vertical channel happens quickly when the front approaches the intersection. However this process will become slow later on. The former case is mainly dominated by local circulation, which will drive the newly arrived front samples into the vertical channel quickly. When it reaches a 'steady' state, the dispersion to the vertical channel will be governed only by slow diffusion. After the species transport is fully developed in the horizontal channel, the total amount of sample in the vertical channel will increase at a slow rate by diffusion leakage.

At a certain time after the sample front passed the channel cross, the applied voltages on the four reservoirs will be switched 90 degree clockwise into the separation case (F/0.05/F/-0.05). A potential difference is established across the vertical channel. The sample in the cross will be truncated and pumped into the down wing channel. Movement

of the sample plug can be seen from a series of concentration contours at different time steps in Figure 5-7. At three different separation time of 1.78s, 3.56s and 5.34s, the sample plug will arrive at three locations (Y=70, 60 and 50) respectively. The sample plug moves downward under the separation potential field. At the longer separation time of 10.68s, it almost reaches the end of the separation channel and then moves into the waste reservoir 4.

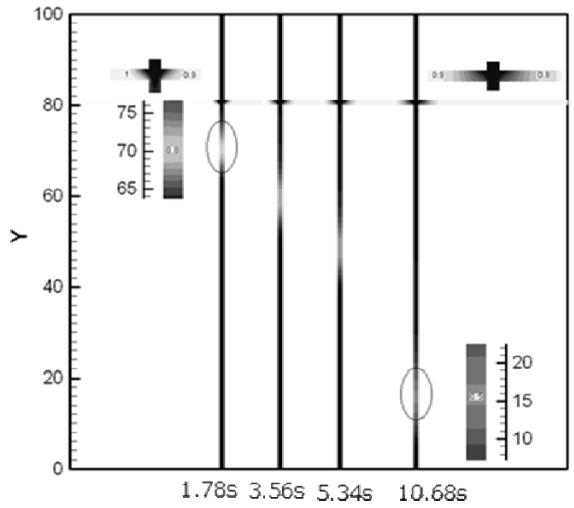


**Figure 5-7** Sample plug movement and evolvement in the vertical channel during separation process.

The diffusion effect can be seen clearly from the dramatic change of sample plug distribution. With time passing by, the sample plug becomes wider and darker. It is due to the high concentration gradient on both edges of the sample plug, which causes a bi-directional diffusion. This phenomenon results in band broadening and peak concentration decrease, which should be minimized as much as possible to achieve high quality separation. In addition, the diffusion also works to change the sample plug shape. Triangle sample plugs in early separation stages becomes rectangular later on. This is because diffusion also happens in the cross-stream direction, because of cross-stream concentration gradients at the interface. Leakage effect caused by the specific potential and flow is also identified in the separation process through the growth of buffer region at the intersection. Species in the horizontal channel is getting more and more contaminated by buffer solution near the channel cross.

### 5.4.3 Multi-species injection and separation

In practical operations, a mixture of all species will be loaded from the common sample reservoir 1. Besides diffusion coefficient, species' movements are also influenced by the individual electrophoretic mobilities, which mainly results from their mass and net charges. Due to differing velocities, it is important to monitor species movement and determine the critical time to switch applied potentials. Three species with different electrophoretic mobilities are studied during injection in Figure 5-8 . As shown before, the diffusion coefficient will have a slight influence on species injection and the same diffusion coefficient with an equivalent $\mathrm{Re}\,Sc_i$ of 25 is applied here. At the same injection time of 13.4s, the positively charged sample has filled up the whole horizontal channel. The front of the neutral species almost reaches the waste reservoir 3, because it doesn't have extra migration effect and moves together with the bulk fluid. The species with a negative electrophoretic mobility just arrives at the channel cross at this time spot because it moves at the lowest speed.

If we switched applied potentials to separation at an injection time earlier than 13.4s, the generated sample plug wouldn't contain any amount of negatively charged species. It will apparently lead to a faulty operation. In contrast, if the applied potentials were switched too late, excessive leakage into the vertical channel would introduce a broad sample plug and then produce low separation resolution. Therefore, it is important to study the transient injection and determine the optimized operation time accordingly.

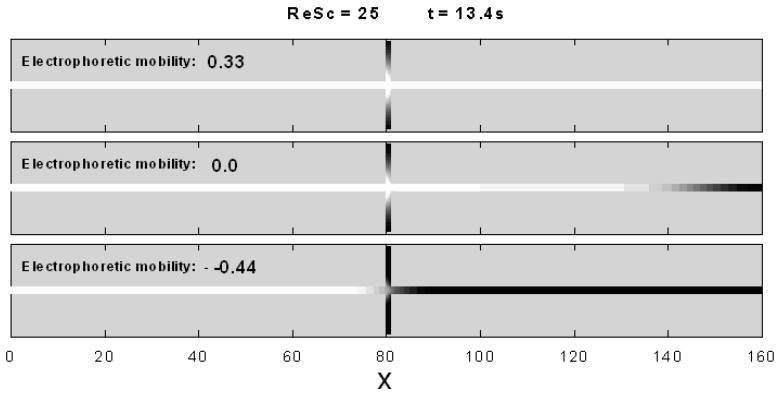


**Figure 5-8** Transient injection process of three kinds of samples: neutral, positively and negatively charged species with different non-dimensional electrophoretic mobilities.

In our default case, the sample plug is generated conservatively by switching applied potentials at the injection time of 35.6s, when the front of slowest species just moves out of the horizontal channel. The injection channel is occupied by all three species and a sample plug including all species will be produced for further separation analysis. Relevant concentration profiles for the state of final injection or initial separation are showed in the left part of Figure 5-9.

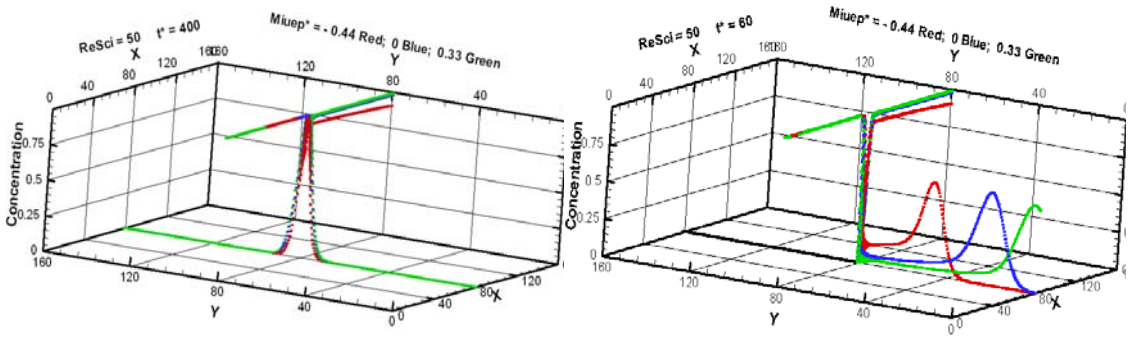


**Figure 5-9** Concentration profile for final injection or initial separation (left) and a certain separation stage (right).

During the injection process, species are provided continuously from the upstream sample reservoir 1. The buffer solution is replaced by species. However, species movement during separation is totally different. Sample plugs will move forward with the buffer solution in the separation process. Because of differing electrophoretic mobilities, their actual velocities are different and thus the species become separated gradually. Although they start to move from the same location simultaneously, different species will pass a detector at differing physical times. In the right part of Figure 5-9, a separation result is revealed by individual concentration profile at a certain separation time of 5.34s. The species are separated into three different groups and the peak concentration for every species is decreased from 1.0 to 0.7 approximately. This extensive band broadening is due to the unavoidable diffusion effect. In fact, species can be detected, sorted and analyzed if the peak concentration is over the detector limit.

## 5.5 Effects of species properties

### 5.5.1 Diffusion coefficients: $\mathrm{Re}\,Sc_i$

Under a specific applied potential field, the electroosmotic flow will be steady for uniform buffer solutions. Once the flow is determined, effect of species' diffusion coefficients, through $\mathrm{Re}\,Sc_i$, can be investigated. As mentioned before, the species' diffusion coefficients are chosen from a typical range of $10^{-9} \sim 10^{-10} m^2/s$ and the magnitudes of typical $\mathrm{Re}\,Sc_i$ are 25, 50 and 100 for test.

For these values of $\mathrm{Re}\,Sc_i$ it is found that the species transport process is highly convection dominated. The effects of bulk flow and individual electrophoretic flow prevail over diffusion effects. With the same electroosmotic flow and electrophoretic mobilities, all three species reach the same location at the same time. This is a significant benefit of the non-dimensional velocity in the manner we chose. The influence of differing diffusivity can be seen from the concentration contours when species passed through the intersection area. In Figure 5-10(a), the non-dimensional electrophoretic mobility is -0.44 and non-dimensional time is 200 after initiation of injection. From the iso-concentration contour plots, the species for $\mathrm{Re}\,Sc_i$ 25 has a higher diffusion coefficient and has diffused into the vertical channel a little more than the other two species. As a result, it will reduce the amount being spread to the downstream right horizontal channel. In addition, the decrease in the concentration contour in the vertical channel could be considered a result of the specific flow circulation occurring locally. Sample leakage to the separation channel is primarily attributed to diffusion and the distortion of the injection electrical field. From the small differences among the contour plots for these three $\mathrm{Re}\,Sc_i$ species, it can be concluded that diffusion effects don't influence the sample plug shape significantly for typical buffer solutions and species.

In Figure 5-10(b), the line concentration along the horizontal microchannel centerline is presented. At the pre-cross non-dimensional time of 100, there is a little concentration difference between the two species for $\mathrm{Re}\,Sc_i$ 25 and 100, which means that convection determines their transport far more than diffusion. When their interfaces reach the cross

at a non-dimensional time of 150, the concentration for $\mathrm{Re}\,Sc_i$ 25 drops faster and this is caused by its extra dispersion leakage into the vertical channel. For the post-cross state at a non-dimensional time of 300, the low concentration for $\mathrm{Re}\,Sc_i$ 100 is also attributed to its small diffusion. Besides the bulk convection, diffusion differences should appear during such a long time period (approximately 27 seconds real time).

The $\mathrm{Re}\,Sc_i$ will influence the band-width of every species in separation process. Because of the short separation time and low diffusion coefficients of the species studied, it is found that there is no obvious influence on separation resolution of the diffusion differences. In both injection and separation process, this kind of convection dominated flow will allow only a very slight influence as a result of the species' diffusion.

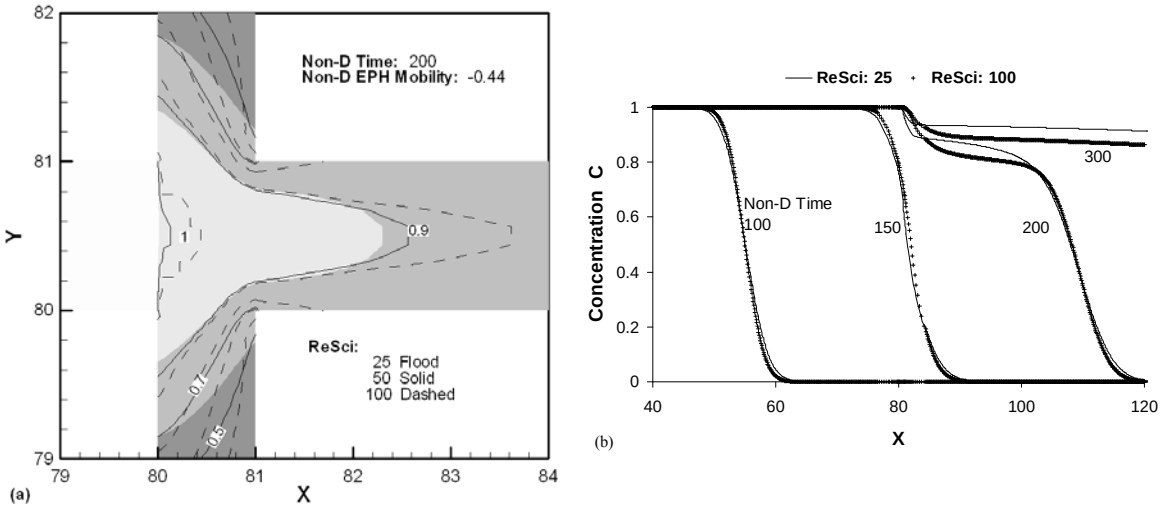


**Figure 5-10** Concentration contours of (a) different $\mathrm{Re}\,Sc_i$ at a certain injection time and (b) centerline concentration comparison of two $\mathrm{Re}\,Sc_i$ at different injection time.

### 5.5.2 Electrophoretic mobility

It should be noted that all the species' electrophoretic mobilities are non-dimensionalized by the buffer electroosmotic mobility of $4.5\times10^{-8}\ m^2/V\cdot s$. Three typical species with non-dimensional electrophoretic mobility of 0, -0.44 and 0.33, are neutral, negative and positive charged respectively. Different electrophoretic mobilities will introduce different apparent velocities for every species; this is the primary mechanism to cause separation

and will have considerable influence on the analysis process. As discussed above, the front of all species will pass through the cross at different injection time, so it is important to study the unsteady injection process and find the optimized time to switch potentials.

During separation, the difference in electrophoretic mobilities accounts for the differences in the species' peak concentration time at the observation station, and accounts for the separation distance between species. In the right part of Figure 5-9, the separation result of three species is clearly exhibited by their centerline concentration at a non-dimensional separation time of 60. Here, separation time refers to time measured after the switch from injection to separation. All three species are assumed to have the same diffusion coefficient with a common $\mathrm{Re}\,Sc_i$ 50. The separation starts after a non-dimensional time of 400 for injection, at which time there is an acceptable balance between species being fully injected and there being low dispersion into vertical channel.

In Figure 5-11, the concentration contours for three species are displayed in parallel at different times during separation. It is clear that the positive electrophoretic mobility moves the species downstream much more quickly. It should be noted that the three images of the sample plug at the top correspond to the final injection state, or initial separation state, and there is a uniform time interval (non-dimensional time of 20) between the adjacent sample plug images for each of the species. In addition, the peak non-dimensional concentration decreases from white (1) to black (0) in the concentration field. This result is comparable to experimental results based on laser-induced fluorescence (LIF) detection of separation analysis where the magnitude of the species' concentration corresponds to the observed intensity of fluorescence.

The species with positive electrophoretic mobility move downward fastest. At the non-dimensional separation time of 60, its interface almost flows into the waste reservoir while the negatively charged species hasn't reached the mid-point of separation channel. Even at the non-dimensional separation time of 120, the species with non-dimensional electrophoretic mobility of -0.44 has just arrived at the location of Y=15. The neutral species with zero electrophoretic mobility moves with the bulk motion velocity and reaches the neutral location as expected. The brightness of the sample plugs becomes less

as the plugs are transported in the separation channel from the cross-channel to waste reservoir $R_4$ as a result of diffusion during the transport down the channel over time. The species in the sample plug will diffuse into the bulk fluids on both sides of the plug. Diffusion can also be seen in the three images at the initial state of separation. The images of the initial sample plugs become narrow and less bright as the non-dimensional electrophoretic mobility decreases from 0.33 to 0 to -0.44. This is because, with a bigger composite (electroosmotic plus electrophoretic) velocity, the positively charge species will arrive at the cross first and stay there longer prior to the electrical field switch, which happens at the same time for all three. This longer residence time allows more diffusion into the vertical channel.

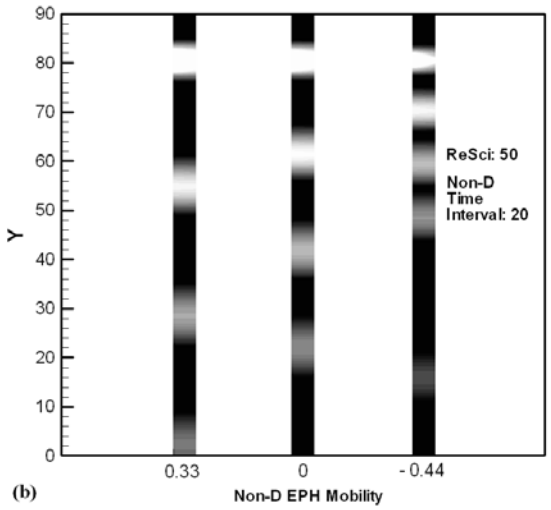


**Figure 5-11** Three species' electrophoretic separation process: sample plugs' evolving movement expressed by concentration contour with a same time interval (non-dimensional time of 20).

## 5.6 Concluding remarks

The complete numerical model has been developed for application to the study of electrokinetic fluid flow and species transport in microchannels. It has been formulated in non-dimensional form and utilizes a unique method to non-dimensionalize the species transient term in the unsteady injection and separation processes. As a result, it is easy to predict where the species front will be at any given time or, conversely, how long it will

take the species front to reach a prescribed location, for example the end of the injection channel or the separation observation station.

Based on a developed finite control volume method, all the governing equations are discretized and solved numerically with reliable algorithms, such as the SIMPLE algorithm for flow field. A non-uniform staggered grid system with 10 control volumes across the channel width and 211 control volumes on each side of the channel intersection provided grid-independent solutions. Convergence studies have been performed to ensure numerical accuracy. A very small iterative convergence criterion was required to ensure iterative convergence, particularly for the potential field since gradients are required to determine electric field strength.

Typical cases for injection and separation are presented showing the corresponding applied potential field and flow field. The electrokinetic transport characteristics for both processes in microchannels are numerically revealed and explained. The effect of the $\mathrm{Re}\, Sc_i$, which characterizes the relative role of convection versus diffusion, is examined for four different values typical of the microchannel separation application. The species' diffusion coefficients are found to have essentially a negligible effect on injection plug shape. In the meanwhile, an application to separate three different but typical species is considered, each species having a different electrophoretic mobility. From the numerically simulated injection and separation processes, the species' differences in electrophoretic mobilities provide us the importance of real-time monitored injection and those differences are also seen to play a key role in the ability to produce and enhance electrophoretic separation.

# Chapter 6

# Conclusions and future work

## 6.1 Conclusions

Through the numerical work in current studies, fluid flow and mass transport phenomenon in microchannels were studied and well understood by three different applications. The complete theoretical model coupled with applied potential field, flow field and species concentration field was constructed with a whole set of governing equations. Based on the reasonable assumptions and simplifications, the problems were studied numerically with our developed codes to simulate the different on-chip fluid flow and mass transport processes. Besides the reliable schemes and algorithms, adequate numerical tests were performed to ensure the accurate results and economical computation. By investigating various controlling parameters and effects, the improved understandings can provide guidance for future enhanced controls and innovative designs of such kinds of lab-on-a-chip/microfluidic chip applications. Different research concerns were put into the three separate projects, and the contributions and recommendations for each of them were outlined as following.

1. In the surface patterning and microfabrication project, attempts were tried to control the width of laminar streams and the width of their interfaces in a cross-linked microchannel network. Different controlled parameters were investigated numerically to achieve this goal. The applied potentials, electroosmotic mobilities of solutions and the channel dimensions (the ratio of horizontal channel width over the vertical channel width) were found to have significant effects to specify the laminar flows in microchannels. However, the diffusion coefficients of various stream solutions would have less influence due to the adoption of these high Peclet number flows. Based on the numerical studying of the parameters mentioned above, different combinations of them will ensure the flow and mass transport within microchannels in a controllable manner. The optimized

configurations can be explored numerically and then be employed for particular surface pattern or microfabrication purposes.

2. For the study of microwashing process with replaced solutions in straight microchannels, attention was mainly paid to the influences of electrolyte solution properties on electroosmotic flow and the coherent solution displacement process. A three-dimensional theoretical model was developed and used to investigate the flow structure, pressure distribution and concentration field evolvement during this typical washing procedure in microchannels. The chemical properties differences of the two replaced solutions were found to have remarkable influences from the numerical results. The induced non-uniformity of solutions' electroosmotic mobilities and electrical conductivities would account for the exceptional change of electroosmotic flow structure, induced pressure field and specific solution displacement process. Some characteristic flows like the inlet/outlet back flows and distorted plug-like velocity profiles were numerically revealed, and corresponding reasons for those phenomena were also explored and discussed in details. A linear effect of applied potential field strength on electroosmotic flow and solution displacement was observed finally.

3. Microchip capillary electrophoresis had broad applications in chemical and biological separation analysis areas. Design and control of this kind of microfluidic chip and related devices were very important. Whereas, a thorough understanding on the fundamental knowledge of involved fluid flow and mass transport process was the basis to fulfill successful designs and controls. A complete non-dimensional model (and maybe a future analysis or design tool) was established in this study. The advantages using it to perform parametric studies include the flexibility it offers to alter each controlling parameter and the physical insight it provides. Through studying the unsteady one-step pinched injection and separation processes within cross-linked microchannels, species transport characteristics, including both species movement during injection and sample plug development in separation, were numerically revealed and discussed. Species' diffusion effect was examined for both processes and it was found to have negligible influence. The separation principle was attributable to species'

electrophoretic mobility differences. Some fundamental phenomena like real-time injection control were well interpreted. Those numerical results were applicable and valuable for further separation evaluation and practical operation.

## 6.2 Future work

### 6.2.1 Experimental validations

In general, theoretical model was developed to study the on-chip fluid flow and mass transport phenomenon in microchannels. The applied potential field, fluid flow field and species concentration field were described and numerically solved for different applications. The results and findings through parametric studies were all based on computer simulations. Various assumptions and simplifications were made in the theoretical model prior to discretizing the differential equations and developing codes. However, the validity and accuracy should be validated by real application in physics, where similar experimental studies are anticipated and recommended.

For example, the surface patterning or microfabrication can be run in the lab-scale to study the deposition or etching process using controlled laminar flow in cross-linked microchannels. The different configurations in terms of these controlling parameters can be explored experimentally and compared with related numerical simulations. Similarly, experiments can be performed to investigate the characteristic flow structure during the displacement process and to validate the distorted velocity field, induced pressure field and non-uniform applied electrical field. For the on-chip species injection and separation for MCE applications, the real biological fragments may not be applicable in current stage, but different substitutes like fluorescent or rhodamine dyes can be applied in the experimental validations. Utilizing the developed LIF detection technique; the on-chip species transport process can be simulated and visualized experimentally.

In a word, experimental validation of above numerical results will be one major branch of future work on current studies. Based on that, some modifications will then be made to the theoretical model. Iterative studies between experiments and numerical simulations will make the model and tool more accurate for effective predictions.

### 6.2.2 Separation analysis and sample pug control for MCE

Due to the broad MCE application and continuable numerical studies, emphasis is put here to address the potential extended research of the on-chip species injection/separation project. So far, a basic understanding of the species transport during pinched injection and separation has been obtained. And the effects of species' properties like diffusivity and electrophoretic mobility on the transport process have also been identified through our numerical simulations. However, the separation process hasn't been revealed and evaluated based on the established complete numerical model.

As future studies, multi-species separation analysis will be performed with some developing evaluating parameters, such as separation resolution for performance judgment, peak concentration for signal detectability and separation speed or efficiency for device reliability. The effects of different injection parameters on separation result can be justified and on the contrary, the separation channel length and resolution can be estimated theoretically. At the same time, the applicability of our numerical prediction can be verified through comparison with the experimental results by other researchers.

In addition, the generated sample plug in the channel cross is identified to play an important role on the electrophoretic separation performance. An optimized sample plug with ideal shape and size is supposed to produce excellent separation result with big separation resolution and high peak concentration. Previous investigators have tried many ways to control the sample plugs, such as developing different injectors (Tee, cross, double-Tee, multi-Tee, etc) and designing various injection modes (pinched, gated, double-L, etc). Based on the developed theoretical model, a multi-stage dynamic injection method is proposed to produce the characteristic sample plugs with desired properties. Employing the standard cross injector and conventional pinched injection mode studied here, this technique mainly relies on the innovative applied potential control, in which parametric studies of applied potentials and precise operation time are essential. In the future studies, other controlling parameters in our complete model, such as channel dimension, solution and sample properties, injector geometry and injection mode, are expected to be explored for featured designs and new controls.

# References


1. Klug, W.S., *Essentials of Genetics*. 2005, Upper Saddle River, NJ: Pearson Prentice Hall.
2. Berthier, J., *Microfluidics for Biotechnology*. 2006, Norwood: Artech House.
3. Vilkner, T., D. Janasek, and A. Manz, *Micro total analysis systems. Recent developments.* Analytical Chemistry, 2004. **76**(12): p. 3373-3385.
4. Dittrich, P.S., K. Tachikawa, and A. Manz, *Micro total analysis systems. Latest advancements and trends.* Analytical Chemistry, 2006. **78**(12): p. 3887-3907.
5. Gao, J., X.F. Yin, and Z.L. Fang, *Integration of single cell injection, cell lysis, separation and detection of intracellular constituents on a microfluidic chip.* Lab on a Chip, 2004. **4**(1): p. 47-52.
6. Hashimoto, M., et al., *Rapid PCR in a continuous flow device.* Lab on a Chip, 2004. **4**(6): p. 638-645.
7. Liu, R.H., et al., *Self-contained, fully integrated biochip for sample preparation, polymerase chain reaction amplification, and DNA microarray detection.* Analytical Chemistry, 2004. **76**(7): p. 1824-1831.
8. Bruin, G.J.M., *Recent developments in electrokinetically driven analysis on microfabricated devices.* Electrophoresis, 2000. **21**(18): p. 3931-3951.
9. Weigl, B.H., R.L. Bardell, and C.R. Cabrera, *Lab-on-a-chip for drug development.* Advanced Drug Delivery Reviews, 2003. **55**(3): p. 349-377.
10. Fu, L.M., et al., *Electrokinetically driven micro flow cytometers with integrated fiber optics for on-line cell/particle detection.* Analytica Chimica Acta, 2004. **507**(1): p. 163-169.
11. Woolley, A.T. and R.A. Mathies, *Ultra-high-speed DNA-sequencing using capillary electrophoresis chips.* Analytical Chemistry, 1995. **67**(20): p. 3676-3680.
12. Liu, S.R., et al., *Automated parallel DNA sequencing on multiple channel microchips.* Proceedings of the National Academy of Sciences of the United States of America, 2000. **97**(10): p. 5369-5374.
13. Sohni, Y.R., et al., *Microfluidic chip-based method for genotyping microsatellites, VNTRs and insertion/deletion polymorphisms.* Clinical Biochemistry, 2003. **36**(1): p. 35-40.
14. Ramsey, J.D., et al., *High-efficiency, two-dimensional separations of protein digests on microfluidic devices.* Analytical Chemistry, 2003. **75**(15): p. 3758-3764.
15. Lagally, E.T., I. Medintz, and R.A. Mathies, *Single-molecule DNA amplification and analysis in an integrated microfluidic device.* Analytical Chemistry, 2001. **73**(3): p. 565-570.

16. Jacobson, S.C. and J.M. Ramsey, *Mcirochip electrophoresis with sample stacking.* Electrophoresis, 1995. **16**(4): p. 481-486.

17. Woolley, A.T., G.F. Sensabaugh, and R.A. Mathies, *High-speed DNA genotyping using microfabricated capillary array electrophoresis chips.* Analytical Chemistry, 1997. **69**(11): p. 2181-2186.

18. Fluri, K., et al., *Integrated capillary electrophoresis devices with an efficient postcolumn reactor in planar quartz and glass chips.* Analytical Chemistry, 1996. **68**(23): p. 4285-4290.

19. Harrison, D.J., et al., *Micromaching a miniaturized capillary electrohophoresis-based chemical-analysis system on a chip.* Science, 1993. **261**(5123): p. 895-897.

20. Harrison, D.J., et al., *Capillary electrophoresis and sample injection systems integrated on a planar glass chip.* Analytical Chemistry, 1992. **64**(17): p. 1926-1932.

21. Lipman, J., *Microfluidics puts big labs on small chips.* Edn, 1999. **44**(26): p. 79-+.

22. Locascio, L.E., C.E. Perso, and C.S. Lee, *Measurement of electroosmotic flow in plastic imprinted microfluid devices and the effect of protein adsorption on flow rate.* Journal of Chromatography A, 1999. **857**(1-2): p. 275-284.

23. Schmalzing, D., et al., *DNA sequencing on microfabricated electrophoretic devices.* Analytical Chemistry, 1998. **70**(11): p. 2303-2310.

24. Xia, Y.N. and G.M. Whitesides, *Soft lithography.* Annual Review of Materials Science, 1998. **28**: p. 153-184.

25. Hunter, R.J., *Zeta potential colloid science*. 1981, London: Academic Press.

26. Ren, C., *Course notes of ME770-Microfluidics*. University of Waterloo.

27. Zimmermann, R., S. Dukhin, and C. Werner, *Electrokinetic measurements reveal interfacial charge at polymer films caused by simple electrolyte ions.* Journal of Physical Chemistry B, 2001. **105**(36): p. 8544-8549.

28. Sze, A., et al., *Zeta-potential measurement using the Smoluchowski equation and the slope of the current-time relationship in electroosmotic flow.* Journal of Colloid and Interface Science, 2003. **261**(2): p. 402-410.

29. Masliyah, J.H., *Electrokinetic colloid transport phenomena*. 2006, Hoboken, New Jersey.: John Wiley Sons Inc.

30. Tabeling, P., *Introduction to microfluidics*. 2005, Oxford: Oxford University Press.

31. Chen, C.H. and J.G. Santiago, *A planar electroosmotic micropump.* Journal of Microelectromechanical Systems, 2002. **11**(6): p. 672-683.

32. Erickson, D., et al., *Electrokinetically controlled DNA hybridization microfluidic chip enabling rapid target analysis.* Analytical Chemistry, 2004. **76**(24): p. 7269-7277.

33. Hu, Y.D., C. Werner, and D.Q. Li, *Influence of three-dimensional roughness on pressure-driven flow through microchannels.* Journal of Fluids Engineering-Transactions of the Asme, 2003. **125**(5): p. 871-879.

34. Lu, F.Z., J. Yang, and D.Y. Kwok, *Flow field effect on electric double layer during streaming potential measurements.* Journal of Physical Chemistry B, 2004. **108**(39): p. 14970-14975.

35. Singh, A.K., E.B. Cummings, and D.J. Throckmorton, *Fluorescent liposome flow markers for microscale particle image velocimetry.* Analytical Chemistry, 2001. **73**(5): p. 1057-1061.

36. Laser, D.J. and J.G. Santiago, *A review of micropumps.* Journal of Micromechanics and Microengineering, 2004. **14**(6): p. R35-R64.

37. Taylor, G.I., *Dispersion of soluble matter in solvent flowing slowly through a tube.* Proc. Roy. Soc. Lond., A, 1953. **219**(1137): p. 186-203.

38. Xuan, X.C., *Joule heating in electrokinetic flow.* Electrophoresis, 2008. **29**(1): p. 33-43.

39. Tang, G.Y., et al., *Joule heating and its effects on electrokinetic transport of solutes in rectangular microchannels.* Sensors and Actuators a-Physical, 2007. **139**(1-2): p. 221-232.

40. Tang, G.Y., et al., *Joule heating effect on electroosmotic flow and mass species transport in a microcapillary.* International Journal of Heat and Mass Transfer, 2004. **47**(2): p. 215-227.

41. Crabtree, H.J., et al., *Microchip injection and separation anomalies due to pressure effects.* Analytical Chemistry, 2001. **73**(17): p. 4079-4086.

42. Walker, G.M. and D.J. Beebe, *A passive pumping method for microfluidic devices.* Lab on a Chip, 2002. **2**(3): p. 131-134.

43. Biddiss, E., D. Erickson, and D.Q. Li, *Heterogeneous surface charge enhanced micromixing for electrokinetic flows.* Analytical Chemistry, 2004. **76**(11): p. 3208-3213.

44. Chang, C.C. and R.J. Yang, *Computational analysis of electrokinetically driven flow mixing in microchannels with patterned blocks.* Journal of Micromechanics and Microengineering, 2004. **14**(4): p. 550-558.

45. Jacobson, S.C., T.E. McKnight, and J.M. Ramsey, *Microfluidic devices for electrokinetically driven parallel and serial mixing.* Analytical Chemistry, 1999. **71**(20): p. 4455-4459.

46. Jacobson, S.C. and J.M. Ramsey, *Electrokinetic focusing in microfabricated channel structures.* Analytical Chemistry, 1997. **69**(16): p. 3212-3217.

47. Yang, R.J., et al., *A new focusing model and switching approach for electrokinetic flow inside microchannels.* Journal of Micromechanics and Microengineering, 2005. **15**(11): p. 2141-2148.

48. Alarie, J.P., S.C. Jacobson, and J.M. Ramsey, *Electrophoretic injection bias in a microchip valving scheme.* Electrophoresis, 2001. **22**(2): p. 312-317.

49. Ren, L.Q. and D.Q. Li, *Theoretical studies of microfluidic dispensing processes.* Journal of Colloid and Interface Science, 2002. **254**(2): p. 384-395.

50. Henry, D.C., *The cataphoresis of suspended particles, Part 1. The equation of cataphoresis,.* Proc. Roy. Soc. Lond., , 1931. **133A**: p. 106–129.

51. Sinton, D., L.Q. Ren, and D.Q. Li, *Visualization and numerical modelling of microfluidic on-chip injection processes.* Journal of Colloid and Interface Science, 2003. **260**(2): p. 431-439.

52. Oddy, M.H., *Electrokinetic transport phenomena*. 2005, Stanford University.

53. Santiago, J.G., et al., *A particle image velocimetry system for microfluidics.* Experiments in Fluids, 1998. **25**(4): p. 316-319.

54. Kane, R.S., et al., *Patterning proteins and cells using soft lithography.* Biomaterials, 1999. **20**(23-24): p. 2363-2376.

55. Kenis, P.J.A., R.F. Ismagilov, and G.M. Whitesides, *Microfabrication inside capillaries using multiphase laminar flow patterning.* Science, 1999. **285**(5424): p. 83-85.

56. Regenberg, B., et al., *Use of laminar flow patterning for miniaturised biochemical assays.* Lab on a Chip, 2004. **4**(6): p. 654-657.

57. Zhao, B., J.S. Moore, and D.J. Beebe, *Surface-directed liquid flow inside microchannels.* Science, 2001. **291**(5506): p. 1023-1026.

58. Birzu, A., et al., *Modelling of spatiotemporal patterns during metal electrodissolution in a cell with a point reference electrode.* Physical Chemistry Chemical Physics, 2000. **2**(12): p. 2715-2724.

59. Evstrapov, A.A., et al., *Rapid analysis of oligonucleotides on a planar microfluidic chip.* Journal of Analytical Chemistry, 2004. **59**(6): p. 521-527.

60. Backhouse, C., et al., *DNA sequencing in a monolithic microchannel device.* Electrophoresis, 2000. **21**(1): p. 150-156.

61. Fu, L.M. and C.H. Lin, *High-resolution DNA separation in microcapillary electrophoresis chips utilizing double-L injection techniques.* Electrophoresis, 2004. **25**(21-22): p. 3652-3659.

62. Esch, M.B., et al., *Detection of viable Cryptosporidium parvum using DNA-modified liposomes in a microfluidic chip.* Analytical Chemistry, 2001. **73**(13): p. 2952-2958.

63. Jiang, G.F. and D.J. Harrison, *mRNA isolation in a microfluidic device for eventual integration of cDNA library construction.* Analyst, 2000. **125**(12): p. 2176-2179.

64. Palkova, Z., et al., *Single-cell analysis of yeast, mammalian cells, and fungal spores with a microfluidic pressure-driven chip-based system.* Cytometry Part A, 2004. **59A**(2): p. 246-253.

65. Huang, Y., et al., *MEMS-based sample preparation for molecular diagnostics.* Analytical and Bioanalytical Chemistry, 2002. **372**(1): p. 49-65.

66. Shapiro, H.M., *Practical fow cytometry* 1995, New York: Wiley–Liss.

67. Miltenyi, S., et al., *High-gradient magnetic cell-separation with macs.* Cytometry, 1990. **11**(2): p. 231-238.

68. Irimia, D., R.G. Tompkins, and M. Toner, *Single-cell chemical lysis in picoliter-scale closed volumes using a microfabricated device.* Analytical Chemistry, 2004. **76**(20): p. 6137-6143.

69. Schilling, E.A., A.E. Kamholz, and P. Yager, *Cell lysis and protein extraction in a microfluidic device with detection by a fluorogenic enzyme assay.* Analytical Chemistry, 2002. **74**(8): p. 1798-1804.

70. Zsido, T.J., et al., *Induction of heat-labile sites in DNA of mammalian-cells by the antitumor alkylating drug CC-1065.* Biochemistry, 1991. **30**(15): p. 3733-3738.

71. Lee, S.W. and Y.C. Tai, *A micro cell lysis device.* Sensors and Actuators a-Physical, 1999. **73**(1-2): p. 74-79.

72. Di Carlo, D., K.H. Jeong, and L.P. Lee, *Reagentless mechanical cell lysis by nanoscale barbs in microchannels for sample preparation.* Lab on a Chip, 2003. **3**(4): p. 287-291.

73. Jamasbi, R.J., et al., *Genetic analysis of Pseudomonas aeruginosa by enterobacterial repetitive intergenic consensus polymerase chain reaction (PCR) and arbitrarily primed PCR : Gel analysis compared with microchip gel electrophoresis.* Infection Control and Hospital Epidemiology, 2004. **25**(1): p. 65-71.

74. Zhou, Z.M., et al., *Determination of SARS-coronavirus by a microfluidic chip system.* Electrophoresis, 2004. **25**(17): p. 3032-3039.

75. Herr, A.E., et al., *On-chip coupling of isoelectric focusing and free solution electrophoresis for multidimensional separations.* Analytical Chemistry, 2003. **75**(5): p. 1180-1187.

76. Xu, F. and Y. Baba, *Polymer solutions and entropic-based systems for double-stranded DNA capillary electrophoresis and microchip electrophoresis.* Electrophoresis, 2004. **25**(14): p. 2332-2345.

77. Breadmore, M.C., et al., *Microchip-based purification of DNA from biological samples.* Analytical Chemistry, 2003. **75**(8): p. 1880-1886.

78. Shevkoplyas, S.S., et al., *Biomimetic autoseparation of leukocytes from whole blood in a microfluidic device.* Analytical Chemistry, 2005. **77**(3): p. 933-937.

79. Taylor, M.T., et al., *Simulation of microfluidic pumping in a genomic DNA blood-processing cassette.* Journal of Micromechanics and Microengineering, 2003. **13**(2): p. 201-208.

80. Anderson, J.L. and W.K. Idol, *Electroosmosis through pores with nonuniformly charged walls.* Chemical Engineering Communications, 1985. **38**(3-6): p. 93-106.

81. Barragan, V.M. and C.R. Bauza, *Electroosmosis through a cation-exchange membrane: Effect of an ac perturbation on the electroosmotic flow.* Journal of Colloid and Interface Science, 2000. **230**(2): p. 359-366.

82. Brechtel, R., et al., *Control of the electroosmotic flow by metal-salt-containing buffers.* Journal of Chromatography A, 1995. **716**(1-2): p. 97-105.

83. Burns, N.L., et al., *Surface characterization of biomedical materials by measurement of electroosmosis.* Biomaterials, 1998. **19**(4-5): p. 423-440.

84. Cikalo, M.G., K.D. Bartle, and P. Myers, *Influence of the electrical double-layer on electroosmotic flow in capillary electrochromatography.* Journal of Chromatography A, 1999. **836**(1): p. 35-51.

85. Cummings, E.B., et al., *Conditions for similitude between the fluid velocity and electric field in electroosmotic flow.* Analytical Chemistry, 2000. **72**(11): p. 2526-2532.

86. Patankar, S.V., *Numerical heat transfer fluid flow* 1980, New York: Hemisphere.

87. Tsao, H.K., *Electroosmotic flow through an annulus.* Journal of Colloid and Interface Science, 2000. **225**(1): p. 247-250.

88. Ajdari, A., *Generation of transverse fluid currents and forces by an electric field: Electro-osmosis on charge-modulated and undulated surfaces.* Physical Review E, 1996. **53**(5): p. 4996-5005.

89. Erickson, D. and D.Q. Li, *Influence of surface heterogeneity on electrokinetically driven microfluidic mixing.* Langmuir, 2002. **18**(5): p. 1883-1892.

90. Keely, C.A., T. Vandegoor, and D. McManigill, *Modelling flow profiles and dispersion in capillary electrophoresis with nonuniform zeta-potential.* Analytical Chemistry, 1994. **66**(23): p. 4236-4242.

91. Long, D., H.A. Stone, and A. Ajdari, *Electroosmotic flows created by surface defects in capillary electrophoresis.* Journal of Colloid and Interface Science, 1999. **212**(2): p. 338-349.

92. Herr, A.E., et al., *Electroosmotic capillary flow with nonuniform zeta potential.* Analytical Chemistry, 2000. **72**(5): p. 1053-1057.

93. Johnson, T.J., et al., *Laser modification of preformed polymer microchannels: Application to reduce band broadening around turns subject to electrokinetic flow.* Analytical Chemistry, 2001. **73**(15): p. 3656-3661.

94. Stroock, A.D., et al., *Patterning electro-osmotic flow with patterned surface charge.* Physical Review Letters, 2000. **84**(15): p. 3314-3317.

95. Ren, L.Q., C. Escobedo-Canseco, and D.Q. Li, *A new method of evaluating the average electro-osmotic velocity in microchannels.* Journal of Colloid and Interface Science, 2002. **250**(1): p. 238-242.

96. Sinton, D., et al., *Direct and indirect electroosmotic flow velocity measurements in microchannels.* Journal of Colloid and Interface Science, 2002. **254**(1): p. 184-189.

97. Pennathur, S. and J.G. Santiago, *Electrokinetic transport in nanochannels. 2. Experiments.* Analytical Chemistry, 2005. **77**(21): p. 6782-6789.

98. Culbertson, C.T., S.C. Jacobson, and J.M. Ramsey, *Microchip devices for high-efficiency separations.* Analytical Chemistry, 2000. **72**(23): p. 5814-5819.

99. Culbertson, C.T., et al., *Microchip separations in reduced-gravity and hypergravity environments.* Analytical Chemistry, 2005. **77**(24): p. 7933-7940.

100. Sinton, D., et al., *Effects of liquid conductivity differences on multi-component sample injection, pumping and stacking in microfluidic chips.* Lab on a Chip, 2003. **3**(3): p. 173-179.

101. Paegel, B.M., R.G. Blazej, and R.A. Mathies, *Microfluidic devices for DNA sequencing: sample preparation and electrophoretic analysis.* Current Opinion in Biotechnology, 2003. **14**(1): p. 42-50.

102. Tian, H.J., et al., *High-throughput single-strand conformation polymorphism analysis on a microfabricated capillary array electrophoresis device.* Electrophoresis, 2005. **26**(9): p. 1834-1842.

103. Patankar, N.A. and H.H. Hu, *Numerical simulation of electroosmotic flow.* Analytical Chemistry, 1998. **70**(9): p. 1870-1881.

104. Ermakov, S.V., S.C. Jacobson, and J.M. Ramsey, *Computer simulations of electrokinetic transport in microfabricated channel structures.* Analytical Chemistry, 1998. **70**(21): p. 4494-4504.

105. Ermakov, S.V., S.C. Jacobson, and J.M. Ramsey, *Computer simulations of electrokinetic injection techniques in microfluidic devices.* Analytical Chemistry, 2000. **72**(15): p. 3512-3517.

106. Bianchi, F., A. Ferrigno, and H.H. Girault, *Finite element simulation of an electroosmotic-driven flow division at a T-junction of microscale dimensions.* Analytical Chemistry, 2000. **72**(9): p. 1987-1993.

107. Mohammadi, B. and J.G. Santiago, *Simulation and design of extraction and separation fluidic devices.* Esaim-Mathematical Modelling and Numerical Analysis-Modelisation Mathematique Et Analyse Numerique, 2001. **35**(3): p. 513-523.

108. Ren, L.Q., D. Sinton, and D.Q. Li, *Numerical simulation of microfluidic injection processes in crossing microchannels.* Journal of Micromechanics and Microengineering, 2003. **13**(5): p. 739-747.

109. Lee, G.B., et al., *Dispersion control in microfluidic chips by localized zeta potential variation using the field effect.* Electrophoresis, 2004. **25**(12): p. 1879-1887.

110. Fu, L.M., et al., *Electrokinetic injection techniques in microfluidic chips.* Analytical Chemistry, 2002. **74**(19): p. 5084-5091.

111. Tsai, C.H., et al., *Experimental and numerical investigation into leakage effect in injectors of microfluidic devices.* Electrophoresis, 2006. **27**(24): p. 4991-4998.

112. Paegel, B.M., et al., *High throughput DNA sequencing with a microfabricated 96-lane capillary array electrophoresis bioprocessor.* Proceedings of the National Academy of Sciences of the United States of America, 2002. **99**(2): p. 574-579.

113. Gao, Q.F., Y.N. Shi, and S.R. Liu, *Multiple-channel microchips for high-throughput DNA analysis by capillary electrophoresis.* Fresenius Journal of Analytical Chemistry, 2001. **371**(2): p. 137-145.

114. Aborn, J.H., et al., *A 768-lane microfabricated system for high-throughput DNA sequencing.* Lab on a Chip, 2005. **5**(6): p. 669-674.

115. Erickson, D., *Towards numerical prototyping of labs-on-chip: modeling for integrated microfluidic devices.* Microfluidics and Nanofluidics, 2005. **1**(4): p. 301-318.

116. Bello, M.S., L. Capelli, and P.G. Righetti, *Dependence of the electroosmotic mobility on the applied electric-field and its reproducibility in capillary electrophoresis.* Journal of Chromatography A, 1994. **684**(2): p. 311-322.